Acoustic Noise Suppression for Helicopter Communication Systems

by

Jeffrey Thomas Evernham

S.B., Aeronautics and Astronautics
Massachusetts Institute of Technology, 1991

Submitted to the Department of Aeronautics and Astronautics
in partial fulfillment of the requirements for the degree of

Master of Science in Aeronautics and Astronautics

at the

MASSACHUSETTS INSTITUTE OF TECHNOLOGY

September 1992

Author .....
Department of Aeronautics and Astronautics
August 25, 1992

Certified by .....
Harold L. Alexander, Assistant Professor
Department of Aeronautics and Astronautics
Thesis Supervisor

Certified by .....
Richard S. Teal, Staff Engineer
Boeing Defense and Space Group, Helicopters Division
Thesis Supervisor

Accepted by .....
Professor Harold Y. Wachman, Chairman
Department Graduate Committee

Acoustic Noise Suppression for Helicopter Communication Systems

by

Jeffrey Thomas Evernham

Submitted to the Department of Aeronautics and Astronautics
on August 25, 1992, in partial fulfillment of the
requirements for the degree of
Master of Science in Aeronautics and Astronautics

Abstract

This document describes the design and implementation of three digital acoustic noise suppression systems for the Boeing CH-47D Chinook helicopter's interphone system. The Chinook's forward transmission produces narrowband noise spikes, or gear whine, which change frequency as the gearbox's rotation rate varies. Three algorithms are explored as possible methods to remove this changing narrowband noise from the pilots' microphone signal in order to increase the signal-to-noise ratio and intelligibility of the pilots' voices. These algorithms are the Least Mean Squared Adaptive Noise Cancellation (LMS) algorithm, the Tracking Filter (TF) algorithm, and the Variable Sampling Rate (VSR) Algorithm.

The LMS and TF algorithms were implemented in computer simulation and in real-time hardware, and were tested with four inputs: sinusoidal, speech, cockpit noise, and cockpit interphone (speech plus noise). A normalized-frequency VSR algorithm was studied as well, but hardware limitations prevented its implementation as a real-time system. The parameters of the LMS and TF systems were varied, and the outputs of the resultant systems were compared with one another and the unfiltered signal. Also, maximum-attenuation systems were implemented to examine the distortion caused by a large number of filters.

The LMS and TF algorithms were found to reduce the noise content at the noise spike frequencies by 10-35 dB, without significantly affecting the signal content of the pilots' voices. The systems were successful at tracking the RPM changes of the forward transmission in order to maintain suppression of the notch frequencies as they changed over time. The noise reduction capability of the two algorithms were comparable for very narrow (less than 5 Hz) band noise, whereas the TF algorithm provided better attenuation for larger bandwidths. However, both systems added distortion to the signal, in the form of a ringing sound at the suppressed frequencies. The ringing sound was stronger for the LMS algorithm than for the TF approach, although the TF algorithm removed more of the pilots' speech frequencies. Using equivalent-parameter systems, tuned to provide a subjective best tradeoff between noise reduction and distortion, the TF algorithm resulted in a slightly better quality

output. These two algorithms do (and the VSR algorithm promises to) improve the sound quality of the CH-47D interphone system, and may be useful in other, similar applications.

Thesis Supervisor: Harold L. Alexander, Assistant Professor
Title: Department of Aeronautics and Astronautics

Thesis Supervisor: Richard S. Teal, Staff Engineer
Title: Boeing Defense and Space Group, Helicopters Division

Acknowledgments

Thanks must be extended to the countless people at Boeing Helicopters who helped me througout this project, but mentioning every one of them would kill too many trees. I will list many on this page; those whom I have overlooked, please accept my apologies. So, thanks go to Angelo "Bring that Back" Drammissi, for ordering parts and hardware for the real-time system, and providing assistance in circuit modification. To Clark Sechler, also for ordering material and constructing circuits. To Ed "The Handyman" Nester, who gave his support to just about every aspect of the real time system and many VAX-IBM-Mac-Other interface tricks, helping to diagnose problems, teach me how to use equipment, debug hardware interfaces, and occasionally providing much-needed stress relief. To Blair "Hardware is Heaven" Harro, who selflessly devoted time and expertise to help debug the multiple hardware problems that occurred during development, from VME interfaces to zero crossing detectors. To Ken "Wire Wrap" Wochele, who designed, constructed, tested, and helped (often on his own time) debug the zero crossing detection systems for both the MIZAR card and the PC interface; good luck with *your* thesis! To Bob Spencer, who furnished help with the acoustics side of the project, providing equipment and observations, as well as making suggestions for the document. To Harry Sternfeld, for his guidance with the project's acoustics side, and also for reading drafts of the thesis. To Perry Zigin-bein, for acoustics help and for digitizing the CH-47 noise on the VAX for analysis. To Nick Albion, for sparking my interest in the initial idea of reducing noise in the CH-47 cockpit. To Rich "Yes, I've got *one* minute" Teal, who also got me interested in the idea, and who provided technical support for the theory and implementation of the real time systems. To Rob "You're Back!" Cloutier, for encouragement and support throughout my time at Boeing. To Dorothy "Time Card" Carroll, for making the ways of the business world easier for a relative newcomer. To Walt Ballauer, for allowing flexibility in my work schedule during the long hours of thesis creation. To the late John Senese, for help with the cockpit interphone system. To Joe Schluck, who assisted me greatly with setup guidance for flight testing, helped to make the

recordings themselves, and who gave me my second helicopter flight (the first on a CH-47). To Phyllis Schultz, for her help with the EIP program from the Boeing side, and a smiling face of encouragement every time I saw her. To Steve "Alarm Clock" Llorente, for providing a haven away from work, stress-relieving tennis, and for waking me up at 7:00 after those 16-hour workdays.

Thanks to those, at M.I.T. and at Boeing, who allowed me to alter the EIP schedule to suit my needs – the project would have suffered greatly otherwise.

There are also many people outside of Boeing who this project would have been impossible without. I extend thanks to Steve Curtain at Ariel, for providing an excellent product and even better support during the purchasing and development stages of the project. To Steve "Athena God" Ellis, who helped to debug my MATLAB simulation code and explained how to make the MIT-Boeing computer connection work. To Liz "What is it now?" Zotos, for handling the bureacracy of mixing business with education. To Tim "Yes No Ok Cancel" Hazen, my long-time partner in DSP and digital circuit labs, for help with DSP techniques, analog filter design, and digitizing the signals for use in the simulation. To Will "Burr" Gorgen, my long-time partner in Aeronautics (among other things), for taking care of MIT-related duties while I was at Boeing, most notably helping with transfer of data and LaTeXcompilation of thesis drafts – now it's your turn. To Jen, for everything she's done for me, but especially her support and understanding during the stressful long hours and weeks of thesis preparation. To Kevin "AutoCAD" Evernham, for the 3-D rendition of the lower planetary gear system. To my parents, for their support, concern, encouragement, and guidance over the last 22 years – much of who I am and what I have accomplished would have been impossible with any others. And, of course, to Sandy "Thesis-by-Mail" Alexander, for his guidance, explanations, instruction, suggestions, and ideas for all aspects of the noise reduction project, and for helping make this document readable and understandable.

I can only hope that all those whom I have mentioned have had as much fun as I have had, and not as much frustration.

Contents

List of Figures

List of Tables

Chapter 1

Introduction

1.1 Project Overview

This document describes the development, testing, and results of applying adaptive notch filter techniques to reduce noise in the interphone system of the Boeing CH-47D Chinook helicopter. Gear whine generated by the forward transmission produces high amplitude, narrowband noise spikes which are picked up by the pilots' microphones and mask their speech, reducing the signal to noise ratio (SNR) in the cockpit radio system and decreasing the intelligibility of pilots' speech. As the rotation rate of the transmission changes during wind gusts and manuevers, the gear mesh frequencies change, "sliding" up and down the frequency spectrum.

Three adaptive filtering techniques were used in an attempt to suppress the noise spikes while leaving most of the desired signal intact, with the hope of increasing the SNR and the intelligibility of the pilots' speech. First, the Least-Mean-Square Adaptive Noise Cancellation (LMS ANC) algorithm was applied to implement notch filters of constant bandwidth whose center frequencies could be controlled by changing the frequencies of reference inputs. The LMS algorithm determines the correlation between the input and reference inputs, and subtracts the integral of this value from the input. The frequencies of the reference inputs were proportional to the rotation rate of the gearbox, allowing the filters to track the frequencies of the gear mesh noise. Second, the Tracking Filter (TF) algorithm, which utilizes quadrature modulation

and a lowpass filter in a feedforward manner to obtain a notch filter, was applied in a similar manner. Last, a Variable Sampling Rate (VSR) algorithm was implemented, which utilized fixed-coefficient notch filters and a sampling rate proportional to the transmission rotation rate. Because the frequencies of digital systems are normalized to the sampling frequency, changing the sample rate changes the frequencies of the filters. The sample rate was proportional to the gearbox rotation rate, allowing the filters to track the gear mesh noise as well.

The three algorithms were first modelled on a computer, to explore their potential, evaluate the effects of nonidealities, and compare the results. Then, the LMS and TF algorithms were implemented in hardware systems and run in the laboratory with recordings from the CH-47D helicopter. The real-time VSR algorithm was not fully implemented due to unforseen hardware limitations of the development system. The VSR algorithm required the least computation time[1], although obtaining a high-frequency, stable signal to drive the sampling rate required careful design of a phase-locked loop frequency multiplier. The LMS algorithm needed a moderate amount of calculation time, and had better frequency-response characteristics than the other two. The TF algorithm required the most computation, but had a better subjective effect on the interphone signal than the LMS approach. All three algorithms proved satisfactory in ideal and nonideal (limited precision) implementations, and when designed carefully, produced comparable reductions in the background noise of the interphone system without greatly affecting the pilots' speech[2]. While formal intelligibility tests were not conducted, the LMS and TF algorithms improved the quality of the interphone signal, providing 10-35 dB of attenuation at the noise spike frequencies, while introducing low to moderate amounts of distortion to the pilots' speech. The distortion was noticeable as attenuated speech frequency bands and a ringing sound present at the attenuated frequencies. The ringing was somewhat more

[1]While the system was not able to run with the variable sampling rate, it was implemented in a normalized form with a constant sampling frequency. Thus, the LTI characteristics of the algorithm were evaluated, but the time-varying effects remain unstudied.

[2]The normalized-frequency VSR algorithm had effects very similar to the TF algorithm, but its attenuation while tracking the gear mesh frequencies remains unstudied.

pronounced with the LMS algorithm, making the TF algorithm slightly more pleasing to the ear.

1.2 Problem Description

The harsh environment of a helicopter cockpit makes it difficult for the pilot and copilot to concentrate on the jobs they must perform. They must constantly monitor their instruments, surroundings, and crew, while enduring continuous vibration, movement, and loud noise. The tasks and environment demand a great deal from the pilots, and any device to lessen the strain they must endure is a welcome addition. Noise is perhaps one of the least controllable and most annoying of these problems, causing increased fatigue, shifts in hearing threshold levels, and reduced intelligibility of communication[15, 25]. Repeated exposure without personal hearing protection (earmuffs, earplugs, etc.) to the noise levels in many of today's helicopters would cause permanent hearing damage. These high levels of noise exist because of system design tradeoffs. A helicopter that was almost noise-free internally would result in extreme performance penalties, so sacrifices (such as the requirement to wear personal hearing protection) are made in order to maximize the aircraft's potential. As a result, high noise levels are present in many of today's helicopters, and the CH-47D is no exception.

1.2.1 Noise in Helicopter Cockpits and a Potential Solution

Excessive noise in the cockpits of helicopters contributes to, among other things, reduced intelligibility of pilot and copilot speech[15, 25, 44]. This occurs because microphones used by the pilots and crew pick up noise inside the helicopter, and transmit this noise over the helicopter's communication system. Many approaches have been tried in the past to reduce this unwanted noise, but as the lifting power of new helicopters increases, previous solutions become less and less effective, and new techniques are sought[40, 44]. A new approach has become feasible with the advent of high-speed Digital Signal Processing (DSP) microprocessors, utilizing the

fact that the noise spectrum is dominated by narrowband noise spikes generated by the forward transmission[7, 25, 41, 44]. These noise spikes degrade the signal-to-noise ratio, making the pilots' speech difficult to understand. Notch filters may be used to decrease the contribution of this narrowband noise to the transmitted signal, without greatly affecting the signal power of broadband speech. This decreases the noise power while leaving the signal power relatively unchanged, resulting in a higher signal-to-noise ratio and better intelligibility. As the rotating speed of the transmission varies over time due to wind gusts and maneuvering, the notch filters must change their center frequencies as well in order to continue suppressing the gear mesh noise. In other words, the filters must track the rotation speed of the transmission. Filters with changing characteristics are difficult to implement using analog techniques, but are quite feasible with the use of DSP algorithms.

1.2.2 Types of Noise and What is Affected

The noise present in the cockpit gets to the pilots' ears by two routes: direct and indirect[25]. Direct noise is the sound that travels from the noise source to the eardrum directly, most often through the pilots' helmet and earcups. Indirect noise is the sound that gets picked up by the pilots' microphones, travels electronically through the communication system, and is then converted to an audible signal by the speaker in the pilots' earcup. Direct noise is experienced only by the pilots and crew in the helicopter, whereas indirect noise is heard by anyone listening to the communication system: the pilot and copilot as well as air traffic controllers, other pilots, ground troops, etc. Both noise sources contribute to reduced intelligibility for the pilots, but only the indirect noise makes the pilots harder to understand by others. Furthermore; this indirect noise, because it is combined in the microphone with what the pilots say, creates a major obstacle to the use of voice recognition (VR) systems. VR systems are becoming feasible as a method to reduce pilot workload in airplanes, but extending their use to helicopters has been hindered by the extremely noisy cockpit environment. If this noise could be suppressed, perhaps VR systems could become an integral part of helicopter avionic systems, and some of the demands

imposed on helicopter pilots could be reduced.

1.2.3 CH-47D Cockpit Noise Characteristics

In examining how to reduce noise in the cockpit, the sources of the noise must be identified. For all helicopters, there are three primary noise sources: the sound of the rotor blades moving through the air, the turning of the gears in the transmission, and the turning of the engine components[44]. The rotors produce loud but very low frequency vibrations which are often transferred to the entire fuselage of the helicopter. Noise from gears in the transmission tends to be narrowband, but has substantial noise power at several frequencies. Engine noise has high power, due largely to its wide bandwidth, and is primarily located in high frequency ranges.

The helicopter used in this project was the Boeing CH-47D Chinook helicopter, which produces a great deal of noise due to its large size and lifting capability. This aircraft generates noise levels as high as 115 dB and 100 dBA[3] inside the cockpit, even with full acoustic treatment[7, 15, 41, 44]. This is mostly due to the large size and lifting capacity of the helicopter; the noise of rotors, transmissions, and engines is a function of the power they must provide or transfer. In fact, the noisiest point in the helicopter is immediately below the forward and aft transmissions[7], and their high noise levels are largely due to the high power transmitted through the gearbox[24]. The CH-47 is therefore a good choice for testing noise reduction equipment for several reasons. First, the noise problem is so evident that a minor improvement will be more noticeable than if the noise were not so severe. Second, noise reduction in such an environment will provide a greater benefit than a proportional reduction in a helicopter where noise is not so severe. Third, if the noise suppression system is capable of reducing such high-amplitude noise, it is also likely to work on lesser amplitude noises; this is not necessarily true the other way around. Therefore, if a

[3]Decibels (dB) is a measure of absolute sound pressure level, defined as 20 $log\frac{spl}{ref}$, where spl is the sound pressure level, and ref is a reference sound pressure level (usually 20 μPa). dBA is the A-weighted sound pressure level, which takes into account the human ear's varying sensitivity to different frequencies. While dBA is most important for measuring intelligibility, the actual level in dB is more important when determining the potential hearing damage that may result.

noise reduction system has the potential for use with various helicopters[4], it makes sense to develop and test the system on a CH-47.

The D-model of the CH-47 has been selected for several reasons. First, it is the most common of the five basic Chinook models, and is manufactured in both military and civilian configurations. Second, they are still being manufactured (unlike the A, B, and C models) and are expected to remain in service for some time. Third, the E model is substantially different, utilizing more modern components, so that a noise reduction system that works on the E model may not work for any of the earlier models.

A diagram of the CH-47D can be seen in Figure 1-1, and shows how the helicopter's specific configuration makes its noise problems unique. First of all, the gas turbine engines that provide its power are located at the aft of the rather large helicopter, so their contribution to the cockpit noise is relatively small. Secondly, the CH-47D is a tandem rotor helicopter, and therefore has a forward rotor and transmission as well as an aft rotor and transmission. The cockpit and the pilots are located very close to the forward transmission and rotors, and as a result, most of the cockpit noise is generated by these sources. Furthermore, the fact that these sources are so close to the cockpit does not allow room for much soundproofing material to be applied. In fact, the forward transmission sits immediately behind and above the two pilots; a pilot with a long arm could touch the bottom of the gearbox casing while still sitting in his or her seat. As a result, the noise from the forward transmission dominates the frequency spectrum of the cockpit.

1.3 Existing Technologies for Cockpit Noise Reduction

Noise in helicopter cockpits is not a new problem. Much time and effort has been devoted to reducing the amount of noise they produce in the first place, and to

[4]Other helicopters have very similar noise problems; Laskin[24] found the UH-1D's noise is dominated by its gearbox as well.

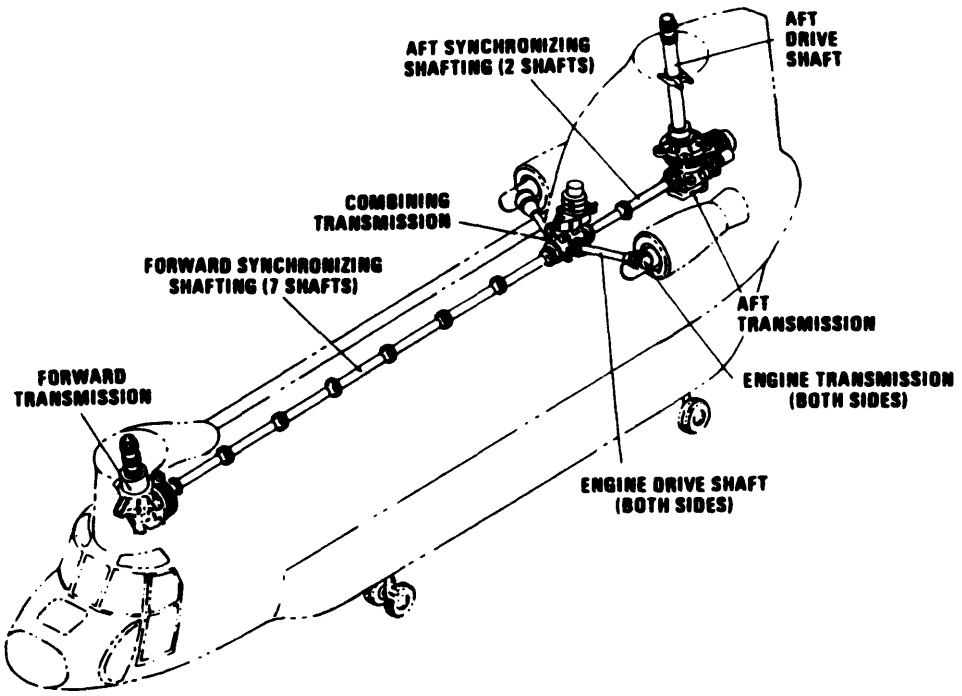

Figure 1-1: Boeing CH-47D Chinook Tandem-Rotor Helicopter

suppressing the noise that they do generate. As the focus of this project is to suppress noise that is already present, the sound-reducing design issues of rotors, gearboxes, and engines will not be explored. However, many other approaches have been used to attack the direct and indirect noise that reaches the pilots, and a brief introduction to these techniques is presented in the following sections. Also included is a synopsis of previous literature on adaptive noise cancellation, the noise reduction technique used in this project.

1.3.1 Suppressing Direct Noise

Perhaps the most obvious solution to reducing the effect of noisy machinery is to isolate the machinery from the operating environment, either by distance or sound absorbing and insulating materials. Because of the design of the CH-47, it is not possible to move the pilots further away from the transmission. However, sound insulation and blanketing can lessen the noise substantially; soundproofing has obtained

reductions of up to 35 dB at speech frequencies in the CH-47 cabin, but cockpit reductions have been limited to no more than 20 dB[5][40]. But, using this sound absorbing material has two drawbacks. First, a lot of insulation is required to obtain substantial dissipation of loud sounds, such as those generated by the tranmission, and second, the insulation is bulky and heavy. There isn't much room in the CH-47 cockpit to place a lot of insulation, and the weight of the material imposes a sacrifice on the performance characteristics of the helicopter. Each additional pound of soundproofing means that one less pound of fuel or other cargo can be carried. This can be a difficult sacrifice to make, especially when lives are at stake; helicopter pilots in Vietnam were known to strip out cabin insulation material in order to obtain as much performance as possible from the helicopter[44]. As a result, better methods have long been sought to provide the same benefits as physical soundproofing, but without its weight and size penalties.

To this end, several alternate and complementary approaches have been found. The simplest of these is isolating the pilots' ears from the noise source, rather than isolating the source from the whole cockpit. This is most often done through the use of insulated helmets and/or noise reducing earcups. Because these treat only the small area around the ear instead of the entire cockpit, the same noise dissipations of other insulating techniques can be achieved with much smaller weight penalties. The attenuation achieved by the standard helmet/earcup combination used on the CH-47 ranges from under 15 dB below 250 Hz to a maximum of about 50 dB near 3500 Hz[15][6]. The drawbacks of this approach stem from the fact that the reduction obtainable is largely a function of the earcup's seal to the pilot's head. The amount of attenuation is directly related to the integrity and force of the seal, so attenuating loud sounds requires high-pressure "bonecrusher" headsets that are often painful and fatiguing, especially when worn for extended periods. Furthermore, while

[5]Even with 95% surface coverage using $1.5\frac{lb}{ft^2}$ blanketing material, cockpit reductions did not exceed 20 dB at speech frequencies. This is largely due to the fact that windows are excellent sound radiators, and the surface of the cockpit of the CH-47 (as with any helicopter) is mostly windows.

[6]This is typical, as most flight helmets achieve more than 30 dB of attenuation at frequencies over 1 kHz[43] but are often limited to a maximum of 13 dB in the 125 and 250 Hz octave bands[14].

these earcups do a good job of attenuating high-frequency noise (above approx. 1000 Hz)[15], they become less effective as the frequency decreases. So, while such earcups are excellent for relatively low-amplitude, high-frequency noise, the extreme volume and lower frequencies of helicopter cockpit noise (especially that of the CH-47) makes these earcups only a partial solution.

A more recent development has been Active Noise Reduction (ANR). An ANR system "listens" to the ambient noise present, and drives speakers to send out an identical noise signal, but 180 degrees out of phase with the original signal. This technique attempts to achieve complete elimination of the unwanted noise through destructive interference. These systems can produce reductions (in the pilot's earcup) of 10-20 dB for low-frequency (below 500 Hz) aircraft engine noise[6, 42, 43], these systems have several drawbacks. First, a microphone must be present very close to the point where the noise is to be cancelled[7], because displacement between the microphone and the zero-noise location affects the phase of the signals. Obviously, phase errors decrease the effectiveness of the system, and enough error (greater than 90 degrees) can actually lead to *constructive* interference, which only worsens the noise. While phase errors do not pose a problem for the use of ANR in an earcup, it does prevent such systems from working in large spaces, such as the cockpit. Second, such systems are limited by their finite response times and the need to listen to the noise present while attempting to cancel it. These two problems can cause positive feedback, where an ANR system actually generates its own noise, causing negative attenuation. For typical systems, this positive feedback can occur at frequencies as low as 1 kHz[42]. Finally, ANR systems do not perform well with extremely high amplitude noise, as the very high sound levels (on the order of 125 dB) can cause the control system to go unstable[43]. Thus, while ANR is attractive for in-the-earcup, low-frequency noise reduction, it does not provide a very good solution to high-frequency, cockpit-wide noise.

[7]Typically, reduction can only be achieved when there is less than half a wavelength distance between the speaker and the microphone[12].

1.3.2 Suppressing Indirect Noise

A limitation of the latter two techniques is that they only attack the direct noise that reaches the pilot's ears. Every time the pilot or copilot tries to talk to the other or transmit a message, his or her microphone picks up all the noise in the cockpit, including any noise that is reduced by his or her earcups. As a result, the pilots is speech mixed with a blast of noise - the indirect noise. While this noise (at the proper volume settings) is not as dangerous to their hearing as the direct noise, it makes their speech difficult to understand, hindering communications between pilot and copilot as well as between the helicopter and external receivers. Furthermore, as described earlier, it is the indirect noise that has prevented the use of VR systems in helicopters. At least four methods (in addition to insulating the entire cockpit from the noise source) have been used in attempts to address the problem of indirect noise.

One approach involves the use of a pressure-gradient microphone, instead of an absolute pressure microphone. By exposing the diaphragm of the microphone on both of its sides, it should only move when a pressure gradient exists[8]. Assuming that the noise field is nearly uniform on both sides of the microphone, the noise impinges equally on both sides of the diaphragm, and it registers nothing. However, when the pilot speaks, his or her voice is present only (or at least mostly) on one side of the microphone, and the resulting pressure gradient is picked up and amplified by the communications system. While such a device has great promise in theory, the improvements actually realized by such microphones have generally been small[25].

Along the same lines, alternate means of picking up the pilots' voices has led to some improvements in reducing the indirect noise. Throat-mounted accelerometers can be used to directly measure vocal cord vibrations to complement and enhance the signal of a standard microphone[35, 46, 47]. Summing the outputs of the microphone and the accelerometers results in a signal with higher intelligibility, because

[8]Most microphones are absolute pressure microphones, with the diaphragm exposed to the ambient air on only one side. These microphones register pressures that are different from the pressure on the inside of the microphone, which is held constant. The relative pressure (what is measured) thus comes from the difference between the two pressures, rather than the pressure gradient between the external and the internal pressures.

the accelerometer is relatively insensitive to acoustic noise. Thus, the microphone provides most of the high-frequency content of the signal, whereas the accelerometer registers more of the low frequencies of the pilot's voice. Dividing the information acquisition in this manner allows better signal-to-noise ratios over the range of speech frequencies (especially if there is a large amount of low frequency noise), resulting in better intelligibilty.

Another approach involves filtering the microphone signal to lessen its signal power at frequencies where the noise is the loudest. While such filtering will affect the speech quality as well (the filter must be applied to the speaker's voice as well as the ambient noise, as the microphone picks up both), the technique has promise for narrowband or well-defined noise spectra. If the noise is narrowband and its frequency is relatively constant, the filter can be designed such that the power of the broadband speech signal is only moderately affected, while the power of the narrowband noise can be greatly reduced. Such filters were used on early production aircraft of the CH-47A helicopter, but their wide bandwidth proved to degrade communication so severely that they were discontinued in later models[25].

More recently, an evaluation of the communication system used in the CH-47 was performed. The results of this analysis concluded that the communication system itself (particularly the resonances of the microphone and the earcup) contributed greatly to the intelligibility problems, because its transfer function is nonlinear, and amplifies many of the frequencies which contain the most noise[25][9]. The transfer function of the standard CH-47 communication system (including microphone, junction box, and speaker output inside the earcup) is shown in Figure 1-2. If the current communication system could be replaced with a linear-response microphone and a redesigned earcup, then perhaps the unwanted noise could be decreased and intelligibility could be increased. An improved design was developed, resulting in the transfer function shown in Figure 1-3[32]. This system obviously has better performance than

[9]More specifically, the intercom system's transfer function has a large peak in the 2500 to 4500 Hz frequency range. Many of the gear mesh frequencies of the transmission fall into this frequency range, and are thus amplified more than the pilot's speech, which consists primarily (for male speakers) of frequencies below this range.

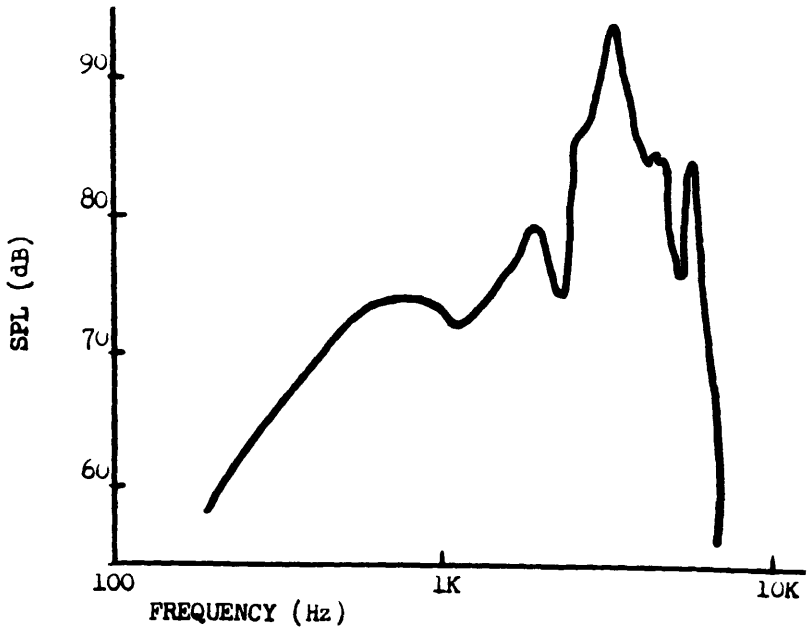

Figure 1-2: Transfer Function of Standard CH-47 Interphone System

the standard configuration and thus provides a more intelligible signal, but very few helicopters were upgraded to the improved communication system. This was largely a result of the fact that the current system is adequate, and the upgrade would require modification of the cockpit hardware, costing money[10].

1.3.3 Summary of Noise Suppression Capability

Even with the many attempts to reduce the noise in the cockpit, problems remain. The extreme amplitude of the noise, scattered over a large range of frequencies, creates a spectrum that is particularly difficult to attack. Furthermore, most of the previous work intends to attack broadband noise, making small gains at many frequencies. While this is adequate for low volume noise, the amplitude of the CH-47D's noise remains high even after subtantial sound treatments, keeping intelligibility low enough that attempts to use voice recognition systems in helicopters have met with repeated failure[45]. Solutions to these problems seem to lie along two separate paths:

[10]The upgrade uses a powered microphone, while the CH-47's standard microphone is an unpowered condenser microphone. Thus, upgrading to the new system would require modification or replacement of the current interphone junction box, in order to provide power to the mike.

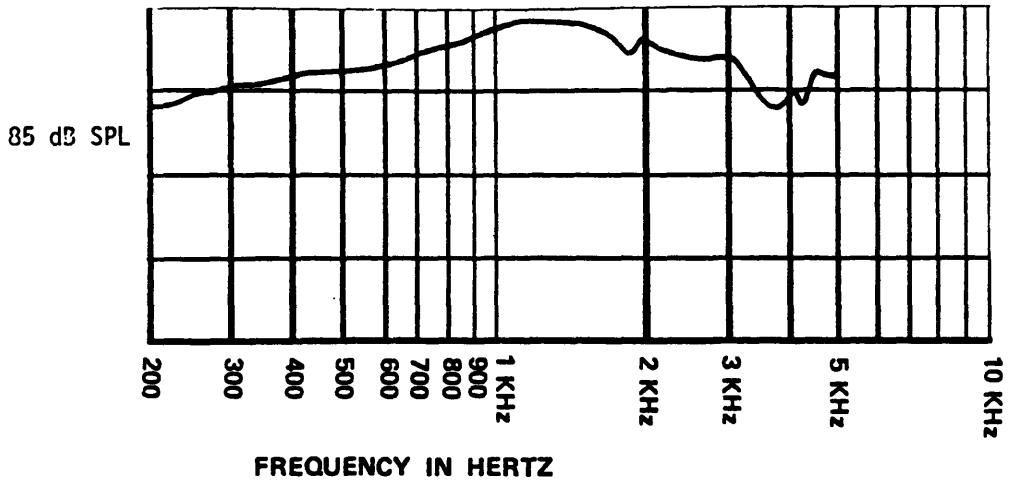

Figure 1-3: Transfer Function of Improved CH-47 Interphone System

combining previous work to gain the best aspects of different suppression techniques, and finding new approaches tailored to the noise spectra that obtain significant noise reductions in the frequency ranges that cause the largest problems. Combining a linear-response interphone system with a microphone and accelerometer input system would certainly improve the quality of speech over the radio system, and matching ANR techniques with good earcups can provide substantial noise reductions over the entire range of speech. However, this project concentrates on utilizing the characteristics of the noise spectra to tailor a noise reduction system to the frequencies of the CH-47's gearbox that are most intrusive. Taking this approach should yield a substantial difference in the signal's unwanted noise power without greatly affecting the desired signal, the pilots' speech. The result is a better signal to noise ratio, critical for the success of voice recognition systems, and better intelligibility for the humans who have to listen to the gear whine picked up by the microphones.

1.4 Proposed Solutions

In order to develop a system that is customized to the sound spectrum of the CH-47D, knowledge of the spectrum is crucial. If some characteristic of the noise can be well-defined, then this knowledge can be used to reduce the noise that causes the greatest problems. The Chinook's noise spectrum has this characteristic, in that the noise created by the forward transmission is periodic in nature, producing narrowband noise spikes. However, while this noise is periodic, its frequency does not remain constant, and a system is needed that can predict or react to changes in the characteristics of the noise. This can be done with an adaptive filter or similarly adaptive system, and the technique of cancelling varying periodic interference is known as Adaptive Notch Filtering, or Adaptive Noise Cancellation (ANC).

1.4.1 Adaptive Noise Cancellation

Many papers have been published exploring techniques of ANC filtering, especially for the retrieval or cancellation of periodic, sinusoidal signals in a noisy environment. Widrow[48] described the LMS ANC algorithm and several of its applications to notch filtering. Also describing the use of this algorithm for notch filtering is Glover[17], who demonstrated that if the reference sinusoid signals have amplitudes of less than one, the resultant notch is of narrower bandwidth, and that a sum-of-sinusoids approach can be used to reduce the required number of reference signals, at the sacrifice of substantial time-variant noise. Clark[10] expanded the basic LMS to a block LMS method, in order to take advantage of parallel processing techniques for MIMO LMS algorithms. The LMS algorithm itself can be greatly simplified if the sampling rate is an integer multiple of the noise frequencies[11], producing better notch filters with large reductions in computation time. Goodwin[16] explored the Kalman filter as an adaptive notch filter, and related its characteristics to the LMS methods. In situations where the input is not well-characterized and LMS performs poorly, the Recursive LMS (RLMS) method can be used[13], at the cost of calculation speed. If low steady state error must be combined with rapid convergence rate, then the inte-

gration constant can be varied over time rather than held constant, called the Variable Step (VS) LMS algorithm[19]. Another option is to utilize the Sequential Regression (SER) method, especially if extremely narrow notches are required[29]. Again, this comes at the cost of higher complexity, especially for MIMO problems. Higher Harmonic Control has been explored by several[18, 36, 37] for elimination of narrowband vibrations, especially as applied to helicopter rotor harmonics. Sievers[38] brought classical control, HHC, LMS, and modern control methods together for comparison in one paper.

1.4.2 Algorithms Examined

There are several DSP algorithms which can be used to implement notch filters with varying center frequencies, three of which were explored in this project. Perhaps the most common approach is to utilize some form of Widrow's Adaptive Noise Cancellation (ANC)[3, 12, 13, 17, 31, 33, 48] techniques, most notably the Least-Mean-Squared (LMS) algorithm, which implements a notch filter whose center frequency can be controlled by changing the frequencies of the sinusoidal reference inputs. In short, the algorithm uses an integrator to progressively estimate the frequency components of the input signal that are near the reference frequency, and uses a feedback loop to subtract this error from the input signal. If the reference input's frequency is proportional to the transmission rotation rate, then the algorithm can be used to cancel the gear mesh frequencies. A second approach, related to this technique, is the Tracking Filter (TF) algorithm[18, 23][11]. This procedure performs the same frequency estimation, but uses a lowpass filter and a feed-forward loop to cancel the noise. The third approach is to utilize the frequency normalization that occurs when sampling an analog signal to control the center frequencies of constant-coefficient filters. In this case, traditional digital notch filters are designed and implemented based on a nominal sampling rate, and as the actual sampling rate changes, their center frequencies will change proportionally with that rate. Thus, if the sampling frequency is pro-

[11]The TF algorithm is a particular implementation of an algorithm more generally known as Higher Harmonic Control, or HHC.

portional to the transmission rotation rate, the notches will reduce the signal power in the desired frequency bands. This approach is called the Variable Sampling Rate (VSR) algorithm. These three algorithms were explored[12] to evaluate their relative effectiveness in improving speech intelligibility in the helicopter cockpit environment.

1.4.3 Testing Procedures and Results

The algorithms were implemented and tested in several ways. First, the LMS and TF algorithms were numerically simulated on a computer. This allowed analysis of their performance under ideal, controllable circumstances, and provided the ability to explore the effects of non-idealities, such as quantization errors. The simulations were run with impulse inputs as well as recorded flight data, providing frequency-domain graphical analyses. These two algorithms were also implemented in 12-bit forms on a Texas Instrument TMS32020 microprocessor. Unfortunately, its speed limitations prevented utilization of this chip for more than one or two notch filters. These two algorithms were also implemented in 14-bit, constant sampling versions on the Motorola DSP56001, as was the normalized version of the VSR algorithm. The systems were tested with frequency-response analysis equipment, to compare to the computer simulation, and several inputs were used to examine the system's characteristics. Speech was used to explore the system's impact on the intelligibility of speech with no noise, and cockpit noise recordings were used to determine how effective the systems were in reducing the transmission's gear whine. Laboratory tests also explored recordings of the cockpit interphone system as a substitute to in-flight testing, to determine their effects on the interphone signal.

The LMS and TF algorithms successfully attenuated the selected gear mesh frequencies, and were able to adapt the filter locations as the transmission rotation rate varied. Both algorithms provided attenuations of 10-35 dB at the selected frequencies, thereby decreasing the noise in the interphone signal. However, they also added

[12]The LMS and TF algorithms were analyzed fully in a simulation and in real-time hardware. The VSR algorithm's normalized frequency response was simulated and run in real-time as well, but the variable nature of the algorithm was not implemented.

distortion to the pilots' speech, evident as a noticeable reduction in the speech's frequency content, and a ringing sound at the attenuated frequencies. The systems' characteristics were tuned by varying the parameters of the system to provide a good subjective tradeoff between noise reduction and speech degradation. The resultant systems, with equivalent design parameters, were compared using speech, cockpit noise, and the cockpit interphone. The LMS algorithm caused a slightly more noticeable ringing, whereas the TF algorithm produced a more noticeable absence of speech frequencies. Subjectively, the ringing was more degrading than the missing frequencies, and the TF algorithm provided slightly better sound quality. Then, to explore the maximum attenuation, notch filters were added to the systems until the computation limits of the processor were reached. The resulting systems provided significant reductions in almost all of the gear mesh noise, but introduced substantial distortion into the speech signal, such that the overall sound quality was reduced. The VSR algorithm was not implemented in real time due to an unforseen hardware limitation, but was run in a frequency-normalized format. The results of this implementation indicate that its characteristics should be very similar to those of the TF algorithm, with substantially reduced computation requirements.

1.5 Reader's Guide to Document

Chapter Two is devoted to characterizing the noise of the helicopter used for this project, the Boeing CH-47D Chinook. It describes the sources of noise, the potential effects of this noise on intelligibility of speech, the way the noise changes over time, and the implications of this variance on the noise reduction algorithms. Chapter Three details the three algorithms used to combat this noise. It explains how the algorithms work, describes practical considerations of the algorithms, and defines the requirements of the reference signal in designing the systems' characteristics. Chapter Four is devoted to the implementation of the algorithms, including data recording, how the algorithms were modelled in computer simulations, and testing procedures. Chapter Five explains the results of the testing, describing how the simulations and

real-time implementations were used to determine the best algorithm design, the results of testing those systems, and recommendations for future work.

Chapter 2

CH-47D Noise Characterization

2.1 General Analysis

The cockpit of the CH-47 is a very noisy environment, due to its proximity to noise sources and its poor sound damping qualities. Noise in the cockpit is reflected off of surfaces such as the windows and instrument panels, and is partially absorbed by the seats, acoustic blankets, and pilots themselves. Some of the obvious sources of this noise include noise from the rotors turning overhead, noise from the forward transmission which sits immediately aft and above the pilots, and to a lesser extent, noise from the auxiliary power units and turbine engines at the rear of the helicopter. Modelling the acoustics of such a complex environment is virtually impossible, and analyzing the problem leads instead to collecting experimental measurements of the noise. Boeing has collected a rather exhaustive library of recordings of cockpit noise, and has attempted to determine the sources of this noise as well as the contribution of each source to the total noise. These analyses are presented and built upon in the following section.

2.1.1 Cockpit Noise Spectra

To identify what noise creates the largest problems for pilots and voice recognition systems, it is perhaps best to first identify the frequency range used for speaking.

For this purpose, the frequency range from 200 to 6100 Hz has been broken down into 20 frequency bands, each of which contributes equally to the intelligibility of adult male speakers[1][1]. These frequency bands are shown in Table 2.1. If each of these frequency bands supplies an equivalent amount to the understanding of speech, removing any one of these bands should have the same effect on intelligibility as removing any other band. This breakdown provides a good start at examining how a noise spike at a particular frequency affects intelligibility. A noise spike will be defined as a narrowband (less than approximately five Hz) noise signal of large amplitude; in the case of the CH-47 interphone system, the noise spike has an magnitude larger than that of the pilot's voice at the same frequency. By this definition, a noise spike will dominate the spectrum of the signal at the frequencies where it is present. So, if a noise spike is present in a larger frequency band (such as that from 5050 to 6100 Hz), it will obscure a smaller percentage of the total frequency band than an equivalent spike in a smaller band (such as 330 to 430 Hz). Thus, the noise spike in the larger band will have a smaller effect on the intelligibility of the voice signal that it is superimposed on. So, reducing a noise spike in a smaller frequency band is more important than suppressing one in a larger frequency band.

Furthermore, the table denotes a good range of the frequencies that compose male speech. Defining an upper limit on the necessary frequency range is important, because a digital system is going to be used. The sampling frequency must be more than twice the maximum frequency desired because of Nyquist's sampling theorem. Of course, the higher the sampling frequency, the less time the microprocessor will have to perform calculations. Furthermore, the input signal will have nonzero magnitude at frequencies above the maximum desired frequency, so an analog lowpass filter must be used to attenuate these frequencies before sampling the signal. This analog filter will need a finite frequency bandwidth above the highest desired frequency in order to achieve adequate rolloff at the Nyquist frequency. Based on the idea that the lower the sampling frequency, the more flexibility will be available in implementing

[1]A similar breakdown for the adult female would undoubtedly be quite different. However, as most Chinook pilots are male, the unusual case of a female pilot was not addressed in this project.

the algorithm on the DSP chip, the sampling frequency should be chosen as small as possible, while allowing for the analog filter and the highest necessary frequency for communication. For instance, if 5000 Hz is chosen as the highest frequency and 3000 Hz is allowed for filter rolloff, we must sample faster than $2(5000 + 3000) = 16$ kHz. This will allow $\frac{1}{16000} = 62.5$ ms for calculation, and if the DSP chip has a clock speed of 5 MHz, then it has an instruction cycle of $\frac{1}{5x10^6} = 200$ ns. Therefore, with this example, the algorithm on the DSP chip must be performed in less than $\frac{62500}{200} = 312$ cycles, including time for the analog-to-digital (AD) and digital-to-analog (DA) conversions. If this is not possible, then the sampling frequency must be decreased so that more time is available to perform the necessary computations. Obviously, however, the highest desired frequency must cover most of the range of speech. The range of speech as defined by the military is identical to that of the frequency response of telephones, spanning from 300 to 3000 Hz[26][2]. Because the noise reduction system will be designed to maximize intelligibility, it will be designed with a substantially larger range (to at least 6 kHz, the point where the CH-47D interphone begins substantial rolloff) so that more of the important speech frequencies are present, and to enable the system to be transferred to other environments where higher frequencies may be more important (such as for female speakers).

Once the maximum frequency to work with has been identified, the next step is to examine the frequency spectrum of the helicopter cockpit. A typical noise spectrum of the CH-47D cockpit is shown in Figure 2-1. The sampling rate for this graph was 12 kHz, and the spectrum represents a data sample of 2.75 seconds. It is obvious from the diagram that there are several noise peaks that are substantially louder than the rest of the noise. The loudest of these peaks occur at around 1500 and 3400 Hz, although there are substantial peaks near 800, 1200, and 3000 Hz as well. These frequencies all fall within the range of speech, and appear to be narrowband noise (note especially the three distinct peaks near 1450, 1500, and 1600 Hz). Such characteristics make these peaks good candidates for suppression, and closer inspection is warranted. Shown in

[2]Note, however, that telephones operate in a largely noise free environment, and intelligibility over phone lines becomes seriously degraded if the background noise exceeds 75 dBA.

All Frequencies are in Hz			
Band No.	Frequency Limits	Center Frequency	Band-Width
1	200-300	270	130
2	330-430	380	100
3	430-560	490	130
4	560-700	630	140
5	700-840	770	140
6	840-1000	920	160
7	1000-1150	1070	150
8	1150-1310	1230	160
9	1310-1480	1400	170
10	1480-1660	1570	180
11	1660-1830	1740	170
12	1830-2020	1920	190
13	2020-2240	2130	220
14	2240-2500	2370	260
15	2500-2820	2660	320
16	2820-3200	3000	380
17	3200-3650	3400	450
18	3650-4250	3950	600
19	4250-5050	4650	800
20	5050-6100	5600	1050

Table 2.1: Frequency Bands of Equal Contribution to Speech Intelligibility

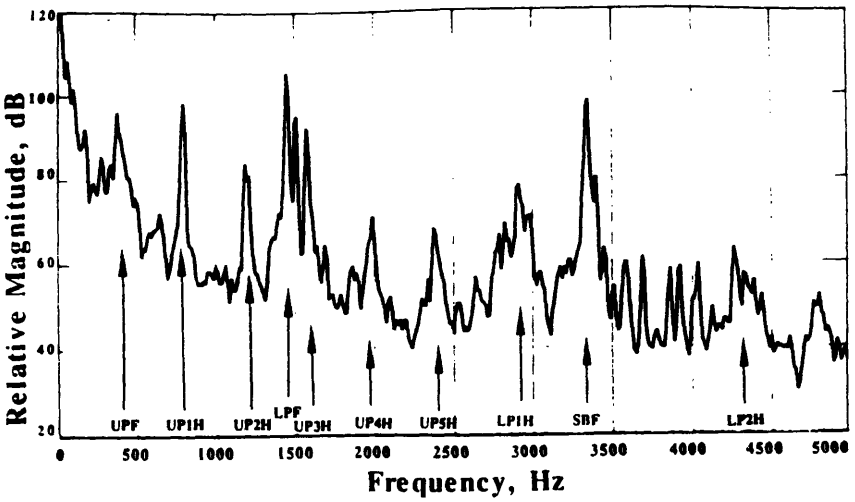

Figure 2-1: Frequency Spectrum of CH-47D Cockpit

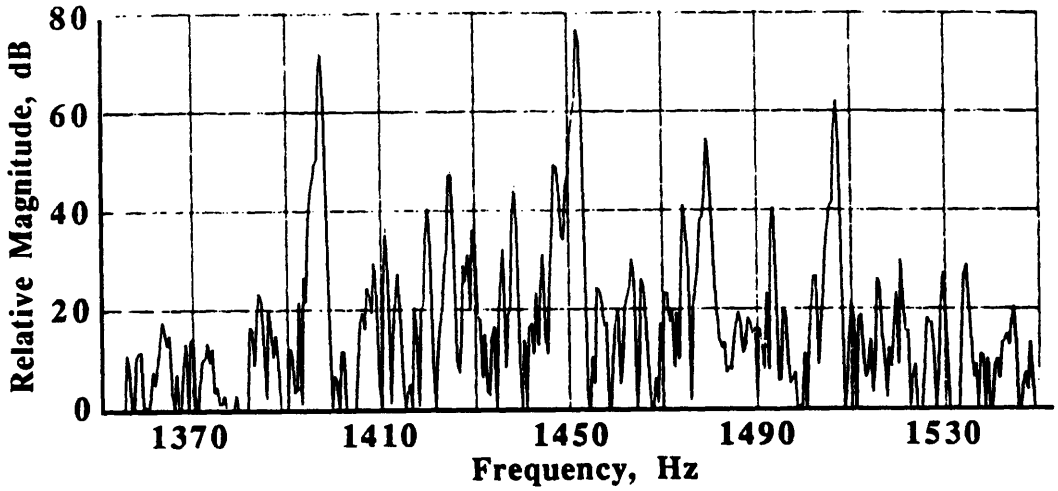

Figure 2-2: Close-up of Frequency Spectrum Near 1450 Hz

Figure 2-2 is a closeup of the highest peak in the frequency spectra. It is apparent in this view that the peak actually consists of several very narrowband noise spikes. These spikes appear to be centered around the peak at 1452 Hz, at roughly ± 13.5 Hz, ± 27 Hz, ± 40.5 Hz, and about ± 54 Hz. Because of the even spacing of these spikes, it is logical to conclude that the peak is actually comprised of a central noise spike and several sidebanded frequencies. All of the spikes have very small bandwidth, on the order of less than 2 Hz. It would therefore seem that removing the signal content at these frequencies could yield a substantial improvement in speech intelligibility.

2.1.2 Primary Noise Sources

Now that the target frequencies for suppression have been identified, the next step is to identify the source of the noise spikes in order to determine how they behave over time. As explained earlier, the two prevalent (very high amplitude) noise sources for the CH-47 cockpit are rotor noise and gear whine noise from the forward transmission. Of these sources, it is easy to determine which could produce high-frequency narrowband noise. The rotors create a low-frequency "whop-whop-whop" sound as they move past the cockpit. The forward transmission, however, generates high-frequency noise due to the interaction of its gears. The action of gear teeth deformations as they come into and out of contact with one another creates high amplitude noise whose signal power is primarily located at a single frequency, called the gear mesh frequency, and its harmonics[5, 24, 25, 34, 39, 41]. If the geometry and speed of rotation of the gears are constant, then the noise that results is a narrowband noise spike at the gear mesh frequency. If the rotation speed and/or number of gear teeth is high, then the resultant gear mesh frequency can be high as well. Based on these observations, it is quite clear that the primary noise source for this problem is the gear whine of the forward transmission.

2.2 Forward Transmission Gear Whine Analysis

In order to fully understand the noise in the cockpit, one must understand precisely how the noise is generated. To this end, the forward transmission of the CH-47D was analyzed in order to determine what gears could create the primary spikes and secondary sidebands visible in the noise spectra.

2.2.1 Gearbox Description

The forward transmission of the CH-47 is designed to offer a high reduction of gear speed, under high torque, with a minimal amount of vibration. To accomplish this, a dual planetary gear system is used. Figure 2-3 shows a 3-D view of the lower (first)

planetary gear system of the forward transmission. It shows that the ring gear, which is stationary, surrounds the four planetary gears, which mesh with a gear at the center of the system, the sun gear. The sun gear's center is stationary, but free to rotate, while the planets are free to rotate and move, but are held together by a brace called the carrier. Driving the sun gear causes, in conjunction with the fixed ring gear, a torque to be applied to the planet gears. This torque causes the planet gears to rotate; as they rotate, the ring gear forces them to translate as well, and their centers orbit in a circle around the sun gear. As the carrier is connected to the centers of the planet gears, it rotates at the orbital speed of the planets. A side view of the complete, two-stage forward transmission can be seen in Figure 2-4. The incoming drive shaft[3] turns a spiral bevel gear to change the rotation axis from near-horizontal to near-vertical, with a reduction in RPM. The near-vertical shaft then turns the sun gear for the lower (first) stage of speed reduction. The torque applied by the central sun gear and the fixed ring gear of the lower stage causes the lower planetary gears (four) to orbit the sun gear. The lower carrier turns at the orbital speed of the lower planet gears, and drives the upper (second) stage sun gear. Just as in the lower stage, this sun gear and the fixed ring gear cause the upper planetary gears (six) to orbit the upper sun gear. The upper planets' carrier then drives the rotor shaft which is connected to the forward rotors. Both the forward and aft rotors have a nominal rotation rate of 225 RPM, or 3.75 Hz[4].

Once the geometry of the gearbox is known, if the rotational speed of one of its components can be determined, it is relatively easy to calculate the rotational speeds of all the gears, and thus their gear mesh frequencies. Before examining the sun-planet gear system, however, consider two interlocking gears with fixed axes of rotation. Because the teeth of these gears must interlock during the entire rotation of

[3]For a diagram showing the drive shaft and tranmission locations in the CH-47, see Figure 1-1. The main drive shaft emanates from the combining transmission, which is a differential gearbox that combines the engine drive shafts. This drive shaft runs both the forward and aft transmissions, and thus the rotors, at the same speed.

[4]D and E models only. The A, B, and C models have the same gearboxes but a nominal rotation rate of 243 RPM (4.05 Hz), while the 47-352 (the RAF's version of the Chinook) has a nominal rotation speed of 250 RPM (4.17 Hz)[34].

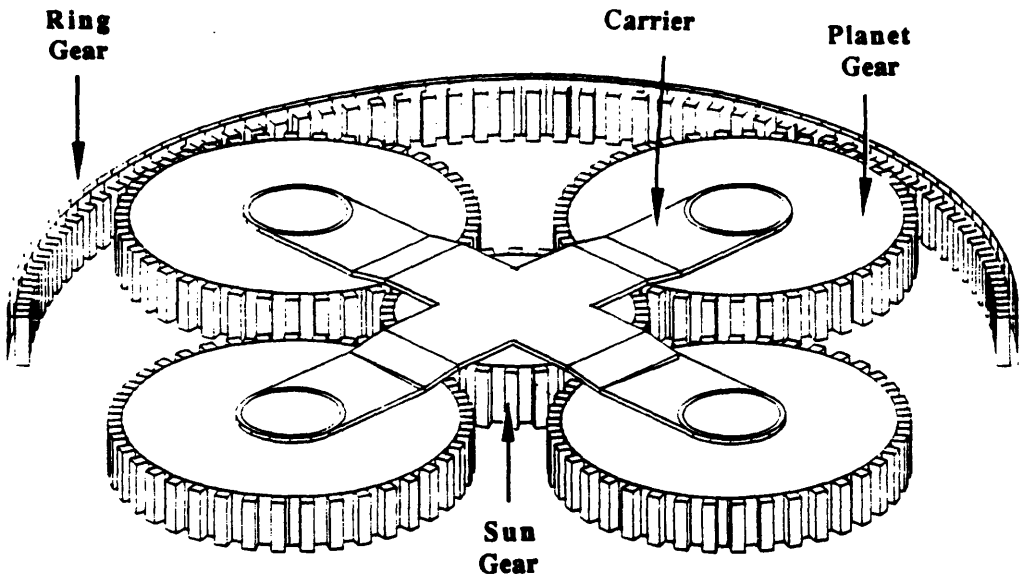

Figure 2-3: Lower Planetary Gear System of Forward Transmission

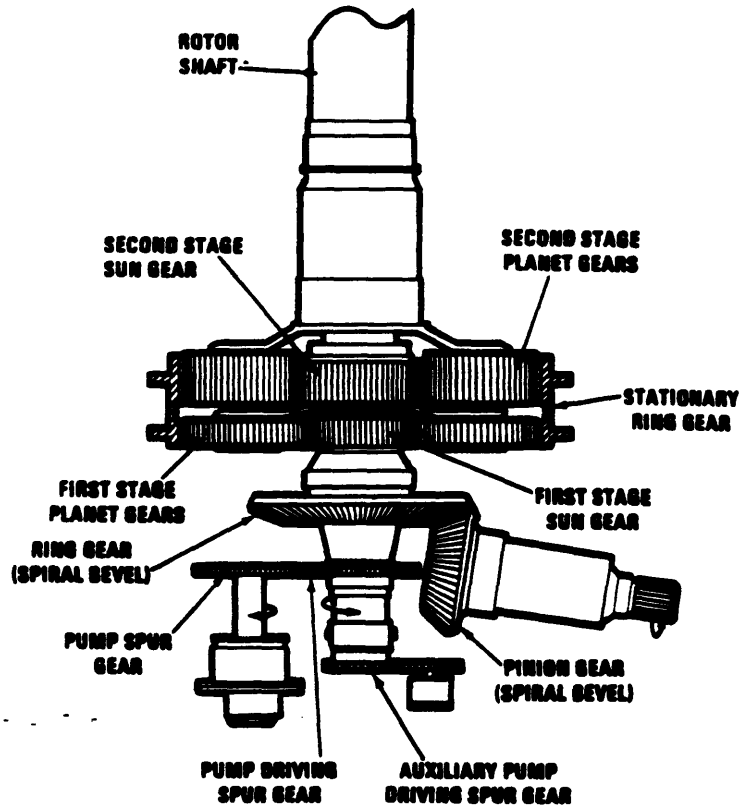

Figure 2-4: Gear System of Forward Transmission (Side View)

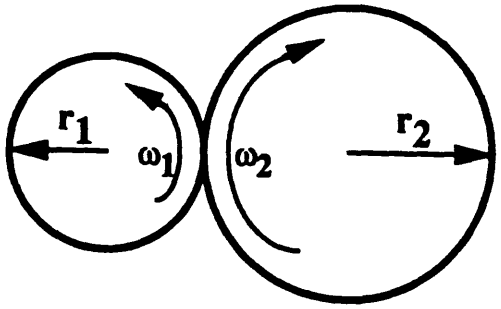

Figure 2-5: Two Interlocking Gears

the gear, the gear teeth must be the same size on both gears. Therefore, the number of teeth on any gear is proportional to its circumference, and thus its radius. So, for the simple 2-gear diagram shown in Figure 2-5,

$$\frac{\omega_1}{\omega_2} = \frac{r_2}{r_1} \tag{2.1}$$

where ω is the rotational speed (angular velocity) of the gear, and r is the radius of the gear. However, a planet-sun combination is considerably more complex. The formulas can be derived from Figure 2-6, which is an overhead view of a single planetary gear stage with four planets.

Here, the subscript $_s$ denotes the sun gear for the stage, and $_p$ represents any of the planetary gears, while $_c$ denotes the carrier. A subscript $_r$ denotes the surrounding ring gear, which remains stationary. With r and ω representing the radius and gear-fixed rotational speed (angular velocity), respectively, for the appropriate gear, the following equations describe the operation of the sun-planet gear system. First, because the ring gear is stationary, the sun will cause the planet gear's edge to move. For an instant in time, the movement can be considered linear, and the center of the gear moves exactly half as far as the inner point (touching the sun gear) of the gear because the outer point's location is fixed by the ring gear. Equation (2.1) can be

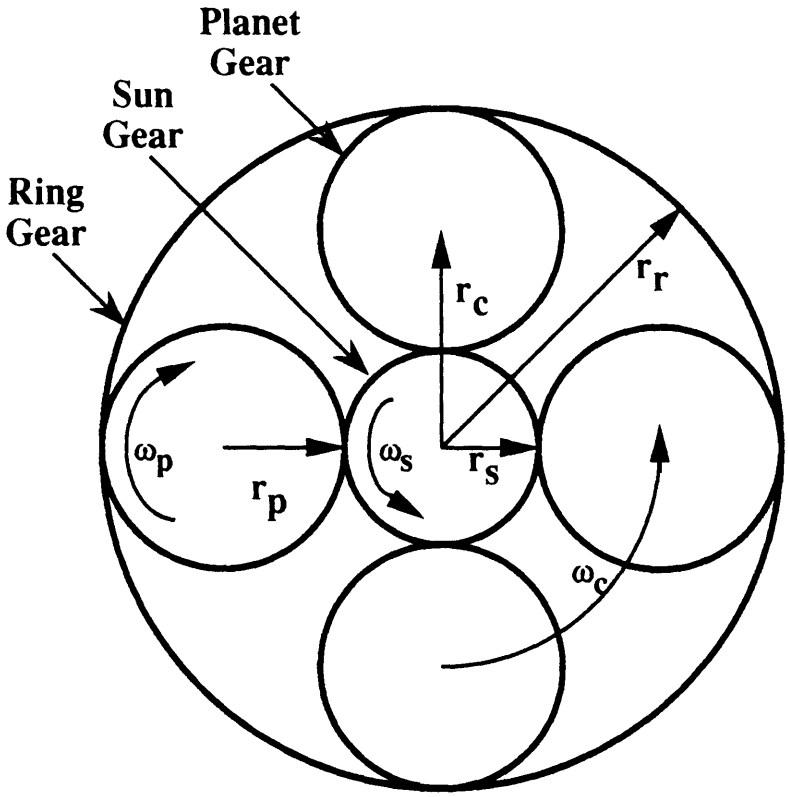

Figure 2-6: Overhead View of a Typical Planetary Gear System

altered to take this into account, resulting in

$$\frac{\omega_c}{\omega_s} = \frac{r_s}{2r_c}. \tag{2.2}$$

Next, consider the planet gear's rotation relative to its neighboring gears[5]. In one full orbit about the sun gear, the number of teeth that come into contact with the ring gear must be equal to the number of teeth on the ring gear. Thus, the planet gear must rotate at a speed that is proportional to the carrier rotation rate, as well as the radius (i.e., number of teeth) of the ring gear. Furthermore, its rotation rate for a given carrier speed must be inversely proportional to its own radius, so that

$$\frac{\omega_p}{\omega_c} = \frac{r_r}{r_p}. \tag{2.3}$$

Next, the ratio of a planetary gear to its adjacent sun gear can be found by multiplying (2.2) with (2.3) to produce

$$\frac{\omega_p}{\omega_s} = \frac{r_r r_s}{2r_c r_p}. \tag{2.4}$$

It is clear from Figure 2-6 that the radius of the stationary ring gear is equal to the radius of the sun gear plus the diameter of the planet gear,

$$r_r = 2r_p + r_s, \tag{2.5}$$

and similarly, the radius of the carrier is equal to the radius of the sun gear plus the radius of the planet gear,

$$r_c = r_p + r_s, \tag{2.6}$$

[5]Due to the translation of the planet gear, its measured rotation rate depends on whether an inertially fixed coordinate frame or a frame fixed to the gear itself is used. The gear-fixed coordinate frame should be used to determine ω, because that is the rotation rate that is used to determine the gear's mesh frequency. Because of this, the gear-fixed coordinate frame is used for the rotation rate derivations.

Gear Description	No. of Teeth	Nominal Rotation Rate RPM	Hertz
Drive Shaft	29	6911.85	115.1975
Spiral Bevel Gear	51	3930.27	65.5045
Lower Stage Sun	28	3930.27	65.5045
Lower Stage Fixed Ring Gear	106	-	-
Lower Stage Planet Gears	39	2232.12	37.2019
Upper Stage Sun (Lower Carrier)	40	821.250	13.6875
Upper Stage Planet Gears	33	722.727	12.0455
Main Rotor (Upper Carrier)	-	225.000	3.75000

Table 2.2: Teeth Per Gear and Rotation Rates of Forward Transmission Gearbox

so that substituting (2.5) and (2.6) into (2.4) results in

$$\frac{\omega_p}{\omega_s} = r_s \frac{2r_p + r_s}{2r_p(r_p + r_s)}. \tag{2.7}$$

Using equations (2.1), (2.7), and the number of teeth on each gear, the nominal angular velocity of all the gears in the transmission can be found from the 225 RPM nominal rotation rate of the rotor. Table 2.2 shows the nominal rotation speeds of each gear in the forward transmission in RPM and Hz, as calculated from the geometry of the transmission's dual-planetary gear system.

2.2.2 Primary Offending Gear Mesh Frequencies

Now that the rotation rates of the gears in the gearbox have been determined, the next step is to calculate the gear mesh frequencies for each of the gears. For two rotating gears, the gear mesh frequency f is the product of the rotational speed of the gear relative to the other gear ω and the number of teeth on that gear n:

$$f = n\omega. \tag{2.8}$$

It is important that ω represent the relative angular velocity, as the ring and planetary gears are meshing with one another and must have equal gear mesh frequencies. The inertially-fixed rotation rate of the ring gear is zero, which would imply a gear mesh

frequency of zero, a clearly incorrect result. However, if the gear-fixed rotation rate is used (in this case, the planet gears are moving at ω_c with respect to the ring gear), then the gear mesh frequency matches that of the planet. Thus, with ω representing the gear-fixed rotation rate of the gear, the gear mesh frequencies of the planet, ring, and sun gears in any planetary gear system can be calculated with the following equations:

$$f_p = r_p \omega_p \tag{2.9}$$

$$f_r = r_r \omega_c \tag{2.10}$$

$$f_s = \omega_s \frac{r_s(2r_p + r_s)}{2(r_s + r_p)}. \tag{2.11}$$

Using Equation 2.8 and the data in Table 2.2, the gear mesh frequencies of the forward transmission were calculated and are shown in Table 2.3. The frequencies in this table can be compared with the spectrum of Figure 2-1, which showed a large spike near 1450 Hz. This is clearly a result of the lower planetary gear meshing, which has a mesh frequency of 1450.875 Hz for a nominal rotation speed. Furthermore, the first harmonic of this frequency is 2901.75 Hz, which is the location of another noise spike. Therefore, the noise spikes present in the CH-47D cockpit are a result of the fundamental and harmonic frequencies of the forward transmission's gear mesh frequencies. Continuing this analysis for all of the large peaks in Figure 2-1 identifies the primary frequency spikes shown in Table 2.4. Note that these frequencies are based on the nominal rotation rate of the transmission, and will change as the speed of the gearbox varies.

2.2.3 Prevalent Harmonics

However, these frequencies do not encompass all of the frequency spikes shown in the previous spectra. The primary frequencies were sidebanded with other frequencies, as examined earlier in Figure 2-2. For this figure, the sidebands were found to exist near the frequencies of the center frequency $\pm 13.5n$ Hz where $1 \leq n \leq 4$. Because

Gear Mesh Description	Frequency, Hz
Spiral Bevel Gear	3340.728
Lower Stage Sun/Planet/Ring	1450.875
Upper Stage Sun/Planet/Ring	397.5000

Table 2.3: Fundamental Gear Mesh Frequencies of Forward Transmission Gearbox for Nominal Rotation Rate

Gear Mesh Description	Frequency, Hz
Upper Planet Fundamental	397.5
Upper Planet First Harmonic	795
Upper Planet Second Harmonic	1192.5
Lower Planet Fundamental	1450.875
Upper Planet Third Harmonic	1590
Upper Planet Fourth Harmonic	1987.5
Upper Planet Fifth Harmonic	2385
Lower Planet First Harmonic	2901.75
Spiral Bevel Fundamental	3340.728
Lower Planet Second Harmonic	4352.625

Table 2.4: Nominal Gear Mesh Frequencies and Harmonics of Forward Tranmission

these sidebands are equally spaced, it is likely that they are the result of harmonics of a fundamental frequency of about 13.5 Hz. Therefore, a physical source that could generate this frequency is sought. This frequency is clearly not present in Table 2.3, but a very likely candidate is the 13.6875 Hz nominal rotation rate of the lower carrier (which is the same as the upper stage sun rotation rate) in Table 2.2. Performing the same analysis for the other primary noise spikes, it is apparent that the lower stage gear mesh frequencies (spiral bevel fundamental, lower planet fundamental, and their harmonics) are sidebanded with the lower carrier rotation rate and its harmonics. Similarly, the upper stage gear mesh frequencies (upper planet fundamental and its harmonics) are sidebanded with the upper carrier rotation rate and its harmonics. Throughout the rest of this document, the fundamental frequencies of important gears will be denoted by xxF, where F stands for the fundamental frequency, and xx denotes the Spiral Bevel (SB), Lower Planet (LP), or Upper Planet (UP) gear mesh frequency, or the Lower Carrier (LC) or Upper Carrier (UC) rotation rate. Harmonic frequencies will be noted by a number followed by the letter H, such that LP1H is the lower planetary first harmonic frequency of 2(1450.875) = 2901.75 Hz.

Thus, the spikes that appear prominently in Figure 2-2 can be referred to as LPF$\pm$LCnF Hz where $0 \leq n \leq 3$. Note that the noise spikes appear at regular intervals, but their magnitude diminshes rapidly as n increases beyond three. More significantly, the loudest noise spikes in the figure occur when $n = 3$, followed by $n = 0$, and $n = 1$. The odd multiples of the carrier frequencies (even harmonics) have substantially smaller magnitudes. This analysis in agreement with experiments performed by Boeing, where the whole forward transmission has been found to vibrate at the LCF and its harmonics. However, it is not known why the third harmonic of the LCF tends to create the highest amplitude sidebands, although it could be attributed to the fact that there are four lower stage planet gears[2][6]. Previous analyses of this

[6]If a manufacturing defect or case mounting caused a bulge in the ring gear, every time a planet gear passed this bulge, additional vibrations would be induced in the transmission. In the case of the lower planet configuration, which has four planet gears, it would then make sense that the fourth harmonic of the carrier frequency (the rate at which the lower planetary gears would be passing the bulge) would cause the greatest disturbance.

phenomenon have concentrated on the resonant frequencies of the gearbox casing, under the premise that excitation near a resonant frequency would result in large oscillations[7].

2.3 Reduction Goal

Based upon this analysis, it is desired to reduce the peaks caused by the forward transmission gear meshing to or below the level of the surrounding background noise. For most of the noise spikes, this will require a reduction of at least 20 dB, and almost 30 dB for the LPF and SBF frequencies. The spikes appear to have a bandwidth of less than 2 Hz[8]; this implies that a very narrowband notch filter may be used. Ranking the relative magnitude of the noise spikes from loudest to quietest creates a prioritized list of the frequencies to be attacked. Then, the system can be designed to accomodate as many peaks as feasible, until the limits of sampling frequency and processing time are reached, or all the desired frequencies have been attenuated. The prominent noise spikes, ranked roughly loudest to quietest, are shown in Table 2.5[9].

2.3.1 Rotation Rate Variance Characterization

Ideally, the rotors of a helicopter turn at a constant rate at all times during flight. However, the forces on the rotor blades change as the helicopter undergoes maneuvers and experiences wind gusts. This change in force on the rotors causes the speed of the

[7]It is interesting to note that the loudest sidebands on the helicopter are not the same as the loudest for a ground-based transmission test stand. Data from the test stand indicates that the loudest sidebands should occur at ± the UC1H frequency; half of the UC3H. This discrepancy has not been explained.

[8]Any frequency spectrum's resolution is limited by the number of points at which the spectrum was calculated. As such, it is impossible to determine the exact bandwidth of the noise spikes. To calculate the spectrum at more points requires a longer sampling of the input signal, and with noise spikes that change frequency, increasing the sample time decreases the accuracy of the noise spike locations. Theoretically, a gear mesh frequency is just that, a single frequency, and the noise spikes should have infinitessimal bandwidth. Of course, this is not practical, and a finite bandwidth is chosen in order to allow for limitations in the frequency analysis methods.

[9]The magnitude of the spikes vary over time as well, so this table should only be used as a guide. It is an approximate ranking based on the average spike magnitudes observed for one particular helicopter.

No.	Gear Mesh Source	Nominal Frequencies, Hz
1,2	LPF ± LC3H	1396.125, 1505.625
3	LPF	1450.875
4	SBF	3340.728
5,6	SBF ± LC3H	3285.978, 3395.478
7,8	UP1H ± UC1H	787.5, 802.5
9,10	UP1H ± UCF	791.25, 798.5
11	UPF	397.5
12,13	UP3H ± UC3H	1575, 1605
14,15	UP3H ± UC1H	1582.5, 1597.5
16,17	UP2H ± UC3H	1177.5, 1207.5
18,19	UP2H ± UC1H	1185, 1200
20,21	LPF ± LC1H	1423.5, 1478.25
22,23	LP1H ± LC3H	2847, 2956.5
24	LP1H	2901
25,26	SBF ± LC1H	3313.353, 3368.103
27,28	LPF ± LCF	1437.189, 1464.563
29,30	LPF ± LC2H	1409.813, 1491.938
31	UP4H	1987.5
32	UP5H	2385
33	LC2H	4352.535

Table 2.5: List of Noise Spikes, Approximate Decreasing Amplitude

rotors (and thus all connecting drive shafts and gears) to vary as well. This variance is minimized in the CH-47 by a speed regulator which attempts to keep the rotational rate of all components constant. However, there is obviously a time lag in this system due to inertial effects and the inherent time constant of any control system. Therefore, the rotation rate of the planetary gear system, and thus the frequencies of the noise spikes, vary over time during the flight. If the noise reduction system is to attack the precise location of the narrowband noise, the rotational speed of the transmission must be known accurately in real time. Furthermore, the bounds of this variance have to be determined in order for the suppression system to accomodate the full range of frequencies it may encounter, and the rate of change is needed to ensure that the system will respond quickly enough to track those changes.

There are two speed regulator systems currently in use on CH-47s. The older regulator (a mechanical governor) is not as effective as the newer Full Authority Digital Engine Controller (FADEC) in maintaining a constant rotation speed. Thus, if the noise suppression system works for the older regulator, it will also work for the newer regulator. Furthermore, most of the CH-47s currently in service do not have the FADEC system, so designing a noise reduction scheme around the FADEC controller provides a system that cannot necessarily be used on helicopters with the older regulator. Therefore, the noise reduction schemes will attempt to suppress noise spikes with the wider and more rapid frequency variations that occur with the older regulator.

The range and rate of rotation speed variance was determined from data recorded by flight test engineers during testing of various CH-47s. If the noise reduction scheme is to handle the most severe variances, then it must be able to suppress the noise spikes during violent maneuvers such as jump takeoffs[10] with a heavily-loaded helicopter. Strip chart records were obtained from Boeing for various helicopters and operating scenarios. Maximum deviations and maximum deviation rates were measured from

[10]A jump takeoff occurs when the helicopter is sitting on the ground, and the pilot pulls up on the collective as quickly as possible. This essentially provides a step input to the pitch of the rotor blades, inducing a great deal of drag and slowing the rotation rate substantially. Under powered flight conditions, this manuever has the most extreme effect on the transmission rotation speed.

the records in order to determine the bandwidth and reaction time regimes, respectively, required of the noise suppression system. A typical strip chart of rotor RPM during a jump takeoff is shown in Figure 2-7. Using graphs similar to these, the maximum experimental deviations from nominal rotation rate (100%) were −9% and 5%. Furthermore, the maximum slope measured was about 14% per second. While this rate variance is indicative of the maximum rate of change that could be expected in normal combat operation, maximum deviation amounts are perhaps better determined from the Operating Limits and Restrictions sections of the CH-47 Operator's Manual. This manual lists the minimum transient rotor rate as 91% of nominal, and the maximum transient rotor rate as 106% of nominal. For reference, the minimum allowable sustained rate is 96% and the maximum allowable sustained rate is 102%. Therefore, the noise suppresion system must be able to handle rotation speeds from 91% to 106% of nominal, at a maximum rate variation of 14% per second[11]. This implies that the notch filter for the LPF noise spike at 1450.875 Hz must be able to suppress frequencies ranging from at about 1320 to 1538 Hz, and must be able to change its center frequency by 203 Hz in one second. The actual range and movement rates of the filter will have to be somewhat higher when measurement and implementation errors are considered, as well as the finite update rate of the system (see section 3.6). Note that it is practically impossible to design traditional filters to suppress this kind of noise, without significantly affecting a large portion of the frequency spectrum. However, certain DSP algorithms can implement adaptive filters with these capabilities.

[11] A CH-47D pilot felt that jump takeoffs were extremely rare events, and that the system should be designed to handle variations from about 95% to 108%, to include autorotation conditions, and a rate variation of less than 10% per second[27].

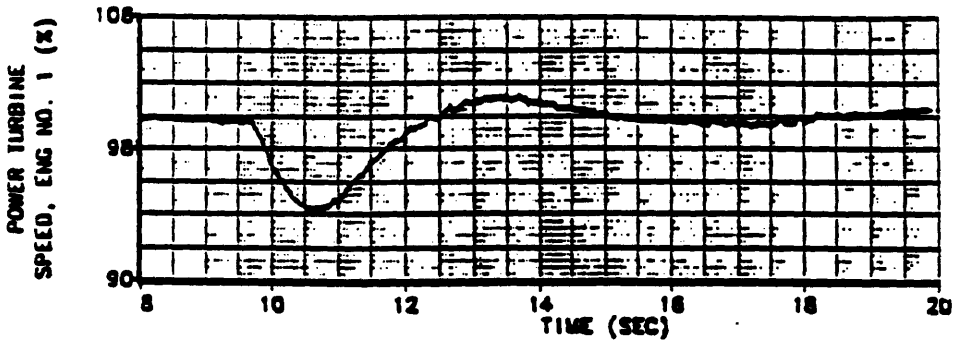

Figure 2-7: Strip Chart Record of Transmission Rotation Rate During Jump Takeoff

Chapter 3

Proposed Solutions

As described in section 2.2.3, a large percentage of the sound power present in the CH-47 cockpit and interphone signal is contained in a few very narrowband frequency ranges. If these frequency ranges could be suppressed or filtered, then a substantial amount of the noise power could be reduced, without greatly affecting the power of broadband speech signals. Applying such a filter to the cockpit interphone system could enhance the signal-to-noise ratio, and therefore increase the intelligibility of the voice signal.

This chapter describes the three algorithms used to attack the gear whine frequencies of the forward transmission: the ANC algorithm (specifically, its LMS implementation), the TF algorithm, and the VSR algorithm. An explanation of the ideas behind each algorithm is presented first, as an introduction to the techniques. After the introductions, the algorithms are analyzed in more detail. The VSR utilizes an entirely different approach than the other two algorithms, so it is treated separately at the end of this chapter, in section 3.5. However, the LMS and TF algorithms are different utilizations of the same core algorithm, the Modulate-Filter-Demodulate (MFD) algorithm. Thus, the MFD algorithm is analyzed in section 3.2, as a prelude to the analyses in sections 3.3 and 3.4.

3.1 Introduction to the Noise Suppression Algorithms

The following three sections introduce the algorithms studied in this project. The ideas behind the algorithms are explained without formula derivations or diagrams, so that the motivations for the algorithms can be described. More formal analyses appear in the subsequent sections.

3.1.1 LMS ANC Algorithm

The LMS algorithm is an elegant means of implementing a notch filter. It multiplies the input signal with a sinusoidal signal of frequency ω_0 in order to determine if the input has a component at that frequency. If it does, then the two signals will be at least partially correlated, and the result of the multiplication will have a nonzero DC component, due to the constant phase difference between the two signals. If the input signal is uncorrelated with the sinusoid, the phase difference is essentially random, and the multiplication results in an output with a DC value that is very close to zero. Thus, the DC component of the product is a measure of the input signal's power content at the frequency ω_0.

The result of the multiplication is then integrated, to obtain a time history of the DC components of the product, and then subtracted from the input signal. Thus, the sinusoidal components of the input at the frequency ω_0 are not present in the system's output. The effect of this integration is to adapt to the frequency content of the input signal, so that the output is always missing the sinusoidal component. If the same procedure is used with a cosinusoidal input of frequency ω_0 as well, then the sinusoidal and cosinusoidal components of the input signal are removed, and the output is completely devoid of the frequency ω_0. Such an implementation has the characteristics of a notch filter placed at the frequency ω_0.

The constant of integration controls how quickly the system adapts to changes in the frequency content of the input signal, and thus determines the bandwidth of

the notch filter. The higher the integration constant, the faster the system responds, and the wider the notch's bandwidth. Perhaps the most powerful aspect of the LMS algorithm, however, is the fact that the notch filter's frequency is controlled by the frequencies of the sinusoidal and cosinusoidal signals. The frequencies of these signals can be changed to control the frequency of the notch filter in real time. Thus, the LMS algorithm can be used isolate a particular component of a signal, even if that component varies in frequency.

3.1.2 TF Algorithm

This algorithm is not quite as intuitive as the LMS algorithm, although it can be understood using frequency domain explanations. Consider the frequency spectrum of an input signal to a discrete-time system. If a notch filter is to be implemented at a frequency ω_0, the frequencies near ω_0 need to be isolated. This can be accomplished by convolving the frequency spectrum of the input with impulses located at $\pm\omega_0$ and lowpass filtering the result. The convolution moves the frequencies near ω_0 to the origin, and lowpass filtereing subsequently removes frequencies that are not near the origin. Convolving once again with the impulses at $\pm\omega_0$ maps the remaining frequency spectrum back out to $\pm\omega_0$. The result is the equivalent of a bandpass filter at ω_0. Then, a bandstop filter can be realized by subtracting this signal from the original input, removing the frequency content of the input signal near the frequency ω_0.

Because convolution in the frequency domain is the same as multiplication in the time domain, this system can be implemented by multiplying the input by a sine or cosine signal of frequency ω_0, lowpass filtering the result, and multiplying once again by the sine or cosine signal. Multiplication with both sine and cosine signals must be performed in order to prevent aliasing that would otherwise result from mapping different frequencies to the same region in the frequency spectrum. So, the complete algorithm involves multiplying the input by sine and cosine signals of frequency ω_0, lowpass filtering the results, multiplying again by the sine and cosine signals, summing the products of the multiplications, and subtracting the result from the input signal.

This is precisely the idea behind the TF algorithm, where a narrowband lowpass filter is used to create a narrowband bandstop filter. When a signal is multiplied by a sine and cosine signal at the same frequencies, it is often said to be modulated, so the core part of the TF algorithm involves a Modulate-Filter-Demodulate procedure, called the MFD algorithm (the summation of the sine and cosine paths is assumed). This algorithm, like the LMS algorithm, implements a narrow bandstop filter centered at the modulation frequency ω_0. If the lowpass filter is designed without a passband, then the TF algorithm implements a notch filter. As with the LMS algorithm, the center frequency of the notch can be controlled by changing the frequencies of the sine and cosine modulation signals.

3.1.3 VSR Algorithm

The VSR algorithm utilizes an approach very different from that of the LMS and TF algorithms to obtain adaptive filters. It utilizes the properties of discrete-time systems to obtain a notch filter with a controllable center frequency. Because all the frequencies of a digital system are proportional to the sampling rate of the system, changing the sample rate of the system changes its frequency response. Therefore, if a digital notch filter is implemented at frequency ω_0 assuming a sample rate of 12 kHz, then if the sample rate is changed to 13 kHz, the frequency of the filter will move to $\frac{13}{12}\omega_0$. Therefore, the VSR algorithm controls the center frequency of the notch filter by changing the sampling rate of the digital system.

3.2 Modulate-Filter-Demodulate Algorithm

First, the effects of the Modulate-Filter-Demodulate[1] algorithm are examined, whose signals will be denoted by the subscript $_{MFD}$. This algorithm forms the key parts of the LMS ANC and TF algorithms, and its block diagram is shown in Figure 3-1. The input is modulated by both a cosine signal (upper path) and a sine signal (lower

[1]See section 3.1.2 for a description of this algorithm's operation.

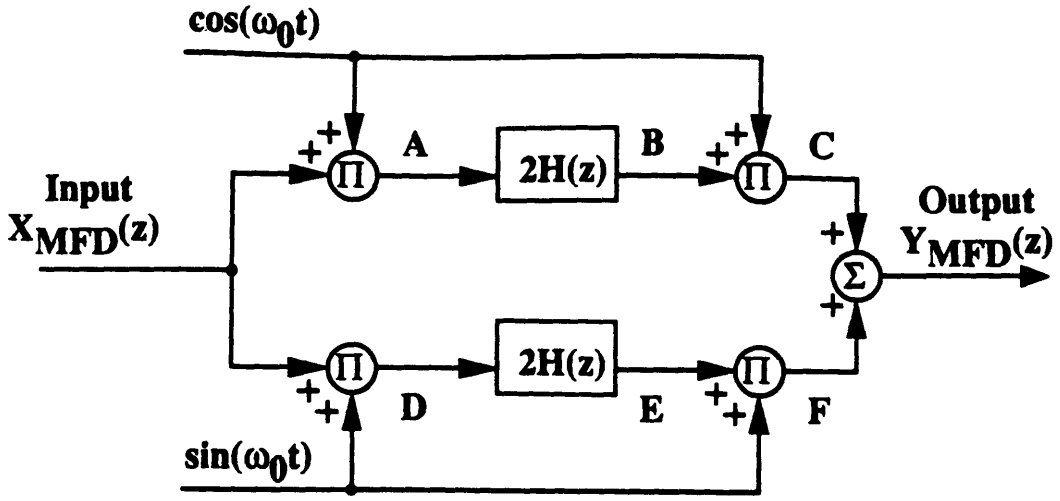

Figure 3-1: Block Diagram of the Modulate-Filter-Demodulate (MFD) Algorithm

path) of frequency ω_0. Then, the signal is passed through identical transfer functions (lowpass filters in the case of the TF algorithm) with a gain of two to account for the modulation's gain of $\frac{1}{2}$. The signals are then demodulated and summed, producing the output. This is clearly a nonlinear system, due to the quadrature modulation. However, if ω_0 is kept constant, the MFD algorithm behaves as a linear, time-invariant (LTI) system[28]. Therefore, standard z-transform analysis applies, and a transfer function may be found for the system. The analysis of the upper and lower paths are very similar (differing only by the $\frac{-1}{j}$ term of the sinusoid's Fourier transform), so only the analysis of the upper path is presented in detail. The input to the MFD algorithm is modulated with a cosine signal of frequency ω_0, whose z-transform is

$$Z(\cos\omega_0) = \frac{e^{-j\omega_0} + e^{j\omega_0}}{2}. \tag{3.1}$$

Thus, given an input of x_n with a z-transform $X_{MFD}(z)$, the z-transform of the modulated signal at A is

$$A(z) = \frac{1}{2}[X_{MFD}(ze^{-j\omega_0}) + X_{MFD}(ze^{j\omega_0})]. \tag{3.2}$$

This signal is filtered by $2H(z)$, which results in the signal at B,

$$B(z) = 2A(z)H(z), \tag{3.3}$$

and demodulated by the same cosine signal. Thus, the output of the cosine-modulated path at C is described by

$$C(z) = \frac{1}{2}[B(ze^{-j\omega_0}) + B(ze^{j\omega_0})]. \tag{3.4}$$

To solve for $C(z)$ in terms of the input, (3.3) is substituted into (3.4), giving

$$C(z) = \frac{1}{2}[2A(ze^{-j\omega_0})H(ze^{-j\omega_0}) + 2A(ze^{j\omega_0})H(ze^{j\omega_0})]. \tag{3.5}$$

Then, substituting (3.2) into (3.5) and combining terms produces

$$\begin{aligned} C(z) \;= \tfrac{1}{2} \;& \Big\{H(ze^{-j\omega_0})[X_{MFD}(ze^{-2j\omega_0}) + X_{MFD}(z)] + \\ & H(ze^{j\omega_0})[X_{MFD}(z) + X_{MFD}(ze^{2j\omega_0})]\Big\}, \end{aligned} \tag{3.6}$$

which is the z-transform of the input after it has travelled through the upper half (cosine-modulated path) of the MFD algorithm. The z-transform of the input after passing through the lower, sine-modulated path (at point F) can be determined in a similar manner, yielding

$$\begin{aligned} F(z) \;= \tfrac{-1}{2} \;& \Big\{H(ze^{-j\omega_0})[X_{MFD}(ze^{-2j\omega_0}) - X_{MFD}(z)] + \\ & H(ze^{j\omega_0})[X_{MFD}(ze^{2j\omega_0}) - X_{MFD}(z)]\Big\}. \end{aligned} \tag{3.7}$$

The output of the MFD block is described by

$$Y_{MFD}(z) = C(z) + F(z), \tag{3.8}$$

and combining (3.6) and (3.7) into (3.8) and simplifying gives the output in terms of

the input,

$$Y_{MFD}(z) = X_{MFD}(z)[H(ze^{-j\omega_0}) + H(ze^{j\omega_0})], \tag{3.9}$$

which implies an overall transfer function of

$$\frac{Y_{MFD}(z)}{X_{MFD}(z)} = G_{MFD}(z) = H(ze^{-j\omega_0}) + H(ze^{j\omega_0}). \tag{3.10}$$

Thus, when ω_0 is constant, the effect of the MFD algorithm is to apply the transfer function $H(z)$ (normally centered at the origin) centered at the frequencies $+\omega_0$ and $-\omega_0$. For example, if $H(z)$ is an ideal lowpass filter with a cutoff frequency of ω_c, the MFD algorithm will act as a bandpass filter centered at frequency ω_0 with a bandwidth equal to twice ω_c. In other words, given an input signal of frequency ω, the output of the MFD algorithm will be be identical to the input at frequencies $\omega_0 - \omega_c < \omega < \omega_0 + \omega_c$, and zero at all other frequencies. If the effects of $H(z)$ are desired at a different frequency, then ω_0 can be changed, and the transfer function will be centered at the new frequency[2]. Thus, the algorithm is ideal for controlling noise with frequencies that change over time. This concept will provide the basis for deriving the transfer functions of the LMS and TF algorithms, which are analyzed in the following sections.

3.3 Least-Mean-Squared Adaptive Noise Cancellation

A common approach to notch filtering, especially when the frequencies to be filtered do not remain constant over time, is known as Adaptive Noise Cancelling. The heart of this algorithm is the use of the MFD algorithm in a feedback loop. A reference signal correlated in an unknown manner with the unwanted noise, but not with the desired signal, is fed into the MFD system, which integrates the correlated components of the two signals. This result is treated as an error signal, which is fed back and

[2]Note that if ω_0 is changed, the system becomes non-LTI, and the derived transfer function is no longer valid.

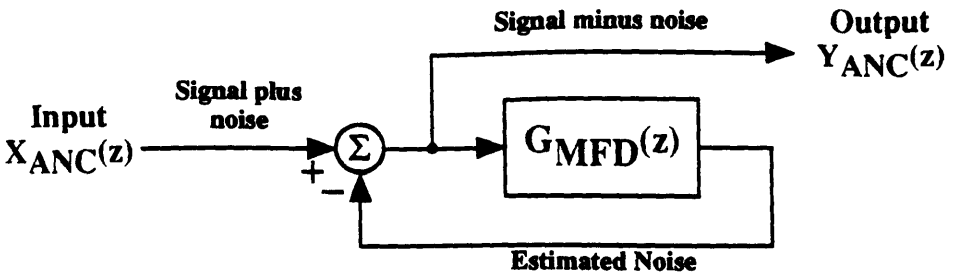

Figure 3-2: Block Diagram of the Adaptive Noise Cancellation Algorithm

subtracted from the input, producing a signal-minus-noise output. This output signal is then used as the input to the MFD algorithm, so that it may determine the amount of the remaining signal that is still correlated with the reference inputs. Thus, the MFD algorithm adapts to changes in the input and reference signals, continually removing the frequencies of the input that are correlated with the reference signals.

If $H(z)$ of the MFD algorithm is the transfer function of a digital integrator, then the ANC algorithm utilizes the LMS approach, and its output power is minimized to its least-mean-square[48]. The LMS ANC algorithm (hereafter referred to as the LMS algorithm) thus converges to a solution which minimizes the signal power according to the spectrum of the reference signals, and once it has converged, it tracks changes in the reference input to keep the output power minimized. This algorithm has several attractive qualities. First, it can be easily expanded in a parallel manner to minimize the signal's frequencies that are correlated with multiple reference signals, rather than just one, as shown in Figure 3-3. Second, the implementation of the LMS algorithm is straightforward and computationally efficient. The core calculations are only five multiplications, four additions, and two memory locations per frequency to be reduced. This algorithm has found widespread use due to its effectiveness, ease of implementation, and minimal computation time requirements.

3.3.1 Transfer Function Derivation

First the transfer function of the ANC algorithm will be derived, and then the specific case of the LMS approach will be examined. The signals of the ANC algorithm will be

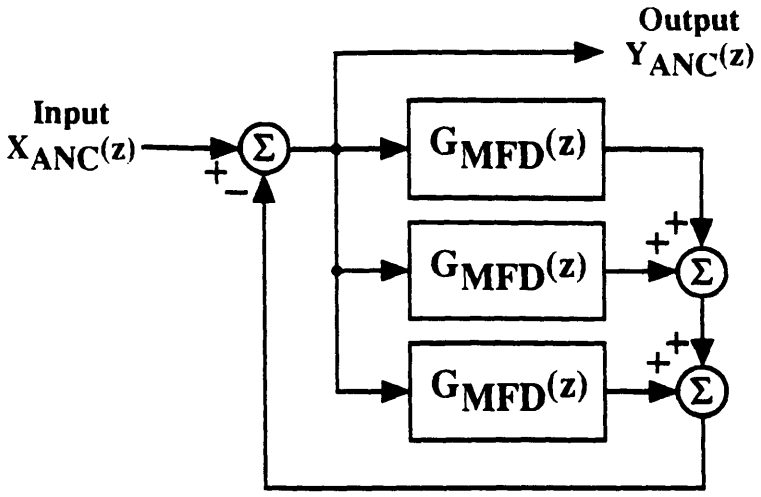

Figure 3-3: Block Diagram of LMS Algorithm for Multiple Notch Filters

denoted by the subscript $_{ANC}$ and its analysis builds upon the earlier derivation of the MFD input-output relations (equation 3.9). Therefore, the following analysis assumes that $G_{MFD}(z)$ is LTI, which is only true when ω_0 is constant. If the z-transforms of the input and output of the ANC algorithm are denoted by $X_{ANC}(z)$ and $Y_{ANC}(z)$, respectively, then the output of the ANC algorithm can be represented by

$$Y_{ANC}(z) = X_{ANC}(z) - Y_{MFD}(z) \tag{3.11}$$

where the input to the MFD part of the ANC algorithm is in fact the output of the ANC algorithm itself,

$$X_{MFD}(z) = Y_{ANC}(z). \tag{3.12}$$

The first step to finding Y_{ANC} in terms of X_{ANC} alone is substituting (3.12) into (3.9), which gives the output of the MFD part of the algorithm in terms of Y_{ANC},

$$Y_{MFD}(z) = Y_{ANC}(z)[H(ze^{-j\omega_0}) + H(ze^{j\omega_0})]. \tag{3.13}$$

Substituting (3.13) into (3.11) results in the output of the ANC algorithm,

$$Y_{ANC}(z) = X_{ANC}(z) - Y_{ANC}(z)[H(ze^{-j\omega_0}) + H(ze^{j\omega_0})], \tag{3.14}$$

and Y_{ANC} and X_{ANC} can be moved to the left-hand side so that the overall transfer function of the ANC algorithm for constant ω_0 is

$$\frac{Y_{ANC}(z)}{X_{ANC}(z)} = G_{ANC}(z) = \frac{1}{1 + H(ze^{-j\omega_0}) + H(ze^{j\omega_0})}. \tag{3.15}$$

Notice that frequency-shifted copies of $H(z)$ (from the MFD algorithm) appear in the denominator. To obtain a notch filter, the magnitude of G_{ANC} should go to zero at ω_0, which can be accomplished if the magnitude of $Hze^{\pm j\omega_0}$ goes to infinity. This occurs if $H(z)$ is an integrator; its magnitude approaches infinity when the input has a DC component. When an integrator is shifted by ω_0, its magnitude goes to infinity if the input has components at that frequency. So, when $H(z)$ is an integrator, then at frequencies near $\pm\omega_0$, the denominator tends towards infinity, and the output of the ANC algorithm appraoches zero. This is, in fact, the theory behind the LMS algorithm, which is analyzed next. For this purpose, let $H(z)$ be a digital integrator with transfer function

$$H(z) = \beta\frac{z^{-1}}{1 - z^{-1}} = \beta\frac{1}{z - 1}, \tag{3.16}$$

where β is the integration constant. Substituting this equation into (3.15) and simplifying results in a transfer function of

$$G_{LMS}(z) = \frac{z^2 - 2z\cos\omega_0 + 1}{z^2 - 2(1 - \beta)z\cos\omega_0 + 1 - 2\beta}, \tag{3.17}$$

which has zeros located on the unit circle at

$$z = e^{\pm j\omega_0} \tag{3.18}$$

and poles placed at

$$z = (1-\beta)\cos\omega_0 \pm \sqrt{(1-\beta)^2\cos^2\omega_0 + 2\beta - 1}. \tag{3.19}$$

Letting $\alpha = 1-\beta$, equation (3.19) can be rewritten as

$$z = \alpha\cos\omega_0 \pm \sqrt{\alpha^2\cos^2\omega_0 + 1 - 2\alpha}. \tag{3.20}$$

This causes the ANC algorithm to act as a notch filter centered at ω_0 whose bandwidth is controlled by α. A pole-zero plot of $G_{LMS}(z)$ for $\omega_0 = \frac{2\pi 1450.875}{16000}$ in the z-plane is shown in Figure 3-4 for $\alpha = .8$. It can be seen that the zeros lie on the unit circle at an angle θ which corresponds to the ratio of the notch's center frequency to the sampling frequency. The poles are located inside the unit circle, near the zeros, but are not located at the same angle. As α is increased, the poles approach the zeros on the unit circle, resulting in a sharper notch (narrower bandwidth). At the limit of α equal to one, the poles lie immediately on top of the zeros, the system becomes marginally stable, and the poles cancel the effects of the zeros, resulting in $G_{LMS}(z) = 1$. Except for this limiting (and physically insignificant) case, note that the depth of the notch is infinite, because the zero is located precisely on the unit circle.

The ability to obtain a notch filter in this manner has several advantages over conventional techniques. First, the bandwidth of the notch is controlled by a single constant, α. Traditional notch filter design requires calculating new coefficients in order to change a filter's bandwidth. Furthermore, the center frequency of this notch filter is controlled by the frequencies of the reference signals, ω_0. Simply altering the frequencies of the sine and cosine signals will change the frequency of the notch. Changing the frequency of a traditional notch filter again requires recalculating the filter's coefficients, a task that is substantially more complex.

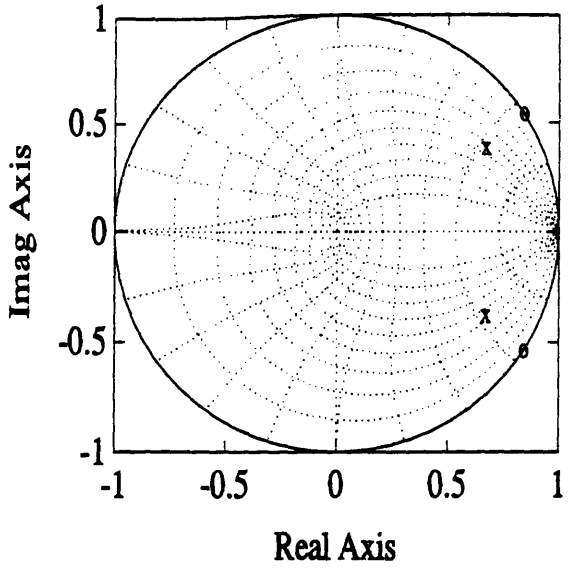

Figure 3-4: Pole-Zero plot of $G_{LMS}(z)$ for $\alpha = .8$

3.3.2 Implementation

There are two implementations of the LMS algorithm that are worth developing. Because the LMS algorithm reduces the signal power according to the frequency content and phase differences of the reference signal, different reference signals will produce different results. The most obvious choice for the reference signals is to use delayed copies of the noise signal as the reference inputs. In the case of CH-47 noise, that requires adding a microphone to the cockpit that registers the ambient noise but not the pilots' voice[3]. The other approach is the notch filtering approach, where a sinusoid and cosinusoid signal at the desired frequency are used; this is the LMS approach that utilizes the MFD algorithm. The theories and constraints of these two approaches are described in the following sections.

[3]Note that, in this case, the transfer function of the LMS algorithm is not represented by Equation 3.17 because the reference inputs are not a sine/cosine pair. Instead, the system response is dependent upon the characteristics of the reference signal. As the cockpit noise is extremely complex, a simple transfer function cannot be derived for this implementation of the LMS algorithm.

Delayed Ambient Noise as Reference Signals

Assuming that the signal from an ambient microphone in the cockpit contains mostly the unwanted noise and little of the desired spoken signal, delayed copies of this signal can be used as reference signals to the LMS algorithm. If a correlation exists between the input and reference signals, the output should be the LMS of the input minus the noise. The potential advantage of this approach lies in the fact that the ambient noise is broad band, and using it as a reference allows the LMS algorithm to attack noise present over a large range of frequencies. However, this can only occur if the phase differences between the input and reference signals are relatively small and do not change substantially over time. If varying phase differences are present, then the signals will not be well correlated and the LMS algorithm will not be efficient at suppressing the noise.

Sinusoids as Reference Signals

When the frequencies of the noise are concentrated in a few well-characterized, narrow bandwidth regions, it is perhaps better to use sine and cosine signals as reference signals for the LMS algorithm. Because the algorithm utilizes phase differences to cancel the noise, the 90 degree phase difference of the reference signals results in a notch filter with infinite attenuation at the frequency of the reference signals. The most significant drawback of this approach is the need to obtain or generate sinusoids at these frequencies. With digital microprocessors, however, it is not difficult to construct accurate sinusoidal signals at multiple frequencies, and this implementation seems well-suited to reduce the nonstationary narrowband noise spikes of the Chinook's forward transmission.

3.3.3 Design Considerations

There are a number of important design considerations to be made when implementing the LMS algorithm. Most of these considerations are tradeoffs between the performance of the system (in terms of reducing the noise without reducing the desired

signal) and ease of implementation (in terms of algorithm complexity and computational requirements). The three primary design decisions for the LMS algorithm are the number of filters to be implemented (i.e., the number of MFD blocks), the type of integrator used, and selection of the speed of convergence.

Number of Filters

The LMS algorithm can be utilized to suppress noise spikes at multiple frequencies. However, each notch requires the generation of a pair of sinusoidal reference signals and uses a two memory locations. The limitation on the number of notches that can be used is primarily a matter of processing speed (although available memory can also be a factor). Each additional notch increases the complexity of the implementation and computation time of the system. Because the CH-47D has numerous noise spikes, it is possible that the algorithm will not be able to attack all of them. As a result, it is important to first apply notch filters to the noise spikes most detrimental to intelligibility. If all of these frequencies can be suppressed and the DSP chip is not utilizing all of its computation time, then filters can be added to suppress the less crucial noise spikes.

Integrator Selection

Selection of the type of integrator is the most basic design criterion of the LMS algorithm. Many different integrators can be used as the $H(z)$ of the MFD block, with different implications for performance and complexity. Using a simple digital integrator (such as that of Equation 3.16) allows an implementation that is computationally efficient, although a more complex integrator may provide better performance in terms of faster convergence, or better notch filter characteristics. For example, if a small width bandstop filter is desired in place of a notch filter, an integrator might be chosen to tailor the pole and zero locations of the LMS transfer function to obtain that kind of frequency response.

Speed of Convergence

The speed of convergence of the LMS algorithm is a parameter that controls how fast the MFD system responds to changes in the reference and input signals. This parameter is tied closely with the integrator selection; for the integrator of the LMS algorithm derived earlier, the integration constant β is the speed of convergence. If the speed is high (fast), then the algorithm will converge quickly and have a short settling time. Unfortunately, the fast convergence will cause the algorithm to respond to frequencies near the reference frequency, resulting in significant attenuation in adjacent bands and increasing the bandwidth of the notch filter. Also, if the convergence speed is extremely high, the LMS algorithm becomes unstable[4]. If the speed is low (slow), then the bandwidth of the notch filter will also be small, because the weights will not respond quickly to other frequencies. However, due to the slower adaptation rate the system will have a larger time constant and will not converge to the LMS solution as quickly. In fact, if variations in the inputs are fast enough, the algorithm may never fully converge.

3.3.4 LMS Algorithm using Ambient Noise as Reference Signals

To determine the potential success of the LMS algorithm with delayed ambient noise as reference inputs, it was modelled in a computer simulation. The simulation used a recording of the cockpit interphone signal as the input, and the reference signals were derived from simultaneous recordings of a microphone added to the cockpit for this purpose[5]. However, the results of the simulation were not promising. The LMS weights did not converge very often, and when they did, the noise reduction in the

[4]Instability in the LMS algorithm occurs when the convergence speed is equal to or exceeds one divided by the largest eigenvalue of the inputs' cross-correlation matrix. As this project is only concerned with the use of narrowband notch filters to attenuate narrowband noise spikes, β remains low and instability of the LMS algorithm is not a concern. The notch filter bandwidth becomes entirely too large for this application long before the system becomes unstable.

[5]The simulation and data recording are described in more detail in the next chapter. However, due to the lack of success with the delayed-noise reference signal approach of the LMS algorithm, its use is not discussed again until the Recommendations section.

interphone signal was not appreciable. This was most likely due to the less than ideal location of the ambient microphone. Because it was not located close to the interphone microphones, the phase of the signals changed over time (especially as the pilots moved their heads), and the phase of the noise in the pilot's interphone signal was completely different from that of the copilot's interphone signal. While better microphone placement or differently tuned algorithms may produce better results, this approach of the LMS algorithm was abandoned for this project due to the time constraints involved and the potential success promised by other techniques[6].

3.3.5 LMS Algorithm using Sinusoidal Reference Signals

As described earlier, using sinusoidal reference signals in the LMS algorithm results in notch filters centered at the frequencies of the reference signals, with a convergence rate and bandwidth controlled by the speed of convergence constant. The number and nominal frequencies of the noise spikes to be attenuated have already been determined, so the remaining design choices are the type of integrator and the bandwidth of the filter. The performance of different integrators was not explored in detail; the simple digital integrator already described provides ample attenuation with minimal computation time, and utilizing more complicated integrators imposes substantial penalties in processing speed. Maximum computation speed is essential for suppressing the large number of noise spikes caused by the CH-47D's forward transmission. The filter bandwidth required to guarantee suppression of the noise spike is determined in section 3.6, and is not discussed here. However, it is useful to examine the ideal frequency responses of the LMS algorithm with several different speeds of convergence (integration constants).

[6]Using an ambient microphone attached directly to each pilots' helmet should provide substantially better phase information than a single microphone placed at one location inside the cockpit. Also, bandpass filtering the reference signal to the frequencies of interest could reduce the overall phase variances in the signals so that better attenuation could be achieved in those bands. However, a substantial challenge still lies in keeping the LMS algorithm converged for each pilot as he or she turns his transmit button on and off. At the very least, a separate system is required for each microphone connected to the interphone system (see section 5.4.4).

Ideal Frequency Response to Constant Frequency

Figure 3-5 shows the ideal Bode response of the LMS system for a constant reference frequency of 1450.875 Hz (the LPF) and integration constants of $\beta = .002$ (solid line), .006 (dashed line), and .015 (dotted line). These values correspond to α values of .998, .994, and .985, respectively. Note that the LMS algorithm achieves an infinute null exactly at the reference frequency, but this is not apparent due to the finite resolution of the frequency response. However, this figure clearly shows how the notch's bandwidth increases as β increases. Also apparent is that the phase angle passes from 180 to -180 degrees at the reference frequency and that the phase deviation at adjacent frequencies also increases with β. Figure 3-6 shows the LMS algorithm with five notch filters (parallel MFD blocks) for constant center frequencies at the lower planetary fundamental frequency, plus and minus two and four times the lower carrier rotational frequency (LPF, LPF$\pm$LC1H, LPF$\pm$-LC3H), again for $\beta = .002$ (solid line), .006 (dashed line), and .015 (dotted line). Note the shapes of the frequency and phase responses between the notch frequencies. At low β, the shapes are practically identical to those seen in Figure 3-5. However, at higher β values, adjacent notches affect one another's performance, resulting in shapes differing from the single-notch response. The frequency response is nearly symmetrical about the frequency that is midway between notches for low β, but becomse very asymmetrical at high β. This is also true of the phase response characteristics between close-proximity notches. An interesting characteristic of the LMS algorithm is that there is always a point of 0 dB attenuation between the notch filters. This is not true of the other algorithms.

3.4 Tracking Notch Filters

The tracking notch filter approach is similar to the LMS algorithm, but instead of using a feedback loop, the MFD algorithm is used in a feedforward manner. The block diagram of the TF algorithm is shown in Figure 3-7, showing how the output of the MFD algorithm is subtracted from the input signal. Thus, if the MFD algorithm isolates the noise in the desired frequency bands, subtracting its output from the input

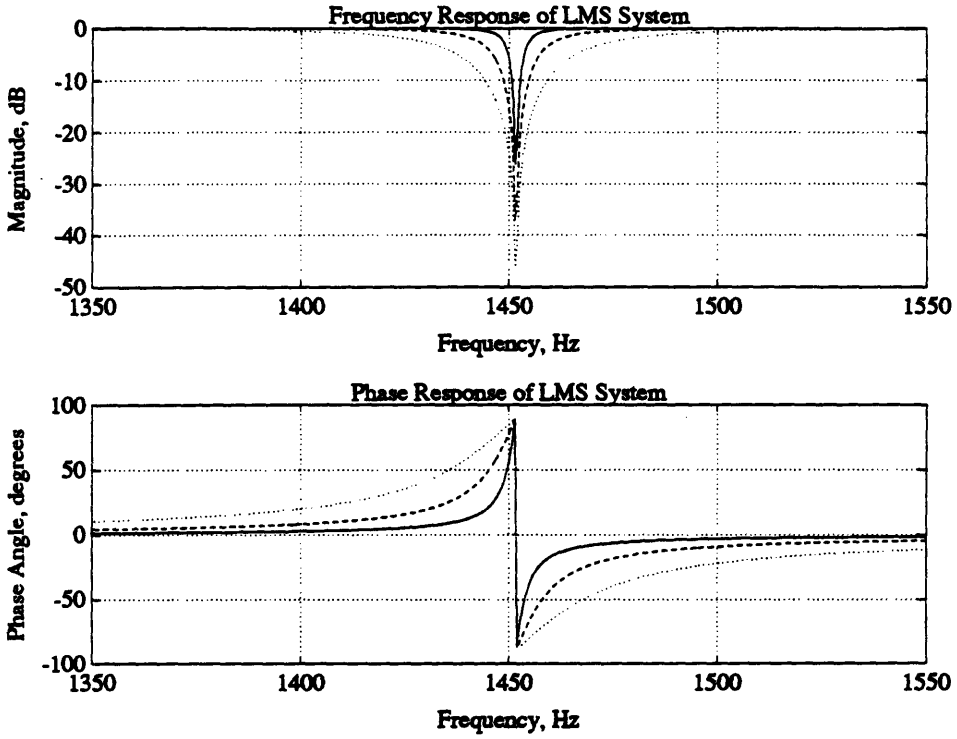

Figure 3-5: Bode Response of One-Notch LMS Algorithm at Constant Frequency

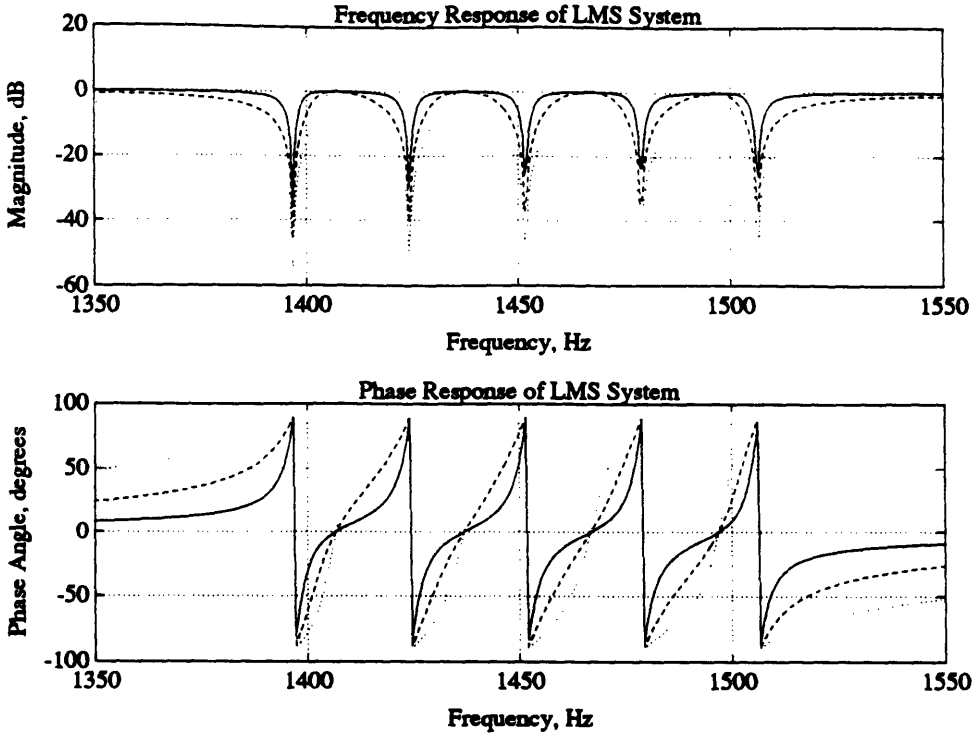

Figure 3-6: Bode Response of Five-Notch LMS Algorithm at Constant Frequency

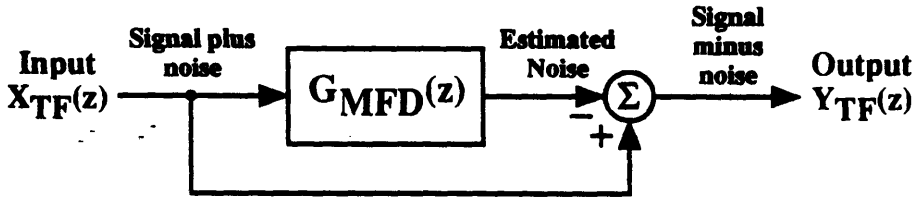

Figure 3-7: Block Diagram of Tracking Filter Algorithm

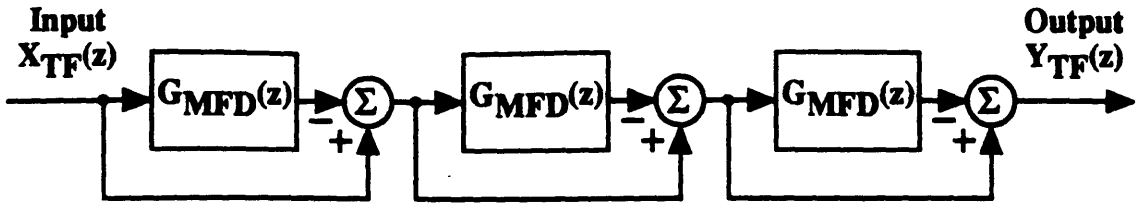

Figure 3-8: Block Diagram of TF Algorithm for Multiple Notch Filters

of the TF system results in a signal-minus-noise output at those frequencies. Like the LMS algorithm, this approach has several advantages over traditional filtering. The center frequency of $H(z)$ is determined by the frequencies of the reference sinusoids, and can be changed in real time. When the TF algorithm is used to implement notch filters, the bandwidth of the notch is controlled by just two related constants. Changing either of these parameters with a traditional filter requires recalculation of the filter's coefficients. Furthermore, multiple notches can be implemented by cascading serial TF blocks, as shown in Figure 3-8. Note that the TF algorithm cannot be used in parallel, as the phase distortions introduced by the lowpass filter will result in different phase delays for each output of the MFD block. Thus, the subsequent summation combines signals of different phase, and the output becomes highly distorted.

While strikingly similar to the LMS algorithm, a few differences are worth noting. First of all, the TF algorithm does not have a feedback component. Furthermore, it does not become unstable, like LMS algorithm can, at very high β (low α). However, it is not as computationally efficient as the LMS algorithm. The input signal must be modulated, filtered, and demodulated for both paths before it is subtracted, requiring at least twelve multiplies, six additions, and four memory locations for each notch filter[7].

[7]These requirements assume that $H(z)$ is a second order IIR filter block. Depending on the exact $H(z)$ used, more memory and/or calculations may be necessary.

3.4.1 Transfer Function Derivation

The transfer function of the TF algorithm is derived using the input-output relation of the MFD algorithm, equation 3.9. The signals in the TF algorithm will be denoted by the subscript $_{TF}$. Assuming that the input and output of the TF algorithm in the z-domain can be represented by $X_{TF}(z)$ and $Y_{TF}(z)$, respectively, and that ω_0 is constant (guaranteeing that the MFD algorithm behaves as an LTI system), the output of the TF algorithm is defined by

$$Y_{TF}(z) = X_{TF}(z) - Y_{MFD}(z) \tag{3.21}$$

and in this case, the input of the MFD algorithm is identical to the input of the TF algorithm

$$X_{TF}(z) = X_{MFD}(z), \tag{3.22}$$

so substituting (3.22) and (3.9) into (3.21) results in the output of the TF algorithm in terms of the input

$$Y_{TF}(z) = X_{TF}(z)[1 - H(ze^{-j\omega_0}) - H(ze^{j\omega_0})]. \tag{3.23}$$

Moving the input to the left hand side of the equation, the overall transfer function of the TF algorithm for constant ω_0 is

$$G_{TF}(z) = \frac{Y_{TF}(z)}{X_{TF}(z)} = 1 - H(ze^{-j\omega_0}) - H(ze^{j\omega_0}). \tag{3.24}$$

It is easy to see that the output of the TF algorithm is the input minus the frequency response of $H(z)$, shifted left and right by the frequency ω_0. Thus, when $H(z)$ is an ideal lowpass filter with cutoff frequency ω_c, the output of the tracking filter algorithm will be identical to the input at all frequencies ω except for $\omega_0 - \omega_c < \omega < \omega_0 + \omega_c$, where the output will be zero. The TF algorithm is now examined for a specific case of $H(z)$, a second-order infinite-impulse response lowpass filter. The

transfer function of such a filter in the z-domain is

$$H(z) = (1-\alpha)\frac{1}{1-\alpha z^{-1}} = (1-\alpha)\frac{z}{z-\alpha}. \tag{3.25}$$

Substituting this function into equation (3.24) and simplifying leads to

$$G_{TF}(z) = \frac{(2\alpha-1)z^2 - 2\alpha^2 z\cos\omega_0 + \alpha^2}{z^2 - 2\alpha z\cos\omega_0 + \alpha^2} \tag{3.26}$$

which has poles at

$$z = \alpha e^{\pm j\omega_0} \tag{3.27}$$

and zeros at

$$z = \alpha^2(1-2\alpha)\cos\omega_0 \pm \alpha\sqrt{\alpha^2\cos^2\omega_0 - 4\alpha^2 + 2\alpha}. \tag{3.28}$$

A pole-zero plot of $G_{TF}(z)$ with $\omega_0 = \frac{2\pi 1450.875}{16000}$ in the z-plane is shown in Figure 3-9 for $\alpha = .8$. Compare this plot with the one shown for the LMS algorithm in Figure 3-4. In this case, it is the poles that are located at the angle θ, not the zeros. In fact, the zeros are outside of the unit circle. This reduces their effect on the system's frequency response, which is evaluated on the unit circle. In the limiting case of $\alpha = 1$, the notch approaches an infinite null as the zeros move toward the unit circle, but once again the poles also converge to the same location. Just as in the LMS algorithm, as α approaches one, the poles move closer to the zeros, resulting in a notch with a narrower bandwidth. Therefore, the fact that the zeros are outside the unit circle imply that, for the same α, the TF system should have a slightly wider notch than the LMS algorithm.

3.4.2 Design Considerations

As with the LMS algorithm, some design tradeoffs must be made when implementing the TF algorithm. These implementation considerations are mostly choices between performance and complexity, trading off the filter's characteristics against ease of implementation and processing time. The two primary design decisions are the number

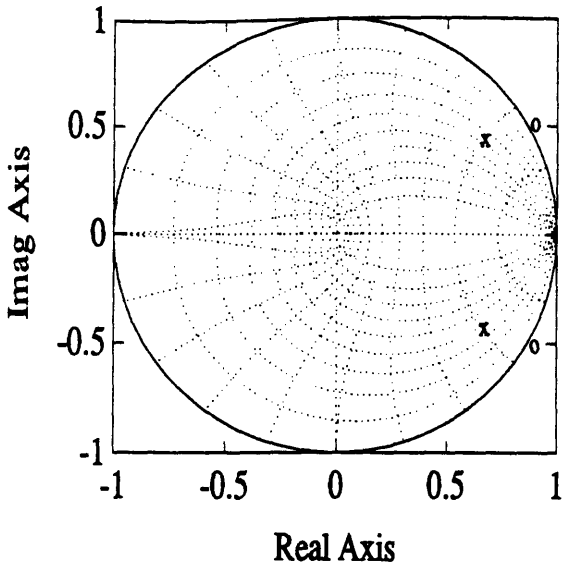

Figure 3-9: Pole-Zero plot of $G_{TF}(z)$ for $\alpha = .8$

of notch filters to be used, and the bandwidth necessary to ensure adequate noise suppression. The issues for selecting the number of filters are the same as those in section 3.3.3. The TF algorithm has processing requirements similar to the LMS algorithm for additional notches, that is, generation of two sinusoidal reference signals and two memory locations for each filter that is implemented. However, due to the increased complexity of the core of the algorithm, the TF approach requires slightly more computation time.

Notch Width Considerations

The first consideration in designing a tracking notch filter is the width of the notch. The filter must be large enough to suppress the noise without attenuating significant amounts of the desired signal. The bandwidth of a notch filter implemented with the TF algorithm is wholly dependent upon the type and characteristics of the lowpass filter $H(z)$.

In fact, the versatility of choosing a lowpass filter for $H(z)$ promises more flexibility than the integrator choice afforded by the LMS algorithm. Lowpass filter design is well-understood, and the TF algorithm allows use of both finite and infinite impulse

response filters, of virtually any order. Theoretically, a sharp lowpass filter with virtually no passband would result in a notch filter, whereas a lowpass filter with a unity passband out to a cutoff frequency ω_c used as $H(z)$ would result in a bandstop filter. This could be useful in applications where the unwanted noise has a wide bandwidth, where the noise is not well characterized or understood, or where many spikes occur so close together that it is more efficient to use one bandstop filter rather than several notch filters to suppress them all.

However, mathematical simulation of higher-order filters did not produce bandstop filters. Instead, they produced notch filters with unusual characteristics. For example, stopband ripple in the lowpass filter caused the TF algorithm to produce gains greater than unity adjacent to the center frequency, before approaching 0 dB gain asymptotically. Also, if the phase response of the lowpass filter crossed through 180 degrees in the pass band, another notch appeared in the TF algorithm due to the phase cancellation that resulted. This phenomenon is shown in Figure 3-10 for a 12th order IIR lowpass filter with a passband of 8 Hz and a cutoff frequency of 10 Hz (sampled at 16 kHz). The Bode response of the filter alone is shown first, above the Bode response of the TF algorithm using that filter (the dotted lines represent the response using quantized coefficients). It is clear that a bandstop filter does not result, but at the locations where the phase of the lowpass filter crosses 180 degrees (where it passes from 180 to -180 degrees on the phase plot), a notch filter appears in the magnitude response. Therefore, the phase characteristics of the lowpass filter affect the frequency response of the TF algorithm, which prevents implementing bandstop filters using the TF algorithm. Further analysis of the phase characteristics of the TF algorithm is required before the possible advantages of customizing $H(z)$ can be realized.

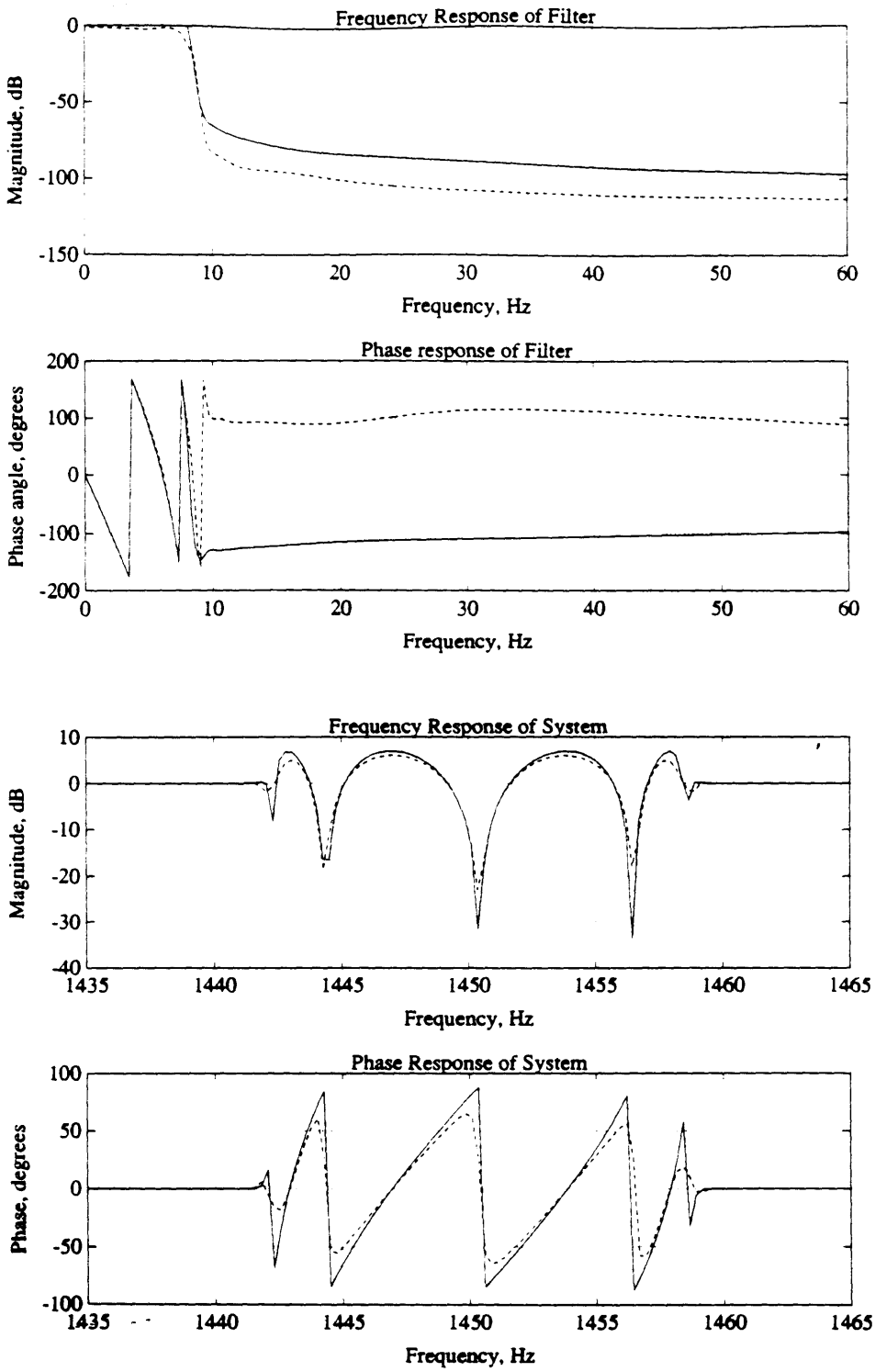

Figure 3-10: Bode Response of High-Order IIR Lowpass Filter and its use in the TF Algorithm

3.4.3 Tracking Filter Algorithm using Finite Impulse Response Filters

The output of a Finite Impulse Response (FIR) filter is solely a function of its input. Thus, FIR transfer functions have only zeros, and no poles. They are always stable, but require very high order to achieve tight filter specifications. They are not very susceptible to nonidealities, such as quantization error, and can be designed to have linear phase, which introduces no relative distortion[30]. Lowpass FIR filters were simulated in the TF algorithm to examine their potential for creating tracking notch filters. While they did produce notch filters, the bandwidth of these notches were quite large. Even for 50-tap FIR filters, the -3 dB bandwidth was still over 170 Hz wide. Due to the poor frequency response characteristics and large computation and memory requirements for such long filters (one multiplication and one memory location is required for each tap), FIR filters were not used in the real-time TF system. Simple, low-order IIR filters provided much sharper notches with significantly reduced compution time.

3.4.4 Tracking Filter Algorithm using Infinite Impulse Response Filters

The output of an Infinite Impulse Response (IIR) filter is dependent upon its input as well as its past outputs. As such, IIR transfer functions implement both poles and zeros, and can usually achieve frequency specifications with much lower order than FIR filters, requiring fewer computations. However, they are not always stable (due to the presence of poles), are much more susceptible to nonidealities such as quantization errors, and can produce substantial nonlinear phase distortion[30]. Various IIR lowpass filters were simulated in the TF algorithm to explore their ability to create tracking filters. As described before, the high-order IIR filters did not fare well in the TF algorithm due to the nonlinear phase distortions they introduced. Furthermore, actually implementing such filters on finite-precision microprocessors would have proved very difficult due to their extreme sensitivity to quantization error. Be-

cause of these problems, high-order IIR filters were not utilized in the real-time TF system. However, low-order (even first order) IIR lowpass filters did perform well, producing narrow notches with high quantization error tolerances and little danger of instability. Therefore, only first-order IIR filters were analyzed in the mathematical simulation and used in the hardware implementations.

Ideal System Response to Constant Frequency

Figure 3-11 shows the ideal Bode response of a few typical first-order IIR lowpass filters used in the TF algorithm. The values of α for these filters are .999 (solid line), .995 (dashed line), and .990 (dotted line). The Bode responses that result when these filters are placed in the TF algorithm with a modulation frequency of 1450.875 Hz (the LPF) are shown in Figure 3-12, again for α = .999, .995, and .990. The frequency response shows a well-defined notch filter centered at the LPF frequency, and the phase response passes from 180 to -180 degrees at the same frequency. The reduced attenuation expected because of the location of the zeros is not noticeable in this plot, primarily due to the high α values. For α close to one, the zero is so close to the unit circle that differences in attenuation between the TF algorithm and the LMS approach are very small. Figure 3-13 shows the Bode responses for the TF algorithm with five notch filters (serial TF blocks) for constant center frequencies at the LPF, LPF$\pm$LC1H, and LPF$\pm$LC3H frequencies with the same filters that were used in the earlier figures. Note that for the wider bandwidth filters (lower α), there is a nonzero attenuation at all points between the notch filters. The filters are so close together that their attenuations combine, so that for α = .99, there is no less than 18 dB of attenuation over a 130 Hz bandwidth. Furthermore, the magnitude and phase characteristics of are symmetrical about the frequency located at the midpoint between the notches, regardless of how close the notches are placed to one another. Both of these characteristcis are in contrast with the LMS algorithm, which always has a point of zero dB attenuation between the notches. Also note that the phase deviation from zero is substantially higher for the TF algorithm than for the LMS algorithm.

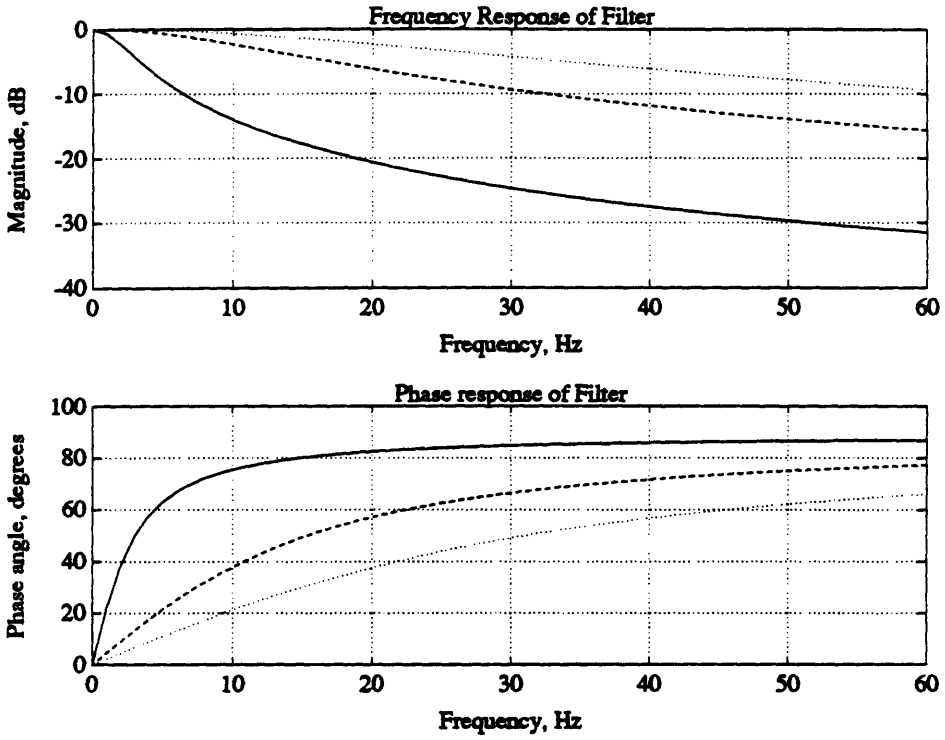

Figure 3-11: Bode Response of First-order IIR Lowpass Filters

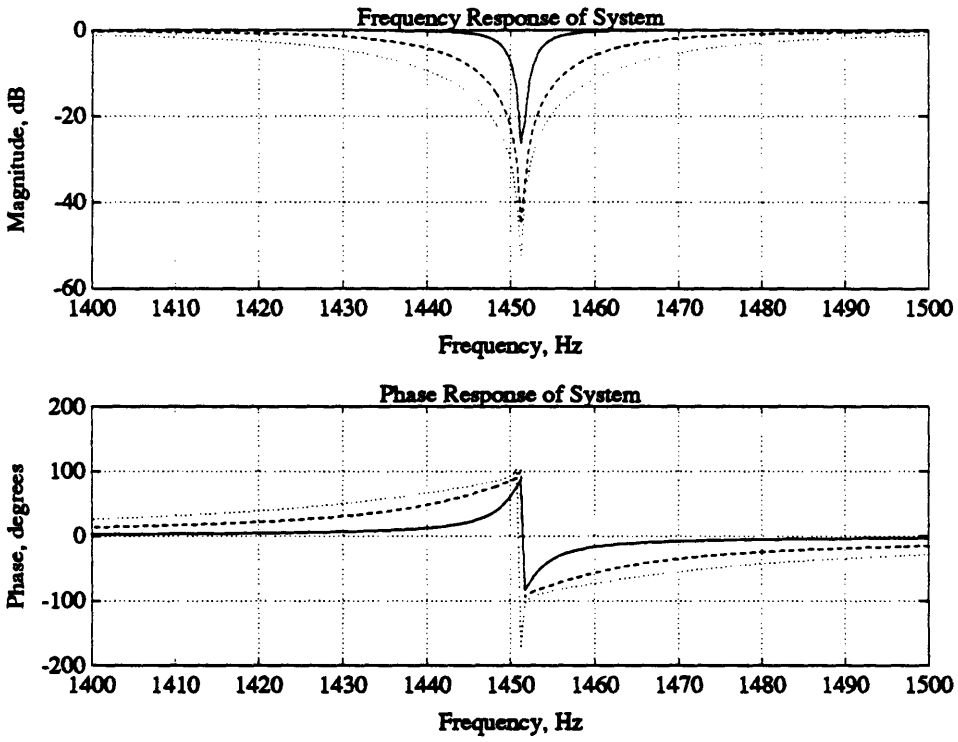

Figure 3-12: Bode Response of One-Notch TF System with First-Order IIR Lowpass Filters at Constant Frequency

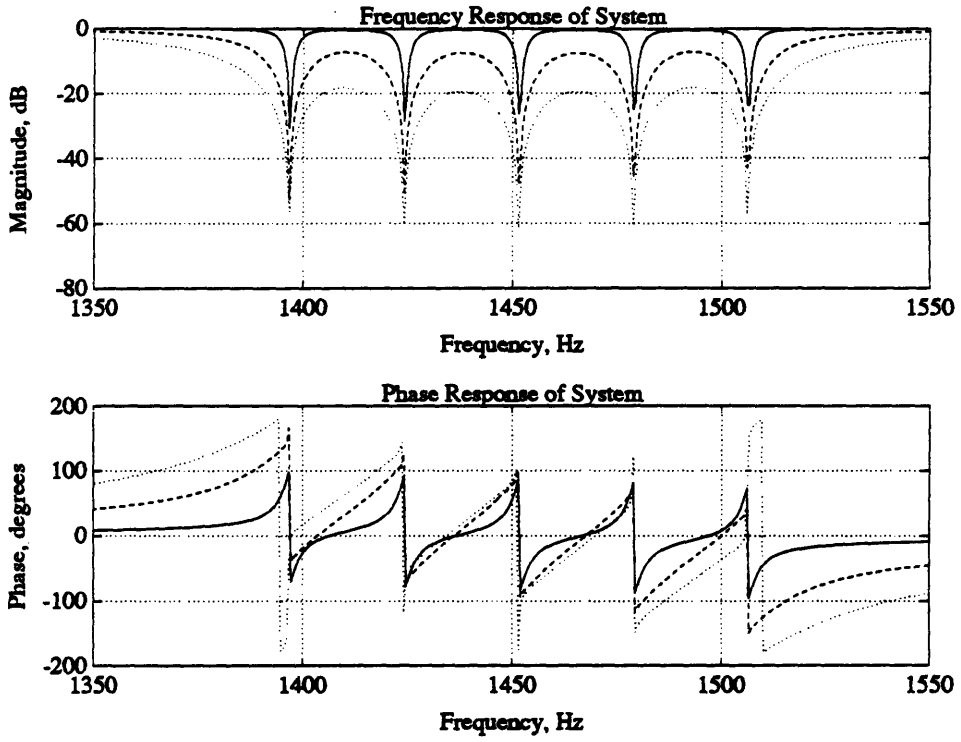

Figure 3-13: Bode Response of Five-Notch TF Algorithm with Five First-Order IIR Lowpass Filters at Constant Frequency

3.5 Variable Sampling Rate Filtering

The last algorithm to be examined is the VSR algorithm, where traditional, constant-coefficient IIR filters are placed at appropriate frequencies, and the sampling rate is varied proportionally to the RPM of the transmission. Because a digital system's operating frequencies are a proportional to sampling frequency, the center frequencies of the filters move as the sampling rate changes. As a result, the filters' centers are proportional to the rotation rate of the transmission, and are thus always aligned with the gear mesh noise spikes. This effect is strictly a result of discrete-time processing; a continuous-time equivalent of this approach does not exist.

This approach has several advantages and disadvantages when compared with the other two algorithms. First of all, it is by far the most computationally efficient of the three algorithms, because the tracking portion of the system is controlled externally of the microprocessor, by the sampling rate. The only calculations that need to be implemented are the difference equations for the filters themeselves, typically four multiplies using six memory locations for each second-order notch filter. Furthermore, no sine or cosine signals need to be generated, a process that eats up substantial processing time in the other two algorithms. As a result, the VSR is certainly the easiest algorithm to implement on a microprocessor, and allows many more filters to be implemented for the same amount of processing time. Furthermore, there are no restrictions on the type of filters that can be used in the VSR algorithm, allowing great flexibility in tailoring the frequency response of the adaptive filter.

However, the VSR algorithm also has a few drawbacks. First, it is not easy to change the filter's characteristics. If a different bandwidth is desired, or if a notch needs to be implemented at a different normalized frequency, then new filter coefficients must be calculated, just as when designing any fixed-coefficient filters. While doing so is not exceedingly difficult, it is certainly more complicated than changing the value of a single parameter, which is all that is needed for the other algorithms[8].

[8]To change the bandwidth, α can be altered directly in the LMS and TF algorithms, and the center frequency can be modified simply by changing ω_0. Filters implemented in the VSR algorithm have coefficients that are calculated based on these parameters, so it is not as easy to alter the filter

Second, the bandwidth of the filter will change as the sampling rate changes. This occurs because *all* of the frequencies of the system are proportional to the sampling rate. While this is a disadvantage when the noise spikes maintain a constant bandwidth (as for the CH-47 transmission noise), it would be a certain benefit if the bandwidth of the noise increased as the frequency of the noise increased as well. A third potential drawback of the VSR algorithm is the requirement of a highly consistent, high-frequency input signal to control the sampling rate. As discussed earlier, the sampling rate must be more than twice the maximum desired frequency, allowing plenty of bandwidth for the rolloff of a lowpass filter. This usually places the minimum sampling rate at or above 12 kHz. This is equivalent to 72,000 RPM, and it is unlikely that any gear or shaft in rotating machinery nominally operates at such a high rate[9]. Therefore, a slower frequency signal must be used as the input to a phase-locked loop (PLL) used as a frequency multiplier, to generate a faster oscillating signal that can be used to drive the sampling rate. The potential problem with such a solution is the fact that the PLL must interpolate between rising edges of the slower frequency in order to generate a faster signal. Slight errors in the interpolated period of the input signal can produce large errors in the sampling frequency, thus moving the filter locations even when the transmission speed has not changed.

3.5.1 Transfer Function Derivation

In the interest of simplicity, the filters used in the VSR algorithm for this project are simple second-order IIR notch filters. When a notch filter is placed at frequency f_0 and the digital system uses a sampling rate of f_s, the transfer function for the VSR algorithm in the z-domain is the same as that of a traditional fixed-coefficient notch filter,

$$G_{VSR}(z) = \frac{z^2 - 2z\cos(\frac{2\pi f_0}{f_s}) + 1}{z^2 - 2\alpha z\cos(\frac{2\pi f_0}{f_s}) + \alpha^2}. \tag{3.29}$$

charcteristics.

[9]In fact, the fastest spinning device in the CH-47D's transmission is the engine itself, which turns at a nominal 18,720 RPM.

The value $\frac{2\pi f_0}{f_s}$ is the normalized frequency of the notch filter, which corresponds to an angle θ in the z-plane[10]. The notch is then designed by placing the zeros precisely on the unit circle (radius = 1) at the angle θ,

$$z = e^{\pm 2\pi j \frac{f_0}{f_s}}, \tag{3.30}$$

and placing the poles at the same angle but with a radius of α less than one,

$$z = \alpha e^{\pm 2\pi j \frac{f_0}{f_s}}. \tag{3.31}$$

The pole-zero plot for the VSR algorithm with a single notch at 1450.875 Hz, a sampling rate of 16 kHz, and $\alpha = .8$ is shown in the z-plane in Figure 3-14. The zeros are located on the unit circle at the normalized angle θ, while the poles lie on the same angle but are closer to the origin. As before, as α approches one, the poles move closer to the zeros, and the bandwidth of the notch filter is reduced. Because the zeros lie on the unit circle, the frequency response of the system has an infinite null at that frequency. It is interesting to compare this pole-zero plot with the pole-zero diagrams for the LMS (Figure 3-4) and the TF (Figure 3-9) algorithms. The LMS algorithm preserves the position of the zeros (thus maintaining the infinite null) but moves the location of the poles slightly. On the other hand, the TF algorithm maintains the position of the poles but moves the zeros outside of the unit circle, sacrificing the infinite null. This is not a major sacrifice for narrow bandwidth filter, because the zero will be very close to the unit circle. For high α, the three algorithms have basically the same pole-zero diagram, because all of the values converge at $\alpha = 1$.

3.5.2 Design Considerations

Just as with the previous two algorithms, there are design tradeoffs to be made with the VSR algorithm. The number of notches implemented, whether they are

[10]In other words, the filter is designed by the ratio of its center frequency to the sampling frequency. In the LMS and TF algorithms, the filter was designed independent of frequency, and the ratio was taken into account during generation of the sinusoidal and cosinusoidal reference signals.

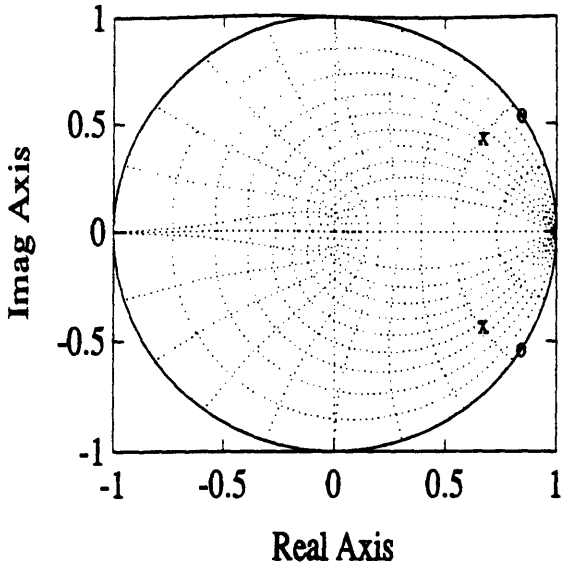

Figure 3-14: Pole-Zero plot of $G_{VSR}(z)$ for $\alpha = .8$

implemented in parallel or serial, and the type of filters used play important roles in the characteristics of the system. The number of filters implemented is decided by the same considerations outlined in section 3.3.3. However, the VSR algorithm has processing requirements that are different from the LMS and TF algorithms. It does not require a pair of generated sinusoidal reference signals, but it does utilize six memory locations for every notch. Furthermore, the core computations required for the VSR are substantially less complex than for the other two algorithms. Because each notch can be implemented in fewer instructions, much more flexibility is available in choosing the number of filters. In fact, it is more likely that the maximum number of filters that can be implemented will be limited by memory constraints and not processing speed.

Parallel or Serial Implementation

Multiple notch filters are not easily implemented in parallel using the VSR algorithm, due to the serial input-output nature of the notch filter itself. There is no feedback or feedforward signal where a subtraction takes place, as in the LMS and TF algorithms. If a parallel approach were used to implement n notches, then the effectiveness (atten-

uation) of each notch would be reduced to $\frac{1}{n}$ its normal amount. Therefore, the VSR algorithm cannot take advantage of parallel processing techniques. However, this is not a significant drawback; because of its extremely low computation requirements, it is unlikely to exceed the ability of even the slowest microprocessors.

Filter Considerations

Just as the previous two algorithms could be altered by changing $H(z)$, the VSR algorithm can be designed with any kind of filter[11]. In fact, any FIR or IIR filter can be implemented, and its frequency response characteristics will remain normalized to the sampling frequency. In the case of notch filters, the important considerations are the depth and bandwidth of the notches. As shown in the transfer function derivation, the depth of the notch filters used in this project are infinite (because the zeros of the transfer function were placed on the unit circle) and the bandwidth is controllable by the parameter α. The VSR will utilize notch fiters with bandwidths slightly wider than the filters described for the LMS and TF algorithms, in order to account for the reduction in filter bandwidth that occurs when the sampling frequency decreases.

3.5.3 Variable Sampling Rate Algorithm using IIR Notch Filters

One problem in analyzing the VSR approach is that it is extremely difficult to model. Most digital systems are not designed to handle variable time increments for sampling, and this is certainly true of computers. Due to the increase in numerical calculations required to keep track of the time that has elapsed, simulating the ideal characteristics of this approach in a numerical analysis program is difficult. Furthermore, if one wishes to analyze the system's ideal response to recorded data, then the data has to be sampled in a variable manner, just as it would be in the actual system. Again, most digital systems are based on a uniform sampling rate, and getting the data to

[11]Furthermore, the filter is implemented in the traditional manner, so that phase distortions do not affect the magnitude response of the filter, as they did in the TF algorithm.

the simulation would require building an interrupt-driven sampling system tied to the rotor rotation speed – just the device needed for implementing the hardware algorithm in the first place! Due to the time constraints on the project and the complexity of such an endeavor, the VSR algorithm was not modelled by a computer simulation.

3.5.4 Simulation of System at Nominal Frequencies

Although modelling the VSR algorithm is difficult, it is fairly straightforward to use standard techniques to obtain its normalized frequency response. This is because the algorithm uses traditional, fixed-characteristic digital filters. These filter equations can be entered into a numerical model to obtain the frequency response for a particular sampling rate, f_s. A real-time system utilizing the VSR algorithm can be expected to have the same frequency response characteristics when it is driven at the same frequency. To examine how the filters might change in frequency and bandwidth, f_s can be altered to obtain the system's frequency response for other sampling rates.

The VSR algorithm's Bode response is shown in Figure 3-15 for five notches with α = .999 (solid line), .995 (dashed line), and .99 (dotted line). The notches are centered at the nominal LPF, LPF±LC1H, and LPF±LC3H frequencies and the sampling rate f_s is the nominal rate of 16 kHz. The responses are very similar to those of the TF algorithm (Figure 3-13), in that for low α, there is always a nonzero attenuation between the notches. The phase deviation that occurs adjacent to the notch frequencies is also similar to that of the TF algorithm, in that there is roughly twice as much phase deviation as in the LMS algorithm for notches with similar bandwidths, but the phase change from 180 to -180 degrees at the notch frequency still takes place.

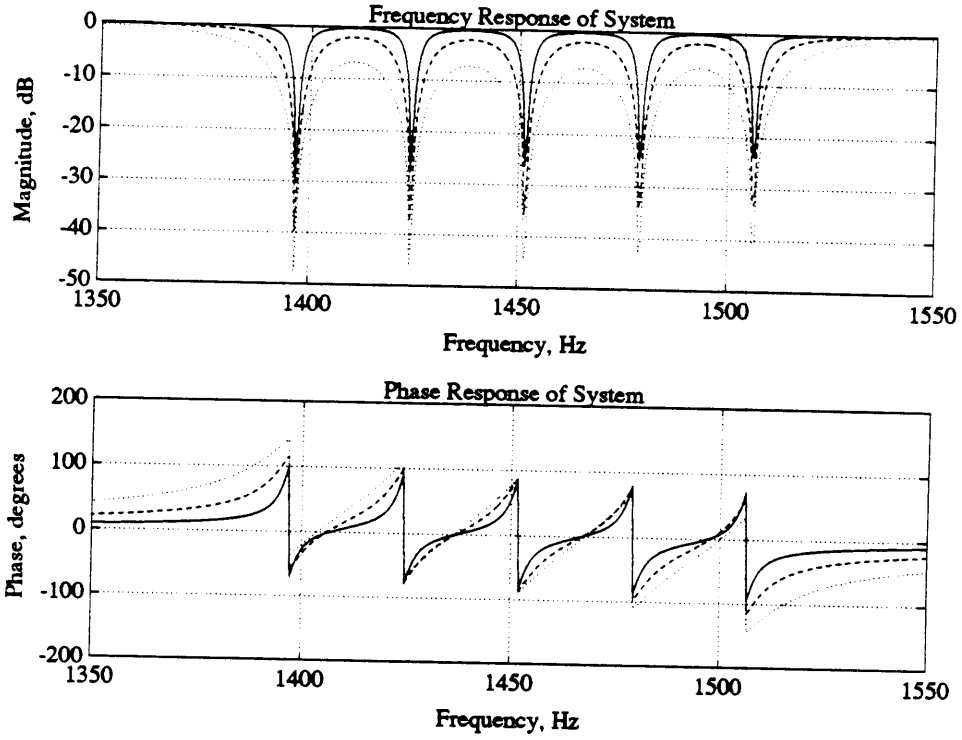

Figure 3-15: Bode Response of Normalized Five-Notch VSR System

3.6 Reference Signal Analysis and Obtaining Frequency Information

All approaches examined in this project require a reference signal of some kind for successful operation. The algorithms need a way to determine the rotational speed of the transmission so that they may calculate the appropriate gear mesh frequencies (LMS and TF algorithms), or to calculate the appropriate sampling frequency (VSR approach). To this end, the LMS and TF algorithms utilize a Frequency Determination System, or FDS, while the VSR algorithm needs a Frequency Multiplication System, or FMS. This section describes the criteria of the input signal, explaining what characteristics were used to evaluate the signals on the CH-47D which could potentially be used as reference signals.

3.6.1 Required Signal Characteristics

The reference signal must meet several criteria in order for it to be able to adequately define the rotational speed and rate of change of the rotor system. The characteristics used to measure the reference signal's performance can be termed resolution, update rate, and accuracy.

Resolution

Resolution is the smallest change in rotation rate that can be discerned from the signal; for continuous systems, resolution is usually infinite. However, for a digital system, the resolution is finite, allowing only discrete values for the calculated frequency. A fine resolution implies that small rate changes in the signal can be measured, while a coarse resolution means that it takes a substantial rate change to occur before the system will be able to recognize the change. It is clear that resolution is very important, because if the rotation rate changes but the system doesn't respond to it, the filter will be acting at the wrong center frequency, and its effectiveness at suppressing the noise will be reduced. Therefore, the system must be able to dis-

tinguish a fine enough resolution that the rotation rate can be determined with a small degree of uncertainty. The frequencies acted upon by the system remain very close to the actual frequencies of the gear mesh, and the attenuation remains high. If the resolution is too coarse, then the bandwidth of the filters must be increased to compensate for the lack of certainty in the reference frequency.

The resolution of the signal depends upon the signal's characteristics as well as the method used to determine the frequency of the signal. In a frequency determination system, or FDS, there are two approaches to calculating the frequency of an oscillating signal: direct pulse counting and gated pulse counting[21]. A sinusoidal (or other periodic) signal can be converted to a square wave (a series of pulses), so that a digital system may implement either of these methods.

Direct Pulse Count A direct pulse count (DPC) is performed by counting the number of pulses that occur in a given amount of time. Knowing the number of pulses n and the duration of the count (gate time) t, the frequency, F, of the signal is easily calculated by

$$F = \frac{n}{t}. \tag{3.32}$$

When performing a direct pulse count, the maximum error occurs when the rising edge of a pulse occurs immediately before the counter starts or stops counting. In the former case, the count is one less pulse than it should be, and in the latter, the count is one more than it should be. These error bounds are used to determine the resolution, R, of DPC by subtracting the smaller from the larger, such that

$$R = \frac{n+1}{t} - \frac{n-1}{t} = \frac{2n}{t}. \tag{3.33}$$

Thus, the resolution of DPC is independent of the frequency of the input signal, but can suffer if the update rate needs to be high (t is small) or the frequency of the signal is low (n is small). This method can experience overflow if there are not enough bits in the counter to keep track of the number of pulses, but this only becomes a problem for fast input signals and slow gate times.

Gated Pulse Count Gated pulse counting (GPC), on the other hand, finds the time between N consecutive pulses by waiting for a rising edge, enabling a counter driven by a high-frequency clock, waiting for an $(N+1)th$ rising edge, and stopping the counter. If the frequency of the clock signal is C and the number of clock ticks that are counted is n, then the frequency F of the signal is found by

$$F = \frac{NC}{n}. \tag{3.34}$$

The maximum errors of this method occur in the same situations as for DPC, that is, the situation when almost $n-1$ clock ticks occur but only n are read, and when almost $n+1$ clock ticks occur but only n are read. Again, the resolution is defined as the difference between the maximum and minimum error cases,

$$R = \frac{NC}{n-1} - \frac{NC}{n+1} = \frac{2NCF^2}{N^2C^2 - F^2}. \tag{3.35}$$

This method has an advantage over DPC in that the resolution can be made as fine as necessary by increasing the clock frequency C. However, it suffers from the fact that the size of the counter is speed dependent, so that for a given number of bits, there is a minimum and a maximum frequency that can be read before the counter overflows or doesn't count at all, respectively. Generally speaking, C should be chosen large enough that the maximum frequency can be read with fine enough resolution, and then the required size of the counter is determined such that an overflow does not occur with the the minimum frequency is applied. If the frequency range is very large or the resolution requirements are very fine, this may demand a counter with a prohibitively large number of bits.

Update Rate

Update rate is the rate at which accurate rotation speeds may be determined from the reference signal. It is primarily dictated by the frequency at which the reference signal oscillates, although a very busy or slow microprocessor could put limits on the update rate as well. Clearly, a slowly oscillating signal has a low update rate,

because it takes a long time for a measurable change to occur in the signal. When a signal oscillates rapidly, discernible changes occur much more quickly, implying a faster update rate. The key concern that results from a slow update rate is that the rotation rate of the rotors may change before the system can react to this change. If this occurs, the filters remain stationary as the noise moves outside the bandwidth of the filters. Therefore, the update rate must be fast enough that the digital system can update the reference frequency before the gear mesh frequencies move outside the filters' effective bandwidth.

Accuracy

Accuracy is a measure of the maximum difference between the calculated value of the frequency and the actual rotation rate of the transmission, neglecting time delays imposed by the digital nature of the system[12]. This value is primarily dependent upon errors in the digital components of the system (such as deviations in the oscillator's clock rate), miscorrelation between the reference signal and the actual gearbox rotation rates (due to lags in the mechanical/electrical systems), and inconsistencies in the analog circuitry used to make the reference signal readable by digital components (i.e., the zero-crossing detector). These errors are hard to quantify, although the errors in the circuit components will most likely be small. Generally, accuracy is not as important a source of error as are resolution and update rate.

3.6.2 Implications for Reference Signal Selection

The maximum variance and rate of change of the transmission rotation speed will dictate a large part of the design of the noise suppression system. In order to determine exactly how these variation characteristics influence the performance of the noise suppression system, their effects are quantified here. Let R be the resolution of the FDS (all values are in Hz unless specified otherwise). Let U be its update rate, and E_{total} its total error (akin to accuracy). The bandwidth of the filter will be

[12]These time delays are accounted for in the update rate of the FDS.

denoted by B_{filter}. Lastly, the maximum variation rate of the helicopter rotor will be represented by V, in Hertz per second. Variables that are a function of frequency will be followed by (F)[13]. To derive the equations governing how these parameters affect one another, consider first a system with infinite resolution (i.e., a system with completely continuous frequency information). In this case, the filter bandwidth will be placed so that its center is perfectly aligned with the noise spike, and the system need not update until the noise spike moves to the edge of the filter's bandwidth. This will occur when the infinitely-thin noise spike travels one-half of the filters bandwidth:

$$U \geq \frac{2V(F)}{B_{filter}(F)}. \tag{3.36}$$

However, the noise spike is not infinitely thin, but instead has a bandwidth of B_{noise}. Thus, the update must occur before the edge of the spike meets the edge of the filter, which is the same as subtracting half of the noise's bandwidth from the filter's effective suppression range. Thus,

$$U \geq \frac{2V(F)}{B_{filter}(F) - B_{noise}}. \tag{3.37}$$

Consider now the effects of an error in the calculation, such that the noise spike may actually be located anywhere within $\pm E_{total}(F)$ of the calculated frequency, so that the necessary update rate becomes

$$U \geq \frac{2V(F)}{B_{filter}(F) - B_{noise} - E_{total}(F)}. \tag{3.38}$$

However, the FDS will not have an infinite resolution, due to its digital nature. Consider the effect that finite resolution will have on the accuracy of the filter placement. If the accuracy of the FDS is infinite (no error), but its resolution is only 10 Hz, then the noise spike must lie within ± 5 Hz of the frequency calculated by the system.

[13]Note that the filter bandwidth, B_{filter}, is shown in the equations as a function of frequency. This is true only of the VSR algorithm; for the LMS and TF algorithms, the bandwidth of the filter is constant.

Thus, resolution effectively contributes to the error of the system such that

$$E_{resolution}(F) = \frac{R(F)}{2} \tag{3.39}$$

and the total error can be broken down into error due to resolution limits, $E_{resolution}$, and the inherent error of the system, $E_{inherent}$ (see the above section on accuracy). Thus,

$$E_{total}(F) = E_{inherent}(F) + E_{resolution}(F), \tag{3.40}$$

and the actual update rate required to ensure that the notch filter always suppresses the gear mesh noise is found by combining (3.39) and (3.40) into (3.38), which leads to

$$U \geq \frac{2V(F)}{B_{filter}(F) - B_{noise} - E_{inherent}(F) - \frac{1}{2}R(F)}. \tag{3.41}$$

The parameters $U, V, B_{noise}, E_{inherent}$, and R are defined by the rotation characteristics of the system to be suppressed (in this case, the CH-47D transmission) and the reference signal. Thus, the primary design choice is the filter bandwidth. For this reason, Equation 3.41 is rearranged to solve for B_{filter}, such that

$$B_{filter} \geq \frac{2V(F)}{U} + B_{noise} + E_{inherent}(F) + \frac{1}{2}R(F). \tag{3.42}$$

Assume that the bandwidth of the noise is 2 Hz and the inherent error is 1 Hz. Also assume that the frequency of the reference signal is 1180 Hz with a maximum variation of 14% (166 Hz/second)[14]. To minimize the filter bandwidth required when using the DPC algorithm, combine equations (3.42) and (3.33) and take the derivative of the result with respect to t, and solve for the point of zero slope,

$$\frac{dB_{filter}}{dt} = 2V(F) + \frac{-n}{t^2} = 0. \tag{3.43}$$

[14]These values approximate the parameters of the signals actually used for the noise reduction system.

The second derivative with respect to t is

$$\frac{d^2 B_{filter}}{dt^2} = \frac{2n}{t^3}, \tag{3.44}$$

which is always positive, so that the zero point of the first derivative identifies a minimum. Thus, 3.43 can be solved to find the update rate that minimizes the necessary filter bandwidth, such that

$$U = \frac{1}{t} = \sqrt{\frac{2V(F)}{n}}, \tag{3.45}$$

and solving results in $U = 18.2$ Hz. Using this update rate to calculate the necessary filter bandwidth results in

$$B_{filter} = \frac{(2)(166)}{(18.2)} + 2 + 1 + \frac{18.2}{2} = 30.3 \ \ Hz$$

This is a rather large bandwidth, considering that some of the notches will be only 27 Hz apart to begin with. As it is the smallest bandwidth attainable, DPC does not yield a high enough resolution/update rate combination to accurately determine the frequency of the reference signal. Therefore, an analysis of GPC is warranted. Unfortunately, the derivative of B_{filter} with respect to t must be solved numerically when using the resolution equation for GPC. Furthermore, the update rate of GPC must be a multiple of the duration of a pulse of the input signal, $\frac{F}{N}$, which leaves only a few discrete values for the update rate. If the straight 1180 Hz signal is used for the FDS, an update rate of .85 ms results. Given the inertia of the transmission system (including gears, rotors, shafts, and engines), it is clear that not much change will take place in such a short period of time. Furthermore, the counters used in the FDS are limited to a 20 MHz clock signal, which would result in a counter value of only 14 bits. In order to increase the number of bits of resolution, the update rate can be decreased by skipping N pulses. If $N = 6$, then the update rate increases to only 5.1 ms, and a slower clock frequency can be used. Choose a 10 MHz clock frequency, and

the resolution of GPC is

$$R = \frac{(2)(6)(10^6)(1180^2)}{6^2(10^6)^2 - 1180^2} = .0464 \quad Hz.$$

Then, the minimum bandwidth of the filter is

$$B_{filter} = \frac{(2)(166)}{\frac{1180}{6}} + 2 + 1 + \frac{.0464}{2} = 4.7 \quad Hz.$$

This is certainly an acceptable filter bandwidth, even when implementing notch filters that are fairly close together[15]. The only remaining concern is that there are enough bits in the counter to prevent an overflow from occurring. The number of bits necessary for these assumptions can be found by finding the number of oscillator clock cycles that will occur in the time that passes between six rising edges of the reference frequency. Thus,

$$Counts_{MAX} = \frac{CN}{F} = \frac{(10^6)(6)}{1180} = 50,848.$$

This many counts can be held in 16 bits ($2^{16} = 65,536$). While this is not a small counter, it is not prohibitively large, either. In fact, single-chip counters are available that contain more than 8 bits, so that this counter could be implemented with only two chips. The high oscillator frequency and counter size are the only real drawbacks of the GPC approach, but these are the tradeoffs made to obtain the resultant combination of high resolution and high update rate.

[15]Note that all filter bandwidths calculated in this section were based on placing a notch filter at the same frequency as the reference signal, 1180 Hz. Because the parameters are a function of frequency, the necessary filter bandwidth increases if the notch filter is to be placed at a higher frequency. For example, to guarantee suppression of the LP2H+US3H frequency of 4407.375 Hz, V becomes 617 Hz per second and R increases to .0869. This results in a necessary filter bandwidth of at least 9.5 Hz for the same GPC-based FDS.

Chapter 4

System Realization

4.1 Choosing the Reference Signal

As described in the previous chapter, all of the algorithms explored in this project require some means of determining the rotation rate of the transmission. Several signals were considered as possible sources for providing this signal, and the characteristics of these signals are discussed in the following sections.

4.1.1 Transmission Accelerometer

Perhaps the most obvious means of measuring the rotation rate is to add an accelerometer to one of the gears in the forward transmission. This approach has an advantage in that it is connected directly to the component that is to be measured, so that there would be virtually no error due to indirect measurement of the transmission rotation rate. However, adding or modifying any hardware on a CH-47 is costly in terms of money, time, and manpower. Due to the relatively short-term nature of the project, and the relatively tight constraints of the IR&D budget, making changes to an existing CH-47 was not deemed feasible. It is worth noting that the CH-47E already has such a device, and the rotor rotation rate is one of the many items that is sent across the helicopter's MIL-STD-1553 data bus. However, the update rate of this signal is apparently only 20 Hz[20], so it would have to have a high resolution

and accuracy to perform better than the rotor tachometer signal chosen for use in the CH-47D. If this is the case, then a noise reduction system implemented on the E model of the helicopter could use the on-board data bus rather than obtaining a reference signal from an analog source.

4.1.2 Blade Tracking Signal

Of the signals already present on the helicopter, the first considered as a possible reference signal was the blade tracking signal. Magnetic strips (called strikers) are placed on the underside of the rotor blades near the rotor shaft. These strips pass over a magnetic phase detector as the rotors spin. This action interrupts the phase detector's magnetic field, creating an electronic pulse (approximately sinusoidal) each time a striker passes it. The result is a series of pulses whose frequency is directly related to the rotor speed.

There were several drawbacks to utilizing this signal as the reference. First, the rotor rotation speed (on the D model) is 3.75 Hz, a very slow rate. Thus, with three rotor blades, the output of the magnetic phase detector includes three pulses per revolution, and thus has a frequency of 11.25 Hz. As discussed in section 3.6, a signal with such a low frequency puts severe restrictions on the capabilities of the FDS, and would require notch filters of very wide bandwidth. Second, the strikers are placed only to indicate which rotor blade is passing; as such, the time of its passage is not important, and the strikers are hand-glued to the rotors. This results in inconsistent placement, which would further increase the error of the FDS. Lastly, one of the blades has two striker plates rather than one[1] which would further complicate the FDS. Because of these difficulties, it was concluded that the blade tracking signal would not provide adequate resolution, update rate, nor accuracy for the FDS.

[1]This is how the test engineers determine which blade is passing: one of the blades produces a double pulse (blade 1) and the subsequent pulses are rotor blades two and three. The blade tracking signal is primarily used for balancing the rotors so that they all fly true, which requires the ability to determine which blade is out of balance.

4.1.3 Aircraft Power

The standard aircraft alternating current power is 3-phase, 400 Hz power at 117 volts. This power comes from generators attached to the main engines. Because the engines, drive shafts, transmission, and rotors are all directly connected, the engine speeds vary with the rotors, and thus the transmission. Therefore, it would be possible to use the nominally 400 Hz signal as the reference signal for the FDS. However, the only requirements placed on the power signal are voltage, rate, and current specifications. As such, the signal does not have to be a clean sinusoidal signal, and the accuracy of the frequency measuring system would be substantially reduced by any high frequency noise or DC variations. While some of these problems may be lessened by the use of lowpass filters or other techniques, the noisy power signal was not used for the FDS in favor of finding a better reference signal source.

4.1.4 Oil Pump Ripple

The oil pump in the CH-47 is driven by a pickup gear off of the forward transmission. Thus, the pump has a cycle rate tied directly to the rotation rate of the transmission. This periodicity could be measured by the addition of a transducer in the oil line to observe transients in the oil pressure. While this is certainly a potential solution, the time and financial constraints imposed by the project did not allow modifications to aircraft hardware.

4.1.5 Rotor Tachometer Signal

Another signal readily available on the CH-47 is the rotor tachometer signal. This signal is created by a generator in the combiner transmission, and is used to drive the rotor tachometer in the cockpit. This analog gauge displays the rotor rotation rate, in percent, so that the pilot can monitor engine speed. If the rate moves outside the operating range, the pilot can alter the power to the transmission to bring the rotation rate back near nominal.

This signal holds great promise for the FDS. The signal is a relatively low-noise

sinusoid with low DC variance, and has a nominal frequency of 1183.17 Hz. The generator's rotor has six strikers, similar to those used for the blade tracking signal, and a single magnetic pickup that detects the passage of each of these strikers. The rotor turns at a nominal 11831.7 RPM, so that six pulses per revolution and sixty seconds per minute translate to an 1183.17 Hz output frequency. While this frequency is high enough to achieve substantial resolution, update rate, and accuracy, there are still two concerns that need to be addressed.

The first is the potential error that could result if the six strikers are not evenly spaced around the rotor. If their spacing is not uniform, then the resulting sinusoid will have slightly nonuniform periods. This nonuniformity could produce errant frequency measurements, and result in misplaced filters. However, due to the tight manufacturing tolerances placed on spinning parts, this error was assumed to be negligible.

The second potential source of error stems from the fact that the measurement system will not be measuring the rotation rate of the noise source directly. Because it is the forward transmission that generates the gear mesh frequencies, and not the combining transmission where the rotor tachometer signal is generated, there is a potential discrepancy between the rotation rate of the gears in the transmission at the front of the helicopter and the rotation rate of the combining transmission, which is located near the engines in the aft of the helicopter. Any discrepancies will result in an error in the calculated forward transmission rotation rate. This potential error is difficult to quantify, but the whole drive system of the CH-47 has to meet extreme tolerances from engine to rotor in order to ensure a long service life. Furthermore, the drive system always rotates in the same direction, and when in normal operation there is always torque applied to the gears[2]. Therefore, it is assumed that discrepancies between the rotation rate of the generator and the rotation rate of the transmission

[2]This is true in all operating conditions except for autorotation, where the engines are disconnected from the drive shafts at the combining transmission. This is a fairly rare occurrence which produces large variations in rotation speed. Because autorotation presents a more difficult tracking problem than normal operation, and because it is not a common occurrence, the noise suppression algorithm was not designed to work in this case.

are negligible and can be neglected for purposes of determining the rotation rate of the forward transmission.

4.2 Data Recording

In order to allow testing of the algorithms in a laboratory environment where conditions could be controlled, the ambient cockpit noise, the interphone signal, and the rotor tachometer signals were recorded. No previous recordings were adequate for this purpose, because there were no synchronized recordings of the cockpit interphone signal and the rotor tachometer signal. These two signals must be recorded simultaneously in order for any of the algorithms to track the transmission rotation rate and thus the gear mesh frequencies over time. To provide the maximum flexibility in testing the algorithms, four signals were desired even though only two are needed to run the noise reduction system. These four signals were the pilot's microphone, the ambient noise in the cockpit, and the left and right rotor tachometer signals. In order to obtain synchronized recordings, a B&K four-track flight-worthy recorder was used to obtain the data. The first track was configured to record the pilot's microphone, the second was connected to a microphone placed in the cockpit, and the third and fourth tracks recorded the two rotor tachometer signals. A schematic showing the connections between the recorder and the helicopter is shown in Figure 4-1.

For the pilot's microphone, an interface had to be built to convert the microphone adapter plugs (type U-93A/U) to a BNC-type connector. The ambient microphone was chosen to be a B&K instrumentation microphone, already designed for use with this recorder. It was mounted above, behind, and to the right of the copilot (i.e., near the middle aft portion of the cockpit), taped to a flexible lifting strap in order to help isolate it from the vibrations of the frame of the cockpit. The rotor tachometer signals were accessed at terminal blocks in the left and right avionics bays of the helicopter, located immediately behind the cockpit. An interface cable ending in a BNC connector was constructed for each rotor tachometer signal. All of these components were then connected to the recorder, which was strapped to a seat in

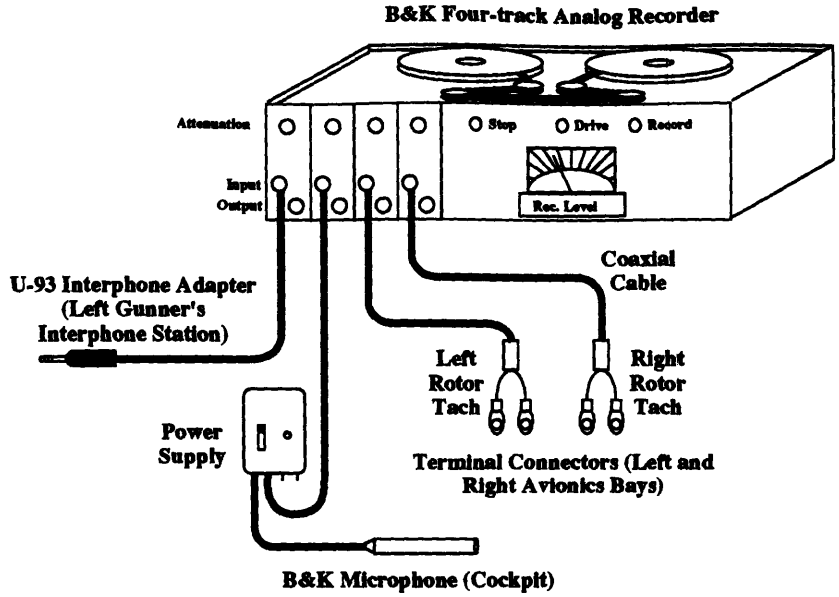

Figure 4-1: Schematic of Recorder Connections

the front of the cabin, immediately behind the avionics bays. The microphone was calibrated before the flight using B&K calibration equipment, and proper recording levels for the four signals were set by adjusting the attenuation of each channel while the helicopter was undergoing preflight checks on the ground.

4.3 Simulation and Modelling

Perhaps the best way to test and see if a digital signal processing system will work is to model it in a computer simulation. The Matrix Laboratory (MATLAB) software provides an excellent environment for working with large arrays of data, and has many built-in signal processing functions required for implementing and analyzing the noise reduction systems described. Therefore, before attempting real-time tests with hardware systems, the LMS and TF algorithms were modelled using MATLAB on Athena, M.I.T.'s computer network. The VSR algorithm was not implemented due to the variable nature of the sampling rate, as explained in section 3.5.3. The modelling approaches and methods are too complex to detail here, but the primary concerns about the implementation and validity of the model are discussed in the

following sections[3].

4.3.1 Implementation Considerations

In order to accurately model the system, care must be taken in converting the real-time design to a software-based simulation. Several concerns had to be addressed in order to gain confidence that the model accurately represented the real-time system.

Calculating the Frequency of the Rotor Tachometer Signal

The real-time system calculates the frequency of the rotor tachometer signal by measuring the time it takes for N rising-edge zero-crossings to occur. Thus, $\frac{N}{\delta t}$ is the rotation rate of the engine (six pulses per revolution). Once this rate has been determined, the rotation rate of any item in the gearbox can be found by multiplying that rate by a constant. Furthermore, the gear mesh frequencies are linearly related to the rotation rates of the gears, so any mesh frequency can be calculated in the same manner. However, determining the times of the zero crossings is not easily done in a simulation, because of the necessity to keep the main and reference inputs synchronized. In order to maintain the correlation of the two signals, they must be digitized simultaneously[4]. The main problem of this approach comes from the fact that the zero-crossing is no longer well-defined once digitization has occurred (only rarely will the sample time exactly coincide with a zero crossing). In order to determine the point of zero amplitude, a linear interpolation algorithm was used to estimate the actual times of the zero-crossings by interpolating between successive negative and positive sample values. The time between two estimated zero crossings was then used in the same manner as the time between rising edges found by the analog frequency measurement system. A graphic example of this interpolation is shown in Figure 4-2

[3]Incidentally, the simulations of the algorithms are what produced the ideal Bode responses shown in the previous chapter. MATLAB provided the capability to obtain frequency responses not limited by hardware considerations, such as finite precision arithmetic.

[4]It would be possible to construct a system to digitize the frequency of the signal rather than the signal itself, much like the actual hardware, but it is easier to calculate the frequency using software algorithms.

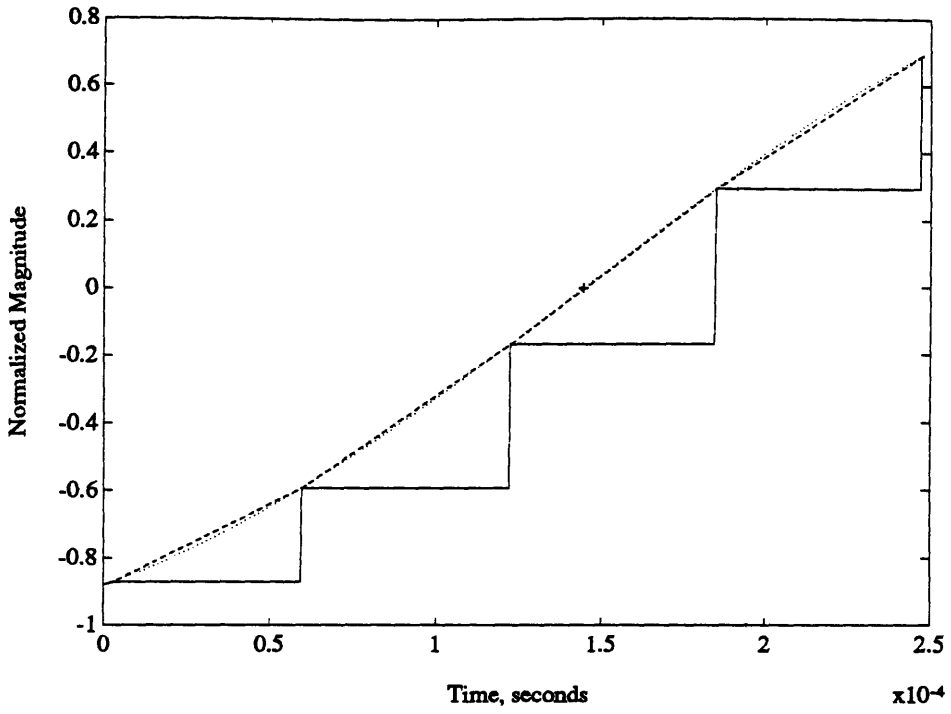

Figure 4-2: Linear Interpolation of Digitized Rotor Tachometer Signal

with a digitized rotor tachometer signal, where the input sinusoid is 1180 Hz, sampled at 16 kHz with 16-bit precision. The solid line represents the digital sampled values (with no error), the dashed line shows linear interpolations between these values, and the dotted line is the actual continuous sinusoid. The plus symbol near the center of the figure denotes the actual zero crossing of the sinusoid, and it can be seen that the dotted line does not pass exactly through its center. This error, introduced by the linear interpolation, must be analyzed to ensure that it will not invalidate the results of the simulation.

This approach has two inherent sources of error that are not present in the analog frequency measurement system (although both are susceptible to noise and DC variations). The first is evident from the fact that the sinusoid is not precisely linear in the region between the negative and positive sample values. As a result, the linear approximation is inaccurate, and the actual location of the zero-crossing will be different from the calculated location. In a worst case, the error due to the non-

linearity is about $8.6 * 10^{-3}\%$[5] for an 1180 Hz signal sampled at 16 kHz, implying a frequency error of about .1 Hz. The second source of error comes from the fact that the rotor tachometer signal has already been sampled, and therefore the magnitude of the sample points has been quantized to the accuracy of the digitization. In this case, the rotor tachometer has been quantized to 16-bit accuracy. Therefore, the actual magnitude deviates by no more than $\frac{1}{2^{15}}$ from the sampled magnitude (one bit is used as a sign bit). If both values have maximum error in the same direction, then this adds $3.5 * 10^{-3}\%$ error. The combined effects of these errors must be taken into account to ensure that the results of the simulation are not jeopardized.

Reducing Noise in the Rotor Tachometer Frequency

Figure 4-3 shows the frequency of the rotor tachometer reference signal as calculated by the simulation. The calculated frequency jumps around erratically by about 5 Hz, indicating a random error of approximately .42%. Clearly, this error is much greater than the predicted error of $1.15 * 10^{-2}\%$, or .137 Hz. Therefore, the jumps in frequency must be due to inconsistent playback tape speed[6]. Lowpass filtering this signal will remove the rapid changes in frequency, resulting in a weighted average of the calculated frequency. Using the output of the lowpass filter should reduce the error introduced by the tape player, and produce a more accurate estimate of the actual rotor tachometer frequency. The result of such a lowpass filter applied to the signal of Figure 4-3 is shown in Figure 4-4. From this figure it can be seen that many of the high frequency components of the signal have been eliminated, and only slow variations remain.

[5]If both points are equidistant from the actual zero crossing, the nonlinearity cancels due to the symmetry of the sinusoid. If one point is very far away and the other is close, then the error is low because the zero crossing is close to one of the data points. Solved numerically, the maximum error occurs when one of the sampled values is about 21% away from the actual zero crossing.

[6]This is likely, because the digitization was performed using a home stereo cassette player, which does not need to have a motor accurate to frequencies in the MHz range.

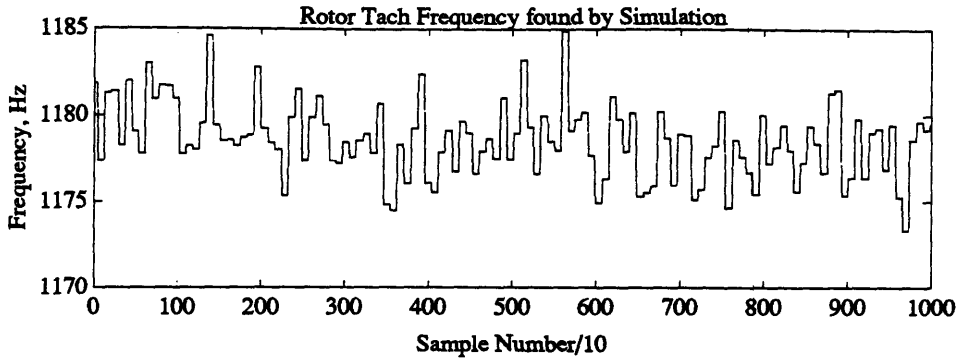

Figure 4-3: Digitally Calculated Rotor Tachometer Frequency

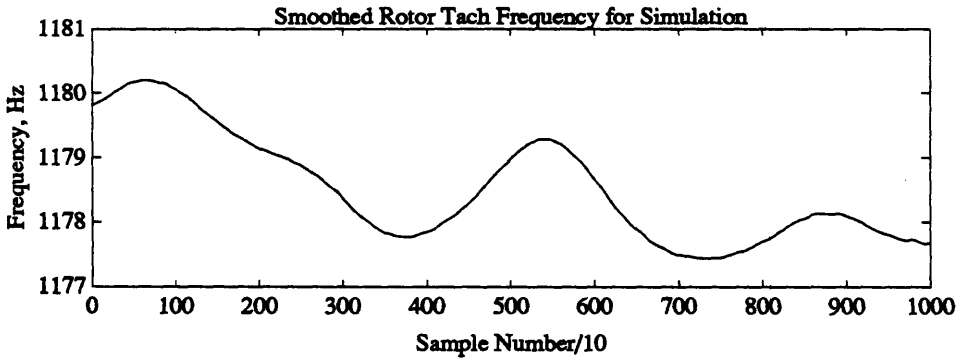

Figure 4-4: Smoothed Rotor Tachometer Frequency

4.3.2 Simulation of the Least Mean Squared Algorithm

Figure 4-5 shows the simulated 5-Notch LMS algorithm's frequency response to the recorded data of the CH-47D[7] in steady, forward flight with a speed of .006 (the dotted line is the input frequency spectrum, and the solid line is the frequency spectrum of the output). Note that at the frequencies of the noise spikes, the signal has been attenuated by 20-40 dB, bringing their spikes' magnitudes down to (or below) the background noise level. Figure 4-6 shows the frequency response of the same system to a recording of the signals at takeoff, when the rotor rotation rate changes dramatically. Note how, even when the gear mesh frequency is rapidly changing, a high-amplitude plateau is visible near the nominal gear mesh frequency. It is clear from the figure that the LMS algorithm has successfully tracked the changing frequency because it reduced the plateaus by approximately 10-20 dB at the LPF and LPF$\pm$UC3H frequencies. It does not appear to have performed as well at the LPF$\pm$UC1H gear mesh frequencies, providing only about 5-10 dB of attenuation. Note, however, the minimal effect of the algorithm between the noise spikes. This is a result of the zero dB point that exists between the notches seen earlier in Figure 3-6. The algorithm does a good job of attenuating the desired frequencies without affecting the neighboring signal content.

4.3.3 Simulation of the Tracking Filter Algorithm

Figure 4-7 shows the frequency response of a simulated 5-Notch TF system to the same in-flight recordings that were used for Figure 4-5. Again, note that the magnitude of the frequency spikes has been reduced by 20-40 dB, enough to bring the magnitude of the noise spikes to or below the background noise. Figure 4-8 is the frequency response of the same system to data recorded from the CH-47 at takeoff. Even at takeoff, when the frequencies of the gear mesh are changing rapidly, the TF system

[7]For this and the next three plots, the input to the system is actually the ambient microphone in the cockpit, and not that of the cockpit interphone system. The reason this input was used is because it is much easier to identify the noise spikes from the gear mesh frequencies. Therefore, it is easier to observe whether or not the algorithm is successfully suppressing the appropriate frequencies. If attenuations are seen in the desired frequency bands, then similar reductions can be expected when using the interphone system as an input. The noise spikes simply show up better when the ambient microphone is used.

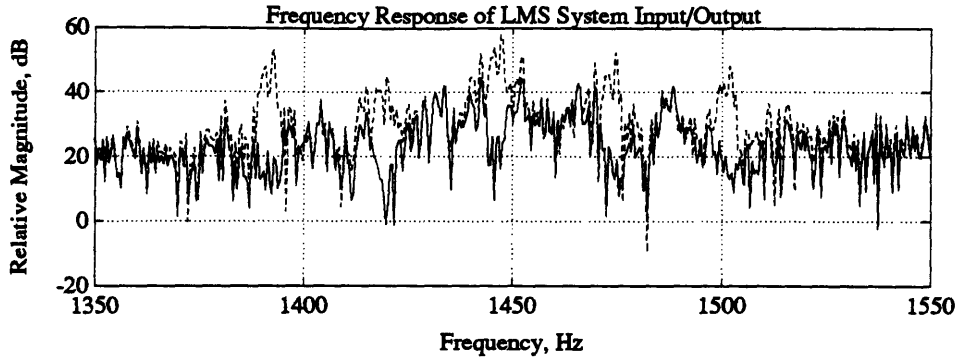

Figure 4-5: Frequency Response of Simulated Five-Notch LMS Algorithm to CH-47D In-Flight Data

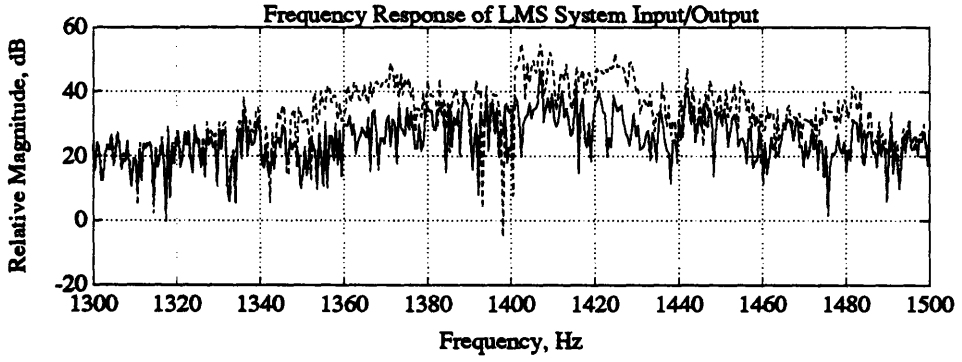

Figure 4-6: Frequency Response of Simulated Five-Notch LMS Algorithm to CH-47D Takeoff Data

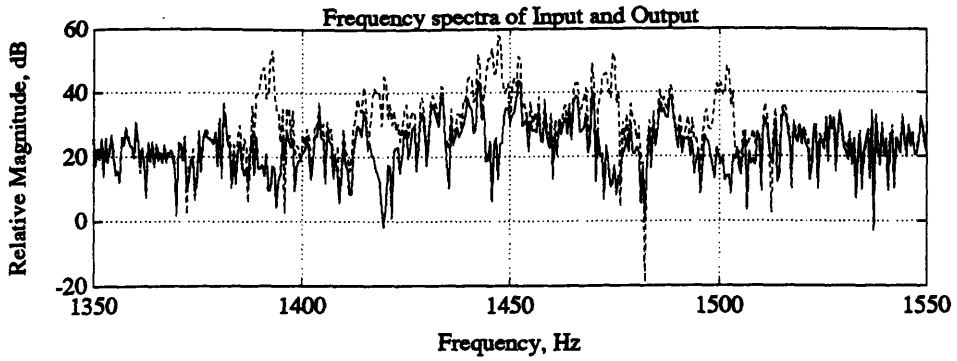

Figure 4-7: Frequency Response of Simulated Five-Notch TF Algorithm to CH-47D In-Flight Data

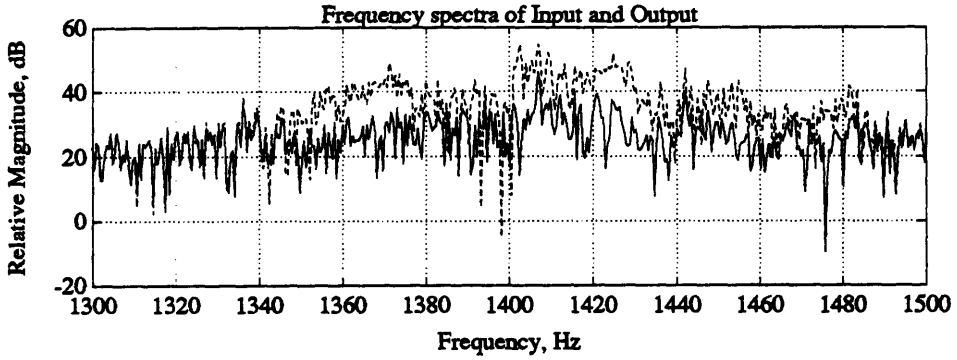

Figure 4-8: Frequency Response of Simulated Five-Notch TF Algorithm to CH-47D Takeoff Data

has sucessfully reduced the noise spikes present in the original spectrum by 10-20 dB. Note that, unlike the LMS algorithm, there is substantial attenuation at frequencies between the noise spike locations. This is due to the fact that neighboring notch filters combine their attenuations for these nearby frequencies. Thus, there is a large range of frequencies with a minimum attenuation that is greater than zero (see Figure 3-13 and its associated description).

4.3.4 Simulation of the Variable Sampling Rate Algorithm

For reasons previously explained (see Section 3.5.3), the VSR algorithm could not be simulated, so no results are available with recorded data. However, the normalized,

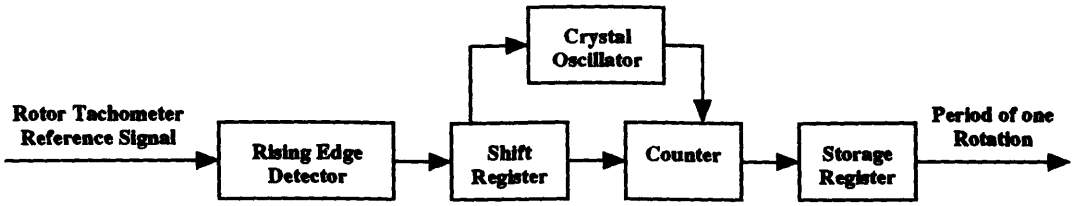

Figure 4-9: Block Diagram of Frequency Determination System

ideal frequency responses are shown in Section 3.5.4.

4.4 Real-Time Implementation

Real-time LMS and TF algorithms were implemented on two different DSP microprocessors, the Texas Instruments' TMS32020 and the Motorola DSP56001, but due to unforseen hardware limitations with the DSP development system, the VSR algorithm was not implemented. Because the standard components of any DSP system are an ADC, a DSP microprocessor, a DAC, and appropriate lowpass filters, the frequency measurement circuitry used to obtain the transmission rotation rate is explained in the following sections.

4.4.1 Frequency Determination System for LMS and TF Algorithms

A block diagram of the FDS is shown in Figure 4-9. The incoming sinusoidal reference signal is converted to a TTL square wave through a diode-capacitor network. Once the start count signal has been given, the counter chip is enabled, and the rising edges of the input are shifted into a shift register. After the $(N+1)th$ rising edge passes ($N+1$ rising edges are equivalent to N full pulses), the output of the shift register turns off the counter and indicates that the count has been completed. The value stored in the counter is sent to the DSP chip, the counter and shift register are cleared, and the process begins again.

4.4.2 Frequency Multiplication System for Variable Sampling Rate Algorithm

The VSR algorithm is based on the premise that the reference signal can be used to drive the sampling frequency of the VSR system through the use of interrupts. In order to do this, a high-frequency, uniform-period reference signal is required. Because the rotor tachometer signal is only around 1180 Hz, and the sampling frequency needs to be in the 16 kHz range, the rotor tachometer signal must be used as the input to a phase-locked-loop (PLL) which multiplies its frequency.

The block diagram for the FMS is shown in Figure 4-10. The incoming reference sinusoid is converted to a TTL square wave through a diode-capacitor network. This square wave is then fed into one of the two inputs of the phase comparator of the PLL. The phase comparator determines the difference in phase between this signal and a fedback signal, and outputs a voltage proportional to this phase difference. This voltage is passed through a narrowband lowpass filter to eliminate any high-freqency components, and is used to drive a voltage controlled oscillator. The output of the VCO is fed through a divide-by-n counter and back into the other input of the phase comparator. Because the PLL matches the phase and frequency of the phase comparator's input signals, the output of the VCO is a square wave at n times the input frequency. This signal can be used to trigger the sampling interrupts for the DSP chip, so that the sampling rate is always proportional to the frequency of the rotor tachometer.

The most critical aspect of the PLL frequency multiplier is the lowpass filter between the phase comparator and the voltage controlled oscillator. This is because the PLL's output between rising edges of the input must be as uniform as possible to ensure a steady sample rate. In order to obtain this consistency, the lowpass filter must have extremely narrow bandwidth in order to filter out the periodic pulses in the output of the phase comparator. Once the components for the lowpass filter have been properly chosen, however, the output of the frequency multiplier holds quite consistent over its n samples. The following section quantifies the error of the

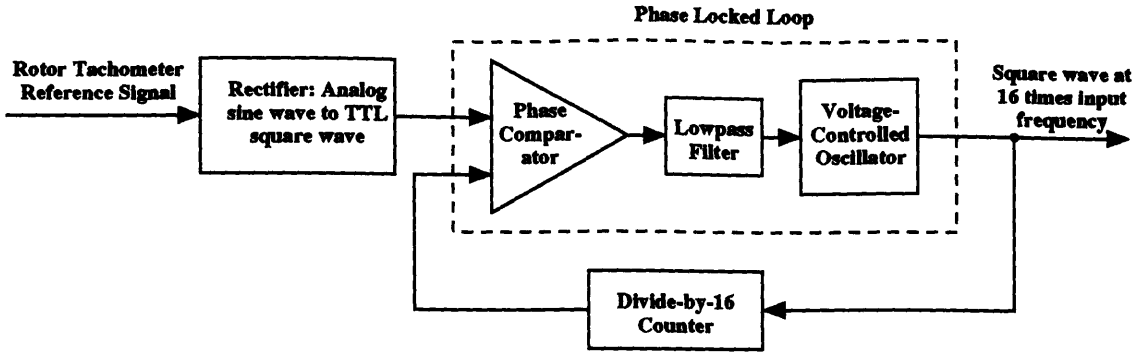

Figure 4-10: Block Diagram of Frequency Multiplier System

frequency multiplier and its effects on the VSR algorithm.

Error Analysis

A divide-by-16 counter was used for analysis of the frequency multiplier, producing a nominal sampling rate of (16)(1183.17) = 18930 Hz. The higher the multiplication rate, the greater the test of the PLL and its lowpass filter; reducing the multiplication factor only improves the accuracy of the frequency multiplier. The input frequency was held at 1183 Hz by using a precision sine wave generator. The output of the PLL was examined using a Hewlett-Packard 1501 logic analyzer, which provides timing information to an accuracy of 10 ns. The times between rising edges of the multiplied-by-16 frequency were measured to examine the variations that occurred between rising edges of the output signal. Several data runs were collected, and the error in the output frequency was found to be no more than .44%. This translates into a variation of up to 6.33 Hz at the LPF frequency. This error must be accounted for in the bandwidth of the notch filter, because there is no way to compensate for this error without redesigning the PLL. This error, $E_{PLL}(F)$ can easily be included in the analysis of section 3.6 by modifying equation 3.42 such that

$$B_{filter} \geq \frac{2V(F)}{B_{filter}(F) - B_{noise} - E_{inherent} - E_{PLL} - \frac{1}{2}R(F)}. \tag{4.1}$$

4.4.3 Implementation on Texas Instruments TMS32020 Microprocessor

Boeing had a VME-based TI TMS32020 development system on-hand, so the first real-time system ran on that processor. The LMS and TF algorithms were successfully implemented, with satisfactory results. The primary drawback to utilizing this chip was its long instruction cycle (200 ns, permitting only 312 instructions when sampling at 16 kHz) and its limited instruction set. Problems with the VME interface, and the fact that four separate hardware systems had to be integrated in order for the noise suppression system to operate, hindered development and further limited the speed of the system. These difficulties combined to result in a limited noise reduction system, one that could implement only two notch filters in the case of the LMS algorithm, and only one filter in the case of the TF algorithm. The VSR algorithm was not implemented because bus errors in the VME data transfer hindered development of an FMS.

Nonetheless, the initial results were encouraging, demonstrating that the LMS and TF algorithms did work successfully on real-time hardware. Narrowband attenuations of over 30 dB were achieved with both algorithms, promising excellent results with a more powerful microprocessor.

4.4.4 Implementation on Motorola DSP56001 Microprocessor

To overcome the limitations of the TI-based system, Boeing purchased a PC-based development system for the Motorola DSP56001 from Ariel Corporation (the PC-56) to continue work on the project. The 56001 purchased had an instruction cycle of only 60.5 nanoseconds (1033 instructions when sampling at 16 kHz), and a more advanced architecture that supported a much more expansive instruction set. Furthermore, the 56001 has a 24-bit architecture (as opposed to the 32020's 16-bit design), which

allows much greater precision for numerical calculations[8]. Also, the PC-based system provided better debugging capabilities, and included on-board ADC and DAC units, simplifying the system and its development.

The TF and LMS algorithms, along with the FDS, were successfully implemented on the DSP56001 system. The details of implementation are too extensive to explain here, but the variables used in testing the algorithms are presented at the beginning of the next chapter.

The VSR algorithm was not implemented on the DSP56001 microprocessor either, due to unforseen hardware limitations of the PC-56. A normalized-frequency VSR algorithm was implemented, however, but because the sampling rate could not be varied, the filters were stationary and the system could not be tested with any of the recorded data.

[8]The dynamic range supported with 16 bit arithmetic is 96.3 dB, whereas 24 bits spans an entire 144.5 dB. While the data was not sampled with 24-bit accuracy, the extra bits provided better overflow protection, higher precision data storage, and more accurate results from calculations internal to the microprocessor.

Chapter 5

Results, Conclusions, and Recommendations

5.1 Implementation

The LMS and TF algorithms were implemented in real-time hardware, in many different configurations and with different input signals. Throughout the testing, the microprocessor ran at 33.6 MHz, and used 14-bit ADCs and 14-bit DACs, maintained 24-bit accuracy throughout compuations and data storage, utilized a 24-bit, 256-value sine lookup table, and a sine increment value that had seven integer bits and 17 fractional bits. The varied parameters included:

1. Sampling rate of 12 or 15.9 kHz.
2. Frequency Determination System utilizing a 10 MHz oscillator, measuring the time for six pulses to pass, or one using a 20 MHz oscillator, counting the duration of three pulses.
3. Reference sine and cosine signals generated by one of two methods: direct table lookup or linear interpolation. The direct table lookup method simply utilized the closest value in the table as the signal amplitudes, whereas the interpolation method calculated the magnitudes of the reference signals by interpolating between the two closest values in the table.

4. Bandwidth of filters (integration constant β of the LMS algorithm, lowpass filter coefficients α and β of the TF algorithm).

5. Number and location of filters (i.e., how many filters were used and which gear mesh frequencies were suppressed).

6. Notch filters of identical bandwidths, independent of the filter center frequency, or filter bandwidths proportional to the center frequency.

7. Using a sinewave frequency generator as the reference input to the FDS, or driving the FDS with the actual rotor tachometer signal.

8. One of four different inputs: sinusoidal (to obtain frequency responses), speech with no noise, ambient cockpit noise, or the cockpit interphone signal (speech plus noise).

The TF algorithm was implemented in both serial and parallel versions, while the LMS algorithm was implemented only in the standard parallel version. As expected, the parallel TF algorithm worked fine for a single notch filter, but did not succeed when two or more notches were placed in close proximity (see section 3.4). The VSR algorithm was implemented in a frequency-normalized version, also at 12 and 15.9 kHz[1]. It was tested with sinusoidal inputs alone, in order to obtain a normalized frequency response, and a speech without noise signal. Because the filters could not track a reference signal, testing with the ambient noise or interphone was not done.

Its frequency responses were practically identical to those of the TF algorithm, just as predicted from the simulation. As a result, it is expected that a fully implemented VSR algorithm would have characteristics very similar to the TF algorithm, but with substantially reduced computation requirements.

[1] Due to an unforseen hardware limitation, the DSP development system was unable to implement the VSR algorithm fully. The sampling rate could not be controlled externally without an extremely accurate PLL with an output frequency in the MHz range, and several modifications to the hardware of the system itself.

5.2 Results

The LMS and TF systems were found to have the following characteristics:

1. The systems were successful in implementing notch filters whose center frequency varied with the frequency of the reference signal, in this case, the rotor tachometer signal.

2. The systems (with filters of adequate bandwidth) were able to attenuate most of the noise spikes selected for suppression even as their frequencies varied over time. However, algorithms that implemented filters with identical bandwidths did not perform as well as the proportional-bandwidth systems when attenuating high frequency noise. This was because the filter bandwidth adequate for suppressing the LPF was too small to guarantee suppression of the more rapidly changing high frequencies, and the amplitude of the high-frequency noise spikes would vary over time.

3. Alternating the sample rates (between 12 kHz and 15.9 kHz) showed no difference in performance, except for the fact that the faster sampling rate resulted in less time available for computation, thereby reducing the maximum number of filters that could be implemented. Also, note that α and β had to be changed proportionally with the sampling rates in order to achieve equivalent attenuation effects.

4. The 20 MHz FDS allowed slightly smaller bandwidths to be used for the filters when compared with the 10 MHz FDS, while still maintaining the tracking capability. With the proper filter design, both performed adequately and were able to attenuate the noise spikes as their frequencies changed.

5. Little appreciable distortion occurred in speech signals for systems with few filters and narrow bandwidths. Filters with extremely narrow bandwidths caused a loud ringing when the speech contained rapidly-changing signals, but the ringing died away quickly.

6. Too many filters with too wide a bandwidth caused substantial degradation of speech signals. The wide-bandwidth systems also experienced ringing, and while the volume of the ringing was lower, it persisted for a longer period of time.

7. Utilizing the less accurate direct lookup method for reference signal generation resulted in substantially worse output effects than the more accurate linear interpolation method. Using the interpolation method resulted in a clean output on an oscilloscope, and largely noise-free audible output. When the direct lookup method was used, the reference signals showed a substantial amount of high frequency noise on the oscilloscope (with a magnitude of roughly 10% that of the input), and resulted in degraded performance that was easily heard. It was clear that the algorithms did not track the gear mesh frequenies well when using the direct lookup approach, due to the distortion present in the reference signals.

8. The effectiveness of a notch filter in attenuating a noise spike was dependent upon how accurately the notch was placed with respect to the noise. Due to the notches' extremely narrow bandwidth at high attenuations, a slight placement error resulted in a very noticeable audible difference. Furthermore, when the filter bandwidth was too small, the system could be heard attempting to track the reference frequency. If the reference frequency changed quickly and the FDS was not able to keep up, the amplitude of the noise spikes increased (the noise spike moved outside the high-attenuation range of the filter) until the system could adapt and realign the notches with the noise spikes.

Several unanticipated characteristics of the CH-47D interphone and its signal noise also became apparent during the real-time tests. These are described below.

1. The loudest noise spikes did not always occur at the calculated gear mesh frequencies described in Chapter Two. All of the calculated LPF and LCF harmonic frequencies were noticeable, from the LPF-LC3H to the LPF+LC3H.

However, there were several frequency spikes between the harmonics, which dominated the frequency spectrum once the others had been suppressed. Furthermore, there were several noise spikes near the UP1H frequency that were not linear combinations of the UPF and the UCF.

2. Several high-magnitude noise spikes were present in the interphone system that were apparently not generated by the forward transmission gear mesh[2]. These spikes appeared at frequencies near 4720, 4732, and 4743 Hz, and had magnitudes approaching that of the LPF frequency. Their source is unknown.

3. When the pilot or copilot used the radio to transmit outside of the helicopter (rather than simply communicating with someone else in the helicopter), the impedance of the interphone line changed. This altered the characteristics of the interphone frequency spectrum. From the signals recorded, the transmitted signal seemed to have less of a noise problem than the internal communication system had when the signal was not transmitted, although this may have been an illusion resulting from the lower overall magnitude of the transmitted signal.

In addition to the above implementations and analyses, the VSR algorithm was implented in a normalized-frequency form, such that fixed-coefficient filters were used with a constant sampling frequency. This system was tested at 12 and 15.9 kHz sampling rates with sinusoids and speech alone as inputs. The system had a frequency response almost identical to that of the TF algorithm, and when speech was used as its input, produced an output that sounded the same as that of the TF algorithm. Due to the fact that the VSR algorithm could not be tested with a variable sampling rate, and the system's extreme similarity to the TF algorithm, the following explanations of bandwidth, filter number, filter placement, ringing, attenuation, and sound quality for the TF algorithm are the same for the VSR algorithm. Because the system could not adapt to changing frequencies of the gear mesh, it was not run with the recorded signals.

[2]This was evident from the fact that the noise spikes appeared very strongly in the interphone signal all the time but did not have substantial magnitude in the ambient microphone signal. This can be seen in the frequency response plots shown in the following section.

5.2.1 Frequencies Suppressed and Filter Characteristics

It was difficult to analyze the systems' performance with a spectrum analyzer due to the constantly changing center frequencies and amplitudes of the noise spikes. However, the spectrum analyzer revealed very clearly when a frequency spike was attenuated successfully, even if listening to the output did not reveal any change. The analyzer also indicated when the filter bandwidth was too small for the noise spike, because the amplitude of the peak could be seen rising and falling on the display. A surprising result was the fact that there seemed to be only a weak correlation with the spectrum analyzer's display and the audible change in the signal. For example, placing a notch at the LPF frequency produced a very significant change in the audible output, as did the LPF$\pm$LC3H frequencies. However, suppressing some frequencies which appeared very loud on the spectrum analyzer (for example, three peaks located near the UC1H frequency) did not produce a substantial change in the audible signal. The effect of suppressing a particular noise spike could not always be guessed by its absolute magnitude, nor its magnitude relative to background noise in adjacent frequency bands. The true test was listening to the signal with and without the suppression to see if the difference was audible.

The systems were fine-tuned by listening to their output with a particular characteristic alternating between two values. For example, the bandwidth of all the filters was alternated, or a particular notch was added or removed from the system. The characteristic that created the best sounding output was then added permanently to the code, and a different characteristic was altered. In this way, the system was iteratively tuned to offer the best subjective performance. The use of 12 notch filters seemed to offer the best tradeoff between noise attenuation and speech distortion. These filters were implemented at the frequencies shown in Table 5.1, using the interpolated sine/cosine amplitude values and the 20 MHz, 3-pulse FDS, while sampling at 12 kHz. The bandwidth chosen corresponded to an α of .988 and a β of .012 at the LPF frequency (β increased proportionally as the suppression frequency increased, and $\alpha = 1 - \beta$). This value was chosen because an α of .990 or higher resulted in noise spikes occasionally leaving the high attenuation region of

No.	Frequency (Hz)	Associated Gear Mesh	α	β
1	800	near UP1H	.99338	.00662
2	1185	UP2H-UC1H	.99020	.00980
3	1207.5	UP2H+UC3H	.99001	.00999
4	1396.125	LPF-LC3H	.9885	.0115
5	1450.875	LPF	.9880	.0120
6	1464.5625	LPF+LCF	.9879	.0121
7	1505.625	LPF+LC3H	.9875	.0125
8	1575	UP3H-UC3H	.9870	.0130
9	1597.5	UP3H+UC1H	.9868	.0132
10	3340.728	SBF	.9724	.0276
11	3395.478	SBF+LC3H	.9719	.0281
12	4732	n/a	.9609	.0391

Table 5.1: Filter Characteristics of "Optimized" LMS and TF Algorithms

the filter. When implementing twelve filters at 12 kHz with a clock speed of 33.6 MHz, neither algorithm taxed the microprocessor's capabilities. The LMS algorithm completed all the calculations for the filters in 28.97 μs, using approximately 35% of the available time. The TF algorithm was slightly less efficient, requiring 38.97 μs for its computations, which is equivalent to nearly 47% of the microprocessor's computing power[3]. For comparsion, a fully-optimized VSR algorithm should take about 4.3 μs to implement 12 filters, or only 5.2% of the processor's capability[4].

To examine the limits of attenuation that can be achieved, and the effect that a large number of filters has upon the output spectrum and clarity of the voice signal, the number of filters in the LMS and TF algorithms was increased until the computation limit of the microprocessor was reached. Filters were added based on a combination of the audible difference in the signal and the effect that the filters had on the frequency response[5]. For the LMS algorithm, this point occurred af-

[3]Note that the algorithms were fairly well-optimized to calculate the system output in a minimum amount of time. However, it is likely that more efficient coding and better memory organization could speed both algorithms up somewhat, although gains beyond about 20% are unlikely.

[4]This is an estimate based on implementing cascaded second-order IIR filters. Such a filter can be executed in only four instructions, with nine more for overhead operations. The ADC and DAC interfaces require only six instructions, plus about ten for interrupt servicing; for twelve filters this is $25 + 4(12) = 73$ instructions, and at 12 kHz the microprocessor can execute up to 1400 instructions!

[5]After about fifteen to twenty filters, it was no longer possible to hear the effect that a single

ter implementing 39 filters, which required almost 82 μs, or 98% of the processor's computation time at 33.6 MHz, sampling at 12 kHz. The TF algorithm reached its maximum at 32 filters, taking 82.7 μs to calculate its output, or 99% of the available time. For comparison purposes, the VSR algorithm will utilize 99% of the available computation time when an estimated 340 second-order IIR sections are implemented. This would allow 340 notch filters, or any combination of notch and other filters that require less than 340 cascaded second-order blocks.

5.2.2 Frequency Response and Input/Output Spectra

The following plots were generated by running the specified input (sinewave, ambient cockpit noise, or cockpit interphone signal) through the specified algorithm (none, "optimized" LMS or TF algorithm, or maximized LMS or TF algorithm) and sending the results to an HP plotter. Significant points about each figure are explained below[6]. The first plot was created using a Solartron frequency response analyzer, while the remaining plots were generated by a Rockland real-time spectrum analyzer. All plots were sent to an HP plotter to create the figures.

Figure 5-1 is a closeup of the frequency response of the "optimized" LMS and TF algorithms in the frequency range of 1350 to 1550 Hz. Both of these algorithms implement seven filters in this frequency range, and the differences in their frequency responses are clear. The LMS algorithm has a point of 0 dB attenuation between every notch filter (note that the y-axis is relative and not absolute attenuation), whereas the TF algorithm has at least 18 dB of attenuation for two bandwidths of about 35 Hz (where two notches are very close to one another) and has at least 8 dB of attenuation over a bandwidth of about 135 Hz. Thus, it is clear that the LMS algorithm provides

notch had on the audible output, so the noise spikes that had the highest peaks relative to the adjacent background noise were suppressed. With the addition or removal of several filters rather than just one, an audible difference in the output noise was apparent.

[6]Note that the plots were not all constructed from precisely identical input spectra. Due to the need to have two simultaneous signals recorded, the only way to perform this analysis without undue overhead was to hand-start and stop the recorder for each system. However, due the audio signal used to cue the start of the analysis and the fact that each spectrum is a time-averaged plot of almost three seconds duration, the plots do accurately represent the attenuation achieved with each algorithm.

better (narrower) notch characteristics, whereas the TF algorithm will result in more attenuation in neighboring bands (the effective bandwidths of the filters are larger). However, for notches that are not close to one another (for example, the left and rightmost notches in the diagram), the bandwidth of the TF filters is smaller than the bandwidth of the LMS filters. Furthermore, the frequency response of the TF algorithm is symmetrical about the frequency that is exactly in the middle of two notches, while the LMS algorithm has an asymmetrical frequency response between notches.

Figure 5-2 shows the spectrum of the ambient noise in the helicopter cockpit. Notice the prevalent spikes near the UPF, UP1H, UP2H, LPF and its sidebands, UP3H, LP2H and its sidebands, and the SBF and its sidebands, as well of the absence of a substantial noise spike near 4730 Hz. Clearly, the magnitudes of the LPF and the SBF frequencies are the strongest, followed immediately by the UP1H, UP3H, and LP2H frequencies.

Figure 5-3 shows the spectrum of the ambient noise in the cockpit after it has been passed through the "optimized" LMS algorithm. Note the substantial reductions of the UP1H (one filter), UP2H (two filters), LPF (four filters), UP3H (two filters), and SBF (two filters). The 12th filter is near 4730 Hz, but the ambient noise does not have a spike near this frequency. It is obvious from the plot that a substantial amount of reduction has occurred at the frequency spikes that have been filtered, resulting in 10 to 30 dB of attenuation.

Figure 5-4 shows the spectrum of the ambient noise in the cockpit after it has been passed through the "optimized" TF algorithm. The filter frequencies are the same as those for the LMS algorithm shown in the previous figure, and it can be seen that the TF algorithm has also successfully suppressed the noise spikes. The TF algorithm shows slightly more attenuation, ranging from 15 to 35 dB at the filter frequencies.

Figure 5-5 is the pilot's microphone signal, as present in the cockpit interphone system. Note the noise spikes at the UP1H, UP2H, LPF, UP3H, LP2H, and SBF frequencies, as well as an additional spike in the 4730 Hz area. Also note the absence of low and high frequencies due to the frequency response of the interphone system

(the UPF spike seen in the ambient noise spectrum is insignificant here). The noise spikes in the interphone are closer to the level of the background noise by 10-20 dB than they are in the ambient noise spectrum, so the audible difference caused by the systems was not as great.

Figure 5-6 is the frequency spectrum of the output of the "optimized" LMS algorithm, using the interphone signal as its input. Again, the noise spikes have been suppressed appreciably, and just as before the attenuation ranges from about 10 to 30 dB. In addition, note the almost 45 dB reduction in the frequency spike near 4730 Hz!

The response of the "optimized" TF algorithm to the interphone input is shown in Figure 5-7, and the selected noise spikes have again been suppressed by about 15-35 dB, except for the spike near 4730 Hz, which has all but vanished after 45 dB of attenuation.

Figures 5-8 and 5-9 show the frequency responses of the maximized LMS and TF algorithms, respectively, when applied to the interphone signal. Note the extreme reduction of almost all significant noise spikes, with attenuations on the order of 30 dB. Note the left over spike near the SBF frequencies in the LMS plot, and how it is attenuated in the TF algorithm. This is due to the 0 dB point of the LMS algorithm and the combining effects of the TF notches; this frequency range utilized only three filters, when five substantial noise spikes were actually present. The TF algorithm caused substantial attenuation at nearby frequencies, whereas the LMS did not. As a result, the neighboring spikes were suppressed more by the TF algorithm than they were by the LMS system. Furthermore, note the spikes still present in the 3500 to 4000 Hz range for the TF algorithm. These spikes remain because the maximized TF algorithm implemented seven less filters than the LMS, and as a result, some of these noise spikes were not filtered.

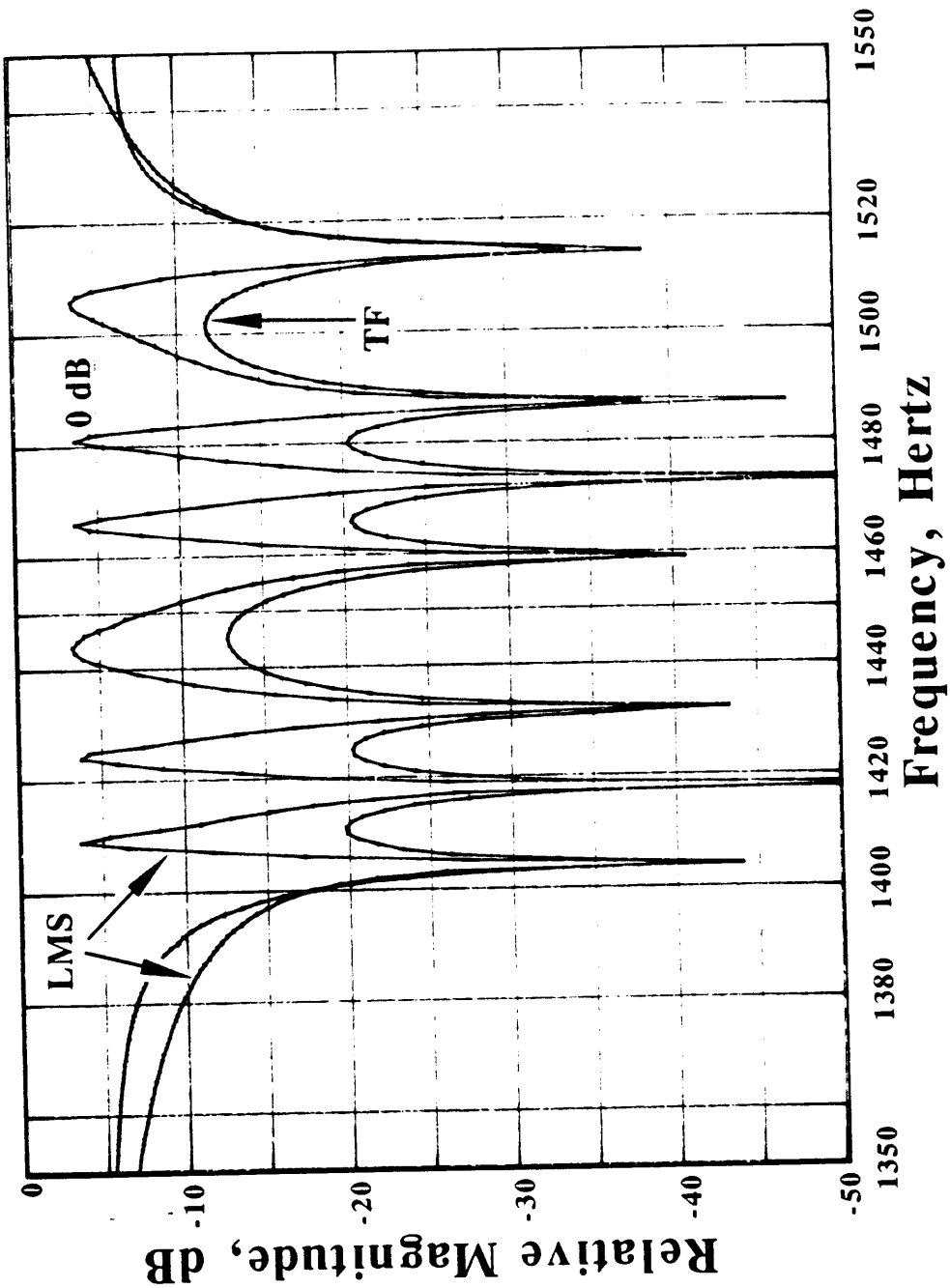

Figure 5-1: Frequency Response of "Optimized" Real-Time LMS and TF Algorithms

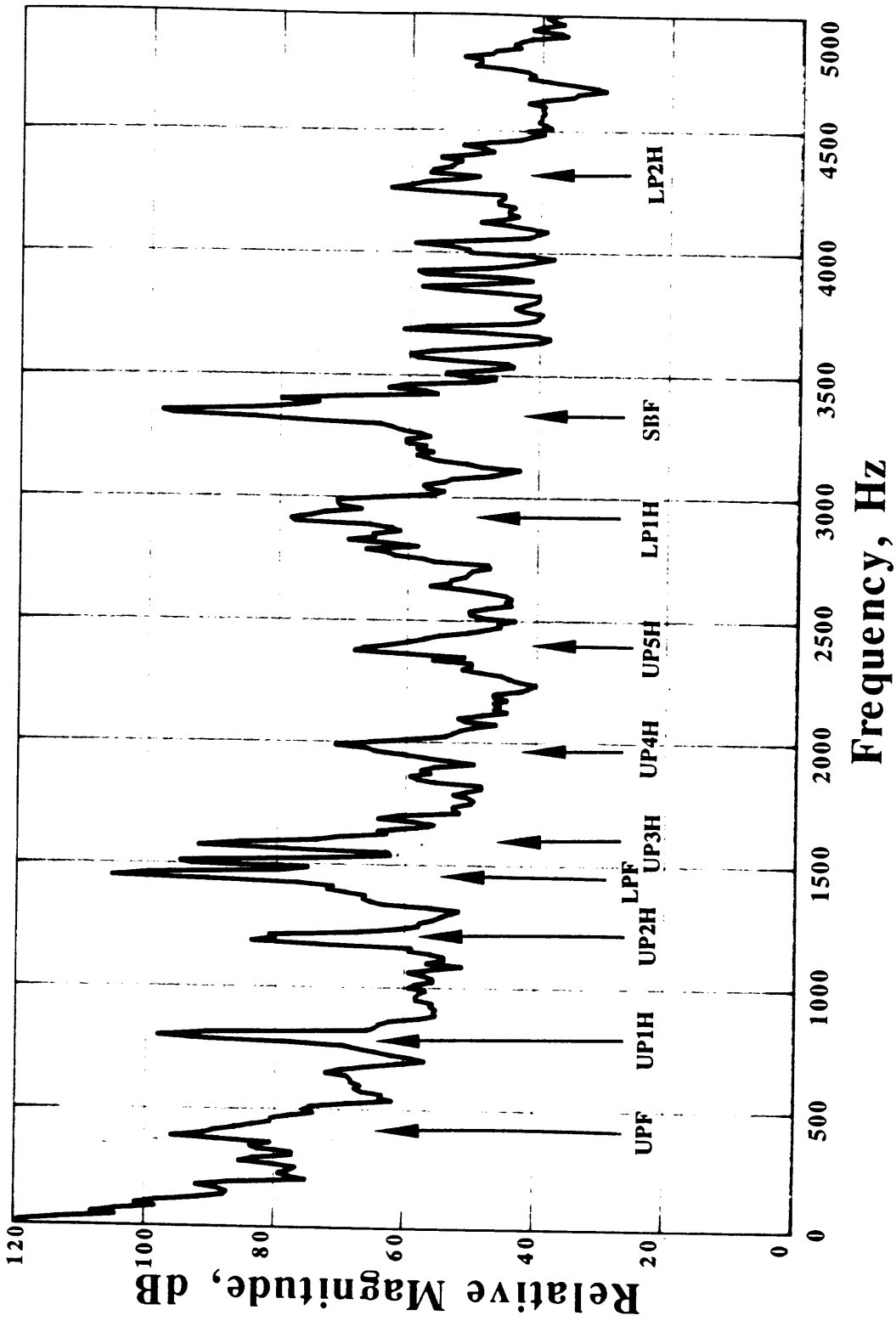

Figure 5-2: Frequency Spectrum of CH-47D Cockpit Noise

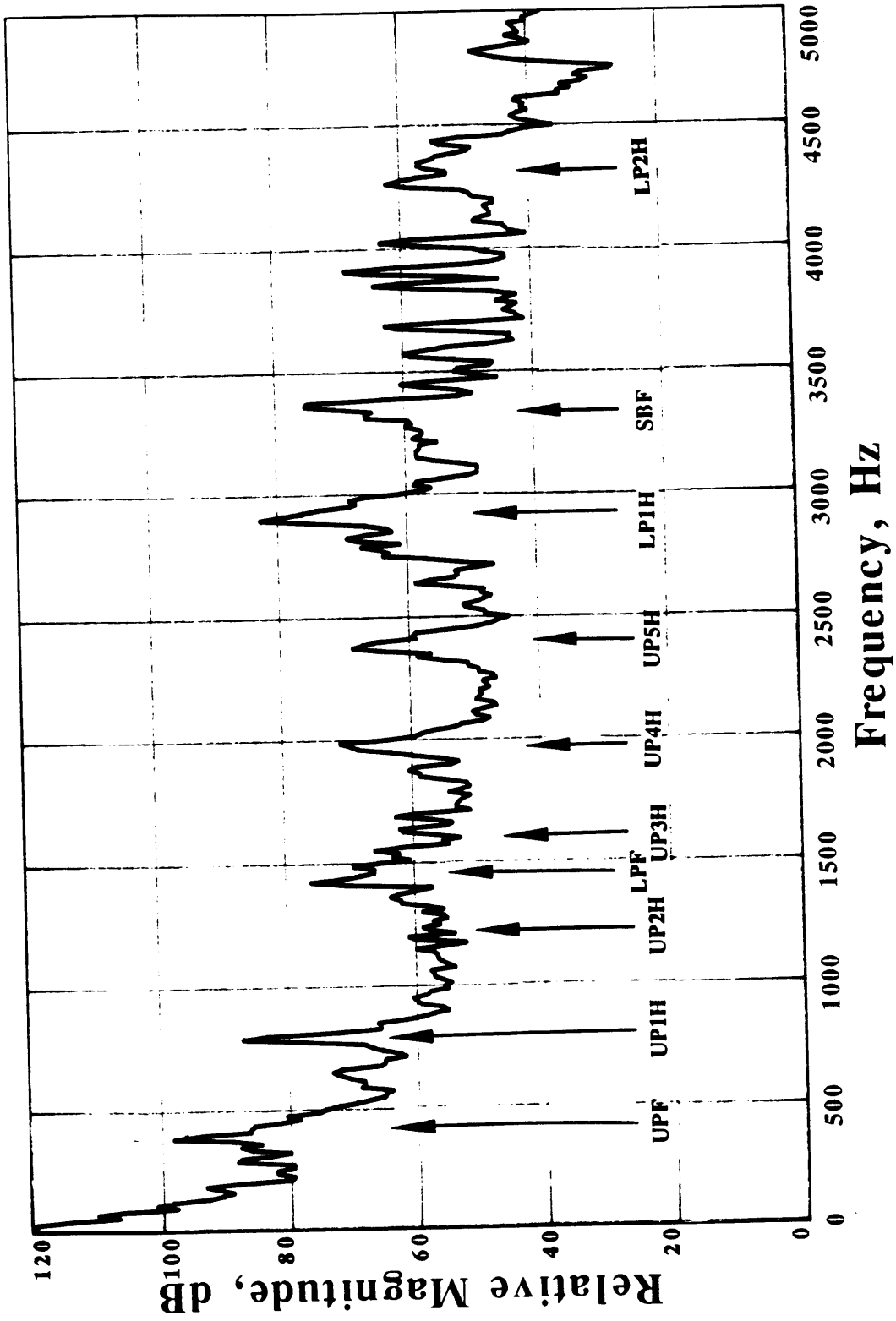

Figure 5-3: Frequency Spectrum of Cockpit Noise after "Optimized" LMS Filtering

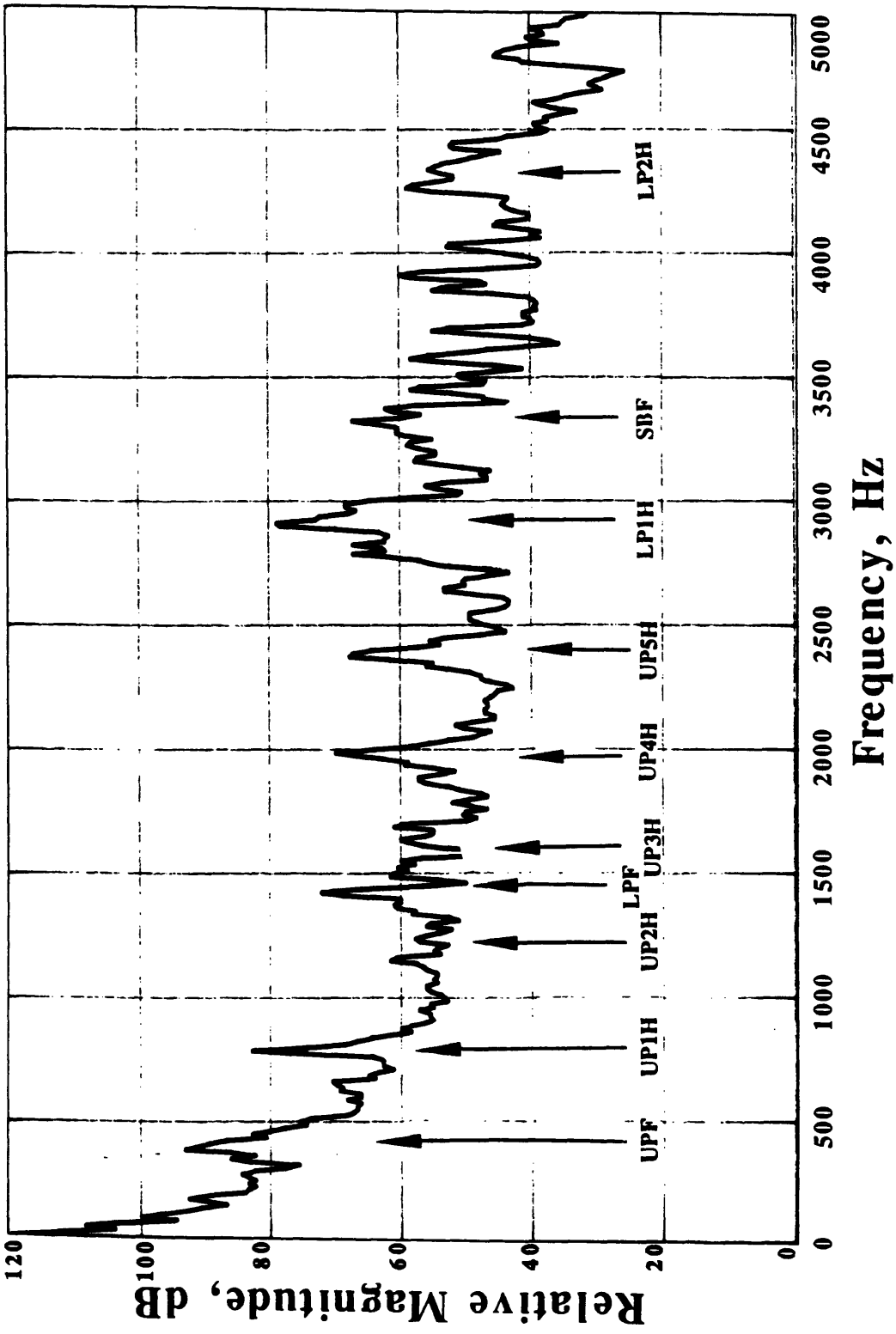

Figure 5-4: Frequency Spectrum of Cockpit Noise after "Optimized" TF Filtering

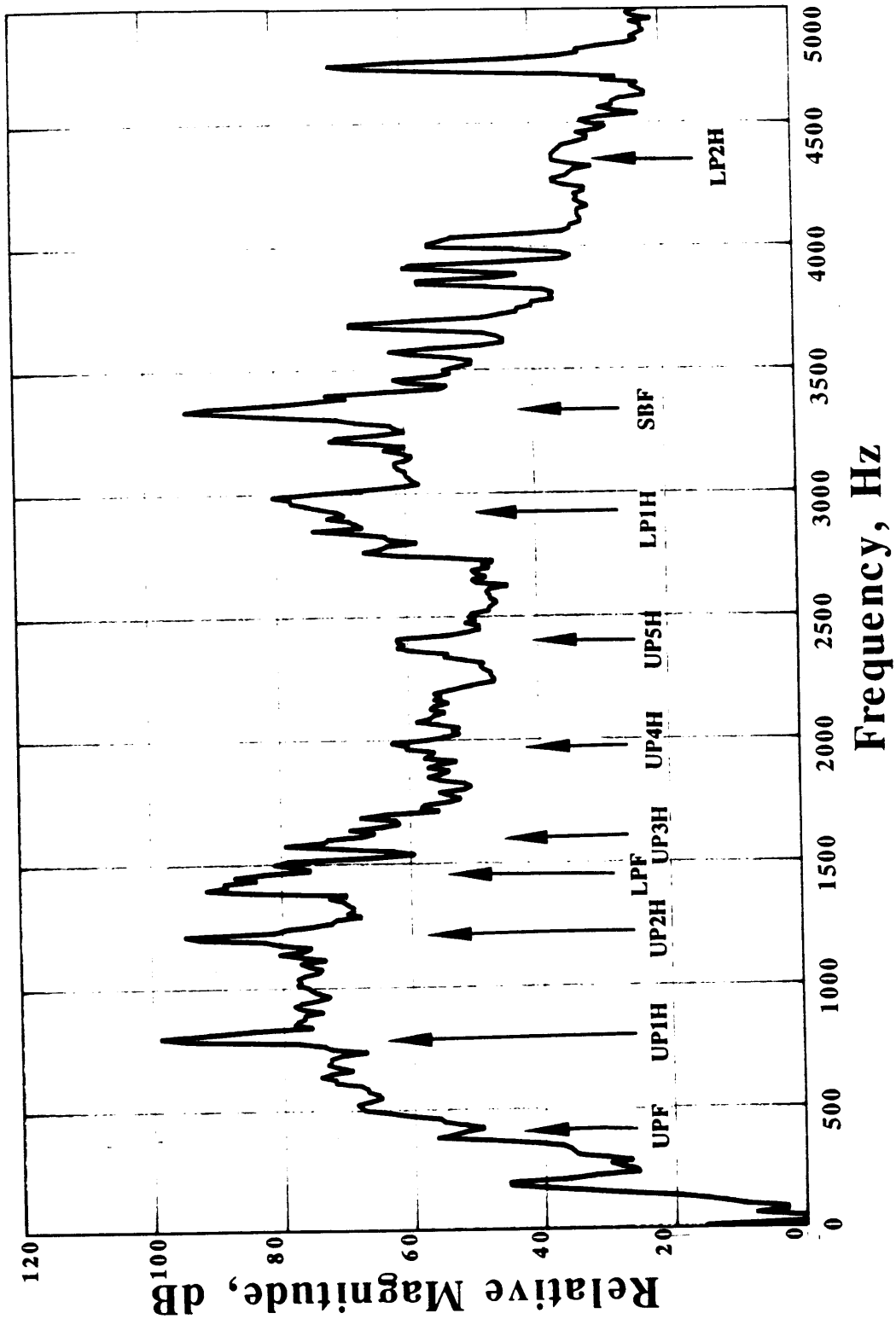

Figure 5-5: Frequency Spectrum of CH-47D Cockpit Interphone System

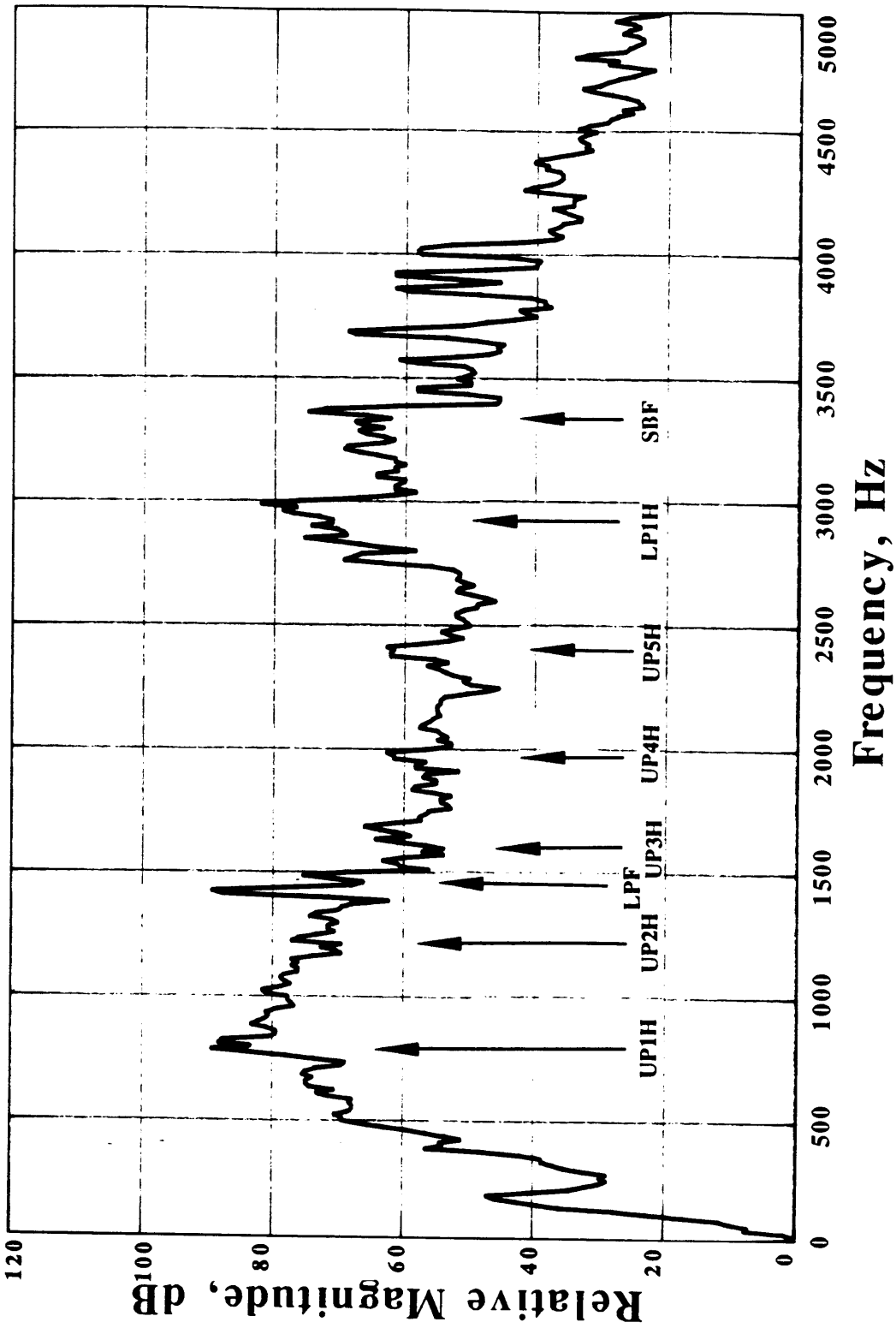

Figure 5-6: Frequency Spectrum of Interphone after "Optimized" LMS Filtering

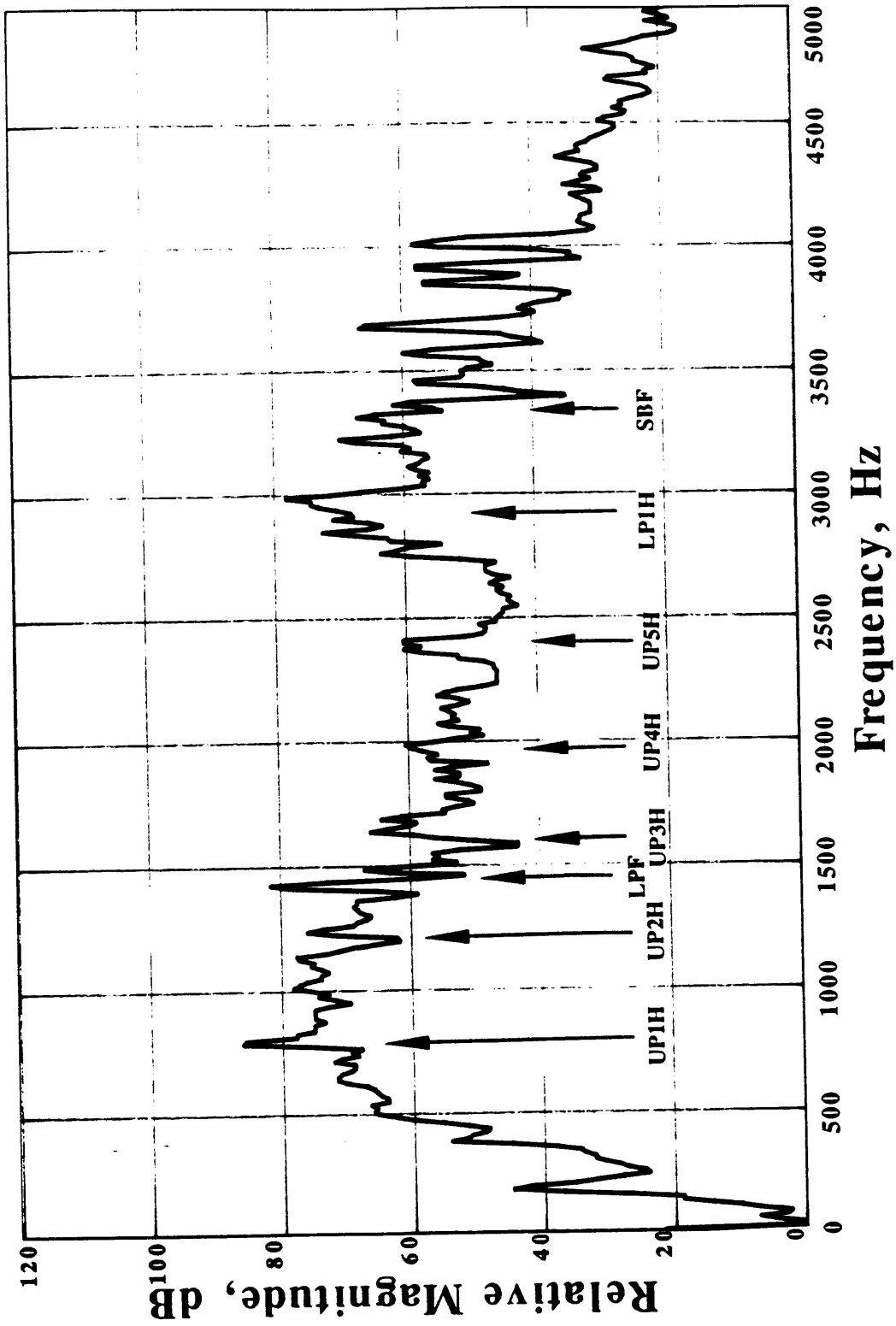

Figure 5-7: Frequency Spectrum of Interphone after "Optimized" TF Filtering

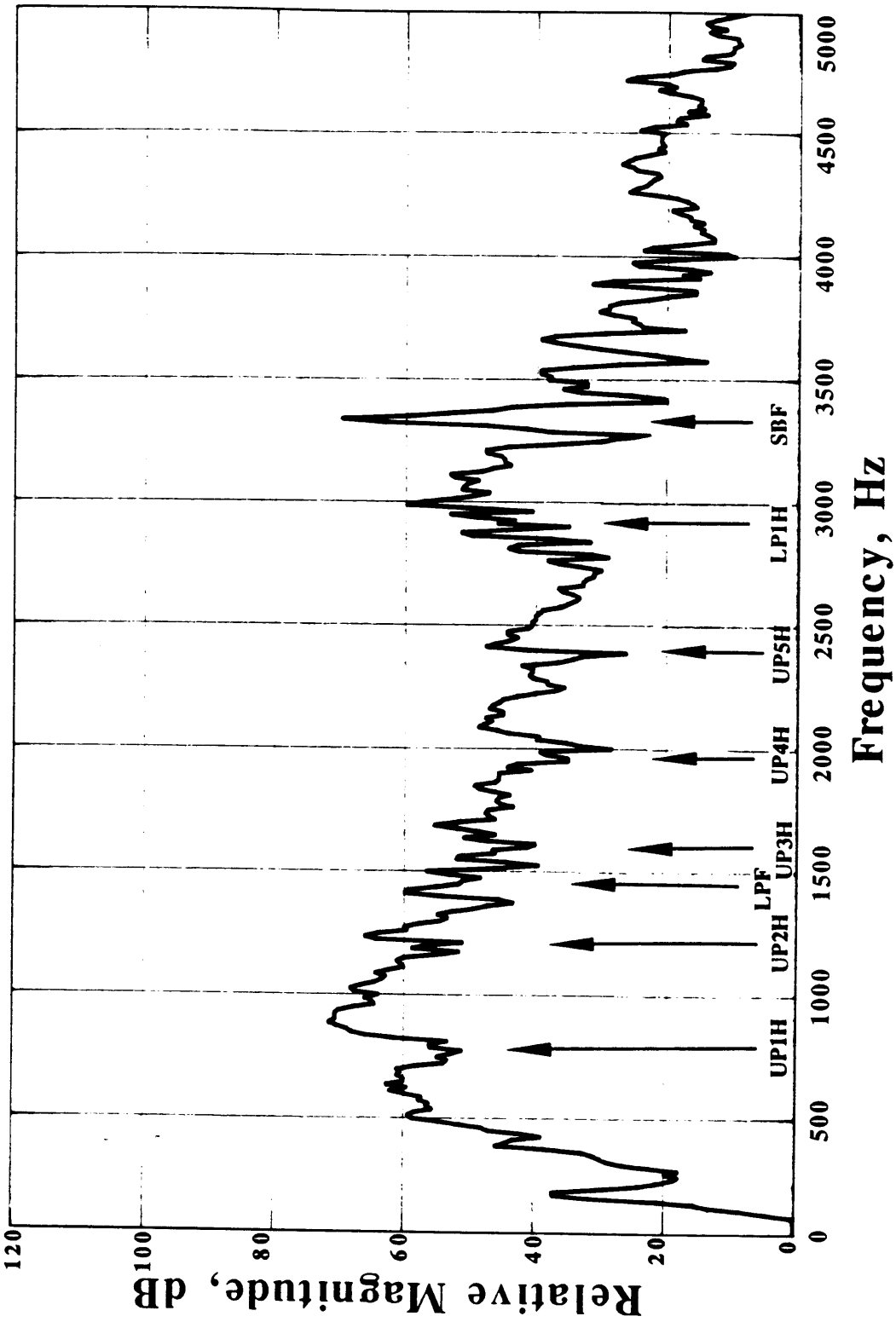

Figure 5-8: Frequency Spectrum of Interphone after Maximized LMS Filtering

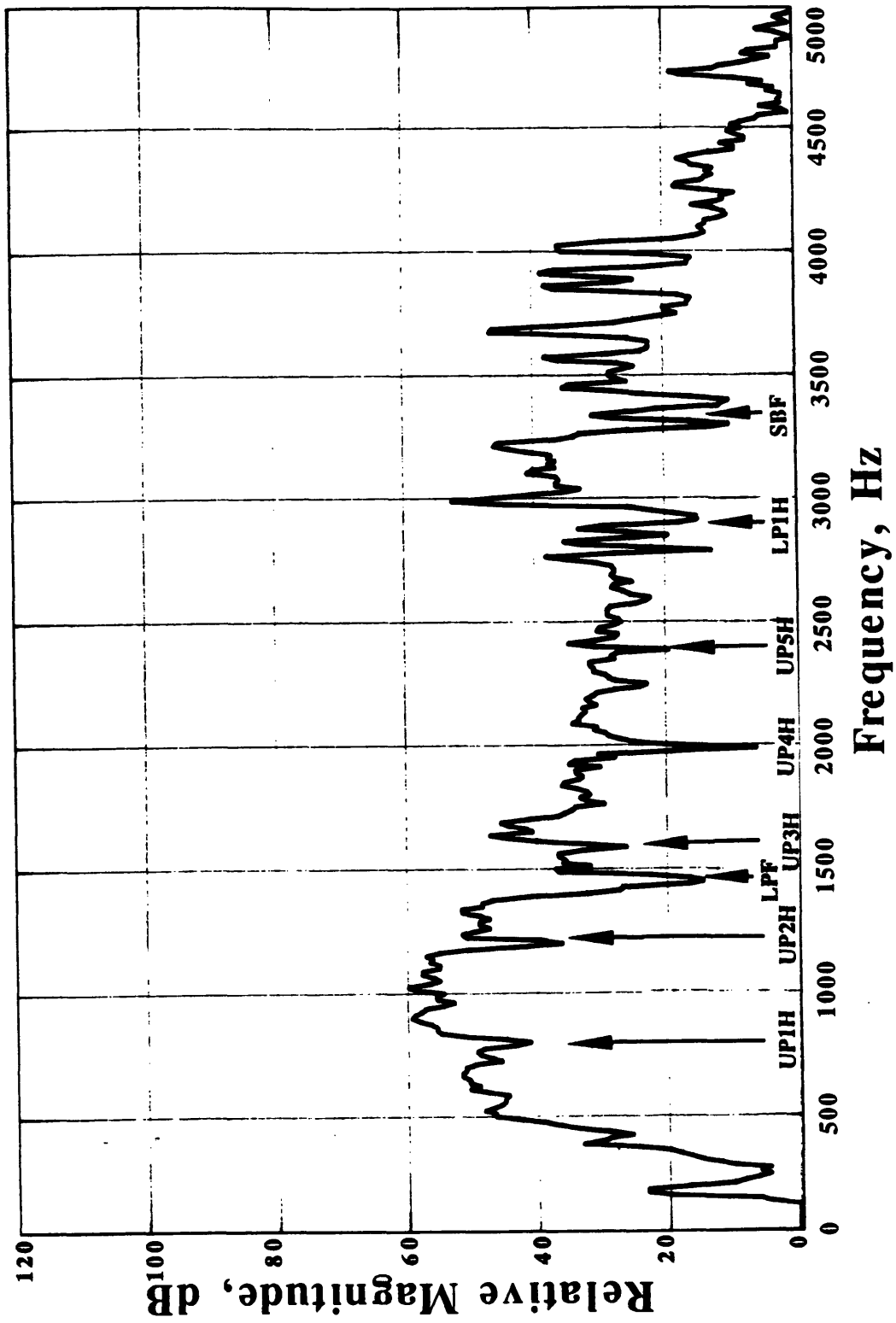

Figure 5-9: Frequency Spectrum of Interphone after Maximized TF Filtering

5.3 Conclusions

The real time systems were able to attenuate the noise spikes in the interphone signal without causing undue distortion to the pilots' speech. While no formal intelligibility tests were performed, the overall sound quality of the interphone signal seemed to improve, provided that the parameters of the algorithms were chosen carefully. The following section describes the subjective testing results of the three algorithms. The second section performs a more analytical analysis of the performance and capabilities of the systems.

5.3.1 Subjective Results

The LMS and TF algorithms were largely successful in attenuating the noise spikes caused by the CH-47D transmission. While the sound quality of the pilots' speech did not improve as dramatically as hoped, the significant noise peaks in the spectrum were reduced to very near the background noise level (a reduction of 10-35 dB), making a "hot mike" situation in the cockpit much less objectionable. Furthermore, the noise spikes were attenuated even when the pilots were speaking, which produced an audible improvement in the sound quality of the signal due to the decreased noise level. As the filters did not greatly affect the pilots' speech, the signal was clearer, more understandable, and less offensive after acted on by one of the "optimized" systems. However, the substantial distortion introduced by ringing did degrade the speech signal if the number and/or bandwidth of the filters was too high. Therefore, it is important to carefully design the systems to find a balance between the amount of attenuation achieved and the amount of distortion added to the speech signal.

The VSR algorithm, while only tested in its normalized-frequency form, had almost identical characteristics to that of the TF algorithm. Therefore, it is believed that the VSR algorithm can offer noise suppression capability and signal distortion levels very similar to those of the TF algorithm, with substantially reduced computation requirements. This algorithm also has the advantage of flexibility in filter design, and should permit implementation of adaptive bandstop, bandpass, lowpass,

and highpass filters, which the LMS and TF algorithms are not capable of doing. Furthermore, these filters could be implemented in FIR forms with linear phase characteristics, with the possible result of substantially decreasing the amount of distortion caused by the system.

When the LMS and TF algorithms are designed to have filters of identical bandwidth (same α values) located at the same frequencies, it is difficult to distinguish between the effects of the two algorithms. While both successfully reduced the noise spikes to the background level, and both algorithms produced ringing, the ringing of the LMS algorithm seemed slightly louder than that of the TF algorithm. On the other hand, the interaction of adjacent notch filters in the TF algorithm caused noticeable amplitude reductions in certain bandwidths of the pilot's voice, which were not as apparent in the LMS system. Subjectively, the ringing had a more degrading effect on the speech signal, and when designed identically, the TF algorithm produced an output with slightly better sound quality. Formal objective testing would have to be performed to more accurately analyze the algorithms' effects on the intelligibility of the cockpit interphone signal.

As a result, the three approaches have the capability to reduce noise in situations where the noise characteristics are similar to those of the CH-47: narrowband, variable-frequency noise spikes whose frequencies are proportional to the frequency of a reference signal. Further development and testing needs to be done to fully develop and test the algorithms presented in this document (especially the VSR algorithm), but the systems can most likely be refined and expanded to handle other circumstances, such as wider bandwidth noise or systems with noise that has less predictable qualities.

5.3.2 Comparison of the Three Algorithms

Although there are certainly more similarities between the effectiveness of the three algorithms than differences, a thorough comparison of the advantages and disadvantages of the algorithms is warranted. While which system produced the largest improvement in sound quality was not determined by formal testing, there are several

areas where comparisons between the algorithms can be done easily. These comparisons are described below.

Pole-Zero Analysis

As discussed earlier, the LMS and TF algorithms can be treated as LTI systems when the modulation frequency ω_0 is held constant. Traditional second-order digital notch filters are designed with zeros on the unit circle at angles $\pm\theta$, where $\theta \leq \frac{\pi}{2}$. These zeros cause the attenuation at the notch frequency, and the steepness of the notch is controlled by the proximity of the accompanying poles, also at angles $\pm\theta$, but inside the unit circle (magnitude less than 1). The closer the zeros and poles are located to one another, the steeper the notch filter and the narrower its bandwidth, although infinite attenuation always occurs exactly at the notch frequency.

The pole-zero analyses of the three noise reduction systems provide interesting results. The VSR algorithm uses traditional fixed-characteristic filters, so its poles and zeros are exactly as described in the previous paragraph. The LMS algorithm preserves the zero locations of the VSR algorithm, but moves the poles. This keeps an infinite null at the notch frequency, but because the poles are now farther away, the bandwidth of the notch filter is larger. Conversely, the TF algorithm keeps the pole locations identical to those of the VSR algorithm, but moves the zeros. As a result, the zeros are no longer located at a position for maximum attenuation, but are moved outside of the unit circle. This distance from the unit circle decreases their effectiveness in attenuating the signal near the desired frequencies, so that the pole's effect is stronger. This produces a more narrowband notch. For high α, this difference is not significant because the zeros are still very close to the unit circle, but it may become a factor as α is decreased and the bandwidth of the notch is increased.

The most significant effect caused by the pole-zero movement became apparent in the frequency response analyses of the algorithms (shown in Chapter Two, and visible in Figure 5-1). For notch filters that are so close together that their frequency response affects one another, there is always a point of 0 dB attenuation between the notches when the LMS algorithm is used. This is due to the fact that the poles of the

LMS algorithm have moved from the traditional notch filter locations, and reduce the attenuation effects of the adjacent filter. This results in a superior notch filter when the primary design concern is minimizing filter bandwidth. The other two algorithms do not guarantee a 0 dB point between notches, and if the bandwidth of the notches is high and they are located close to one another, the minimum attenuation between the notches may be high. For the TF notches shown in Figure 5-1, their close proximity, combined with an α of .988, resulted in a minimum attenuation between the notches of 8 dB over a 135 Hz frequency band, and a minimum 18 dB reduction spanning a 35 Hz frequency range. However, it should also be noted that, for isolated notch filters of identical α, the LMS algorithm produces a notch with a wider bandwidth than that produced by the TF or VSR algorithms. So, depending on the type of filters desired, the LMS algorithm may have an advantage over the TF and VSR algorithms.

Ease of Implementation and Calculation Requirements

While the implementations of the LMS and TF algorithms were similar, both requiring sinusoid and cosinusoid signal generation, the VSR algorithm sidestepped this requirement by using the sampling frequency to control the filter frequencies. This moves much of the calculation burden out of the microprocessor and into support circuitry, in this case a PLL. As a result, the VSR algorithm was by far the most computationally efficient of the three systems, reaching the microprocessor's computation limit only after implementing an estimated 340 second-order IIR filters (the LMS and TF algorithms were limited to 39 and 32 filters, respectively). Furthermore, the VSR algorithm provides great flexibility in the design of adaptive filters, allowing any kind of band pass/reject filter to be used in an adaptive form. However, it is not easy to control the filter parameters over time, and it is more difficult to design the filters in the first place than with the other two algorithms. Also, it may be difficult to obtain an accurate, consistent, high-frequency reference signal whose frequency is proportional to the frequencies of the noise (which is required to control its sampling rate). However, if this signal is available, the VSR algorithm is almost certainly the system of choice due to its flexibility in tailoring the system's frequency response and

its minimal computation requirements[7].

The LMS and TF algorithms require external circuitry (an FDS) of comparable complexity to that needed by the VSR algorithm (an FMS), but the design of the FDS is not as difficult as that of the FMS. Furthermore, both algorithms require substantially more computation from the DSP chip, because of their need for digitally generated reference signals[8]. Furthermore, the LMS and TF algorithms are not well-suited to implement filters other than notch filters. Thus, if other types (lowpass, highpass, bandstop, etc.) of filters are desired, the VSR algorithm holds a clear advantage. However, if the reference signal does not lend itself to controlling the DSP chip's sample rate, or if the system only needs to have notch filters, the LMS and TF algorithms can be used quite effectively to attenuate noise spikes of varying frequency. In this case, the LMS algorithm holds two advantages. First, it is more computationally efficient than the TF algorithm, as it is able to take advantage of parallel processing techniques. As a result, more filters can be implemented using the LMS approach than the TF approach. Second, for notch filters close together, the LMS algorithm always has a point of 0 dB attenuation, resulting in a more narrowband notch filter than when the same filters are implemented in the TF algorithm. Therefore, if the number of required filters is high and the bandwidth of the filters needs to remain narrow, even for notches that are close together, then the LMS algorithm is better suited to the problem than the TF approach. So, if the noise reduction application needs wider bandwidth notch filters (or indeed bandstop filters; the additive attenuation between notches can be used to simulate a bandstop filter), then the TF algorithm is probably a better choice. When all design considerations are equal, the TF algorithm had a more favorable effect upon the cockpit interphone signal in subjective audio tests.

[7]This, of course, assumes that the VSR algorithm has virtually the same effects on the audible signal as the TF algorithm. Based upon the analyses of this project, this is believed to be the case, although the VSR algorithm was not run with the recorded data.

[8]The reference signals could be externally generated instead, but this would require two ADC channels for each notch filter to be implemented. While possible, such a design is not very practical for multiple notch filters because of the cost of ADC chips and the software overhead needed to read their values. Furthermore, generating the signals themselves would be hardware-intensive, most likely requiring PLL circuitry for each notch filter.

Overall Evaluation

Due to the great advantages of minimal computation time and the ability to implement different kinds of filters, the VSR algorithm is most likely the best of the three algorithms when used to suppress variable frequency noise spikes. However, if a consistent, high-frequency reference signal is unobtainable, then the LMS and TF algorithms both provide viable alternatives. If the number of filters to be implemented is high, or approximate bandstop filters are not desired, then the LMS algorithm is the better choice. If, however, computation time is not a critical concern, or a bandstop filter is needed, the TF algorithm is a better choice due to its ability to simulate a bandstop filter when notches are placed close together. If there are no design concerns that lead to one algorithm over the other, then the TF algorithm should be used because it does not produce as much ringing as does the LMS algorithm.

5.4 Recommendations for Future Work

As implemented, the systems were successful in attenuating the primary noise spikes present in the CH-47D interphone system. However, there are several improvements that could be made to the real-time system in order to improve its performance. These possible improvements and areas requiring further study are split into two categories below. The first five sections deal with alterations or improvements that could be made to the system to improve its performance in the specific case of suppressing CH-47D interphone noise. The last section describes a more general area for future research, which could expand the potential applications of the LMS and TF algorithms. The capabilities of the algorithms may extend well beyond the scope of their implementation in this project, and further analysis is warranted.

5.4.1 Real-Time Implementation and Testing of the VSR Algorithm

The VSR algorithm was not implemented during this project due to unforseen hardware limitations, so its true characteristics could only be guessed at, based on the responses of the other two algorithms and the responses of the normalized VSR algorithm. In future efforts, the VSR algorithm should be implemented and studied in a real-time system (simulating the algorithm is difficult) to determine its transient characteristics and its audible effect on the cockpit interphone signal. While it is expected that the results will be very similar to those of the TF algorithm when implementing IIR notch filters, the VSR algorithm holds two possibilities for improvements which cannot be realized in the LMS or TF systems. First, the ability to implement different filters, such as bandstop filters, may be able to remove several noise spikes that are located close to one another without introducing as much distortion as when they are removed one by one with notch frequencies. Second, and perhaps the most promising aspect of any of the algorithms, is the ability to implement FIR filters in the VSR algorithm. With this capability, the filters could be designed to have linear phase characteristics, which, while increasing computation time, could produce appreciably less distortion that their IIR counterparts. If the same noise reductions could be achieved without the ringing present in the current systems, then a very significant improvement in the intelligibility of the cockpit interphone signal could be realized.

5.4.2 Error Reduction, Update Rate improvements of FDS

The accuracy and update rate of the FDS could be improved to provide better tracking of the reference input frequency. Some of the faster rotor tachometer variations allowed the noise spikes to move outside of the filters' effective ranges, temporarily increasing the noise. While this can be somewhat compensated for by increasing the filter bandwidth, doing so is not as attractive a solution as making better measurements of the rotor tachometer signal in the first place. If the system could respond

more quickly and more accurately, the filter bandwidth necessary to ensure attenuation could be reduced.

5.4.3 Flight Testing

A logical extension of the current project is to flight test one or more of the noise suppression systems on-board a CH-47D aircraft during flight. This would be necessary as a proof-of-concept test for the algorithm, and the system could be verified in the high-vibration environment of the helicopter. Furthermore, the system's effectiveness could be tested in a real time, immediate-response scenario, where the pilot could perform abrupt maneuvers in an attempt to cause the system to lose track of the noise spikes, and turn the system on and off at will to analyze any improvements in the quality of the signal. Flight testing was planned for the noise reduction systems studied in this project, but was not completed at the time of this writing.

5.4.4 LMS Algorithm with Delayed-Noise Reference Signals

As explained in Chapter Three, there are two implementations of the LMS algorithm that are commonly used. Only one was explored in detail for this project, the implementation that uses sinusoid and cosinusoid signals at the frequency to be attenuated as the reference inputs. The other approach involves using delayed noise signals as reference inputs. While this latter implementation of the algorithm was not successful in simulation, there are several possible explanations. First, a single cockpit microphone placed at a fixed location was used as the reference noise source. This causes problems when the pilots move their heads, because the phase difference between the interphone signal and the reference microphone changes rapidly. Furthermore, the phase difference between the pilot and copilot's microphone signals are completely different, and switching from one to another would undoubtedly cause the algorithm to fail. A possible solution to this problem is to utilize a separate reference microphone for each pilot, mounted to his or her helmet. That way, the phase differences

should be relatively well-behaved as the pilots turn their heads, and because each interphone microphone has its own reference microphone, the phase difference in the other pilot's signal will not affect the algorithm. Another possibility of improving the performance of this implementation of the LMS algorithm is to bandpass the reference microphone signal to leave only the frequencies of interest. That way, the phase differences in other frequency bands of the signal do not greatly affect the LMS calculations, and the algorithm is better able to supress the noise signals in the desired bands.

5.4.5 Characterization of Gearbox and Interphone Noise

A better analysis and understanding of the noise spikes created by the gearbox would simplify determination of what frequencies the filters should be suppress. A substantial amount of the implementation time was spent hunting for the loudest noise spikes, and accurately determining or confirming their frequencies. If the spikes' amplitude and frequencies could be determined through analytical research, ranking them loudest-to-quietest on average across multiple helicopters, much of the tedious experimenting would be unnecessary. Furthermore, the fact that the analysis in Chapter Two did not exactly identify all of the noise spikes indicates that there may be substantial variations between different helicopters, or harmonic frequencies may be present that were not revealed by the analysis. If a large scale noise survey of CH-47D transmission noise were undertaken, the fundamental gear mesh spikes and their sidebanded harmonics would be better understood.

Also, two problems with the interphone system should be addressed. First, the source of the noise spikes near 4730 Hz should be identified. While these spikes are narrowband and of high amplitude (characteristics of a gear mesh frequency or harmonic), they do not appear in the recordings of the ambient microphone. This seems to indicate that their source is not the gearbox, but something internal to the interphone system. The source of this noise needs to be identified. Furthermore, the changing impedance of the interphone system should be analyzed more closely to determine what effect that has upon the noise reduction algorithms. The results of

such an analysis could be used to improve the noise reduction systems over the full range of conditions that they would experience in the Chinook.

5.4.6 Combining Noise Reduction Techniques

Many of the noise reduction techniques that have already been used in the CH-47 were used individually, in order to determine the improvements achieved by the technique. However, as explained in Chapter One, many of the techniques are complementary in terms of what kind of noise problem each addresses. Combining these techniques and systems into one helicopter would undoubtedly cause substantial reductions in the noise heard by the pilots, both direct and indirect. Furthermore, combining systems that treat the indirect noise would undoubtedly increase the quality of the interphone signal as well. The right combination of these approaches could probably yield a signal-to-noise ratio good enough that VR on a helicopter might become feasible.

5.4.7 Experimentation with $H(z)$

Chapter Three derived the LTI transfer functions of the LMS and TF algorithms for specific cases of $H(z)$ in the MFD algorithm[9]. However, other transfer functions may be obtained using alternate systems as the $H(z)$. For example, the TF algorithm was simulated with the use of high-order lowpass filters in an attempt to obtain bandstop filters, but phase problems affected the output, resulting in distorted notch filters. Perhaps other transfer functions used in the MFD algorithm could result in different adaptive filters, which could expand the application of these two algorithms.

[9]Specifically, a simple integrator was used as $H(z)$ in the LMS algorithm and a second-order IIR lowpass filter was implemented as the $H(z)$ for the TF algorithm.

Bibliography

[1] Acoustical Society of America. "American National Standard Methods for the Calculation of the Articulation Index." American National Standards Institute, Inc., New York, New York, 1970.

[2] Harold L. Alexander. Assistant Professor, M.I.T. Department of Aeronautics and Astronautics. Personal communication, 1992.

[3] Harold L. Alexander. "Analog Adaptive EKG Noise Canceling System." Stanford University, 1982.

[4] Roger Alwang. Propulsion Technologies, Boeing Defense and Space Group, Helicopters Division. Personal Communication, 1991-92.

[5] R. H. Badgley and T. Chiang. "Reduction of Vibration and Noise Generated by Planetary Ring Gears in Helicopter Aircraft Transmission." ASME Paper 72-PTG-11, 1972.

[6] Bose Corporation. *User's Manual for Bose Noise-Reducing Headset.*

[7] Thomas S. Bragg. "Acoustical Study of the CH-47B (Chinook) Helicopter." U.S. Army Human Engineering Laboratories, Technical Note 4-68, Aberdeen Proving Ground, Maryland, March 1968.

[8] Robert Brashears, et. al. "Filter for Speech Enhancement in Helicopter Communications." Drexel University Senior Design Project 87-15, 1987.

[9] Jeffrey W. Chan and Carol A. Simpson. "Comparison of Speech Intelligibility in Cockpit Noise Using SPH-4 Flight Helmet with and without Active Noise Reduc-

tion." National Aeronautics and Space Administration, USAAVSCOM Technical Report 90-G-1, Ames Research Center, July 1990.

[10] Gergory A. Clark, Sanjit K. Mitra, and Sydney R. Parker. "Block Implementation of Adaptive Digital Filters." *IEEE Transactions on Acoustics, Speech, and Signal Processing*, vol. ASSP-29, no. 3, June 1981, pp. 744-752.

[11] Stephen J. Elliott and Paul Darlington. "Adaptive Cancellation of Periodic, Synchronously Sampled Interference." *IEEE Transactions on Acoustics, Speech, and Signal Processing*, vol. ASSP-33, no. 3, June 1985, pp. 715-717.

[12] Stephen J. Elliott, Ian M. Stothers, and Philip A. Nelson. "A Multiple Error LMS Algorithm and Its Application to the Active Control of Sound and Vibration." *IEEE Transactions on Acoustics, Speech, and Signal Processing*, vol. ASSP-35, no. 10, October 1987, pp. 1423-1434.

[13] L. J. Eriksson, M. C. Allie, and R. A. Greiner. "The Selection and Application of an IIR Adaptive Filter for Use in Active Sound Attenuation." *IEEE Transactions on Acoustics, Speech, and Signal Processing*, vol. ASSP-35, no. 4, April 1987, pp. 433-437.

[14] S. E. Forshaw, J. M. Rylands, and R. B. Crabtree. "Evaluating the Effectiveness of Active Noise Reduction in Flight Helmets." Defence and Civil Institute of Environmental Medicine, DCIEM no. 88-RR-34, Downsview, Ontario, August 1988.

[15] Thomas A. Giordano and Gerard C. Keane. "The Effect of Helicopter Noise on Communication and Hearing." U.S. Army Electronics Command, Research and Development Technical Report ECOM-4140, Fort Monmouth, New Jersey, August 1973.

[16] Graham C. Goodwin, Robin J. Evans, Rogelio Lozano Leal, and Robert A. Feik. "Sinusoidal Disturbance Rejection with Application to Helicopter Flight Data

Estimation." *IEEE Transactions on Acoustics, Speech, and Signal Processing*, vol. ASSP-34, no. 3, June 1986, pp. 479-484.

[17] John R. Glover, Jr. "Adaptive Noise Canceling Applied to Sinusoidal Interferences." *IEEE Transactions on Acoustics, Speech, and Signal Processing*, vol. ASSP-25, no. 6, December 1977, pp. 484-491.

[18] Steven R. Hall and Norman M. Werely. "Linear Control Issues in the Higher Harmonic Control of Helicopter Vibrations." Presented to the 45th Annual Forum of the American Helicopter Society in Boston, Massachusetts, May 22-24, 1989.

[19] Richard W. Harris, Douglas M. Chabries, and F. Avery Bishop. "A Variable Step (VS) Adaptive Filter Algoithm." *IEEE Transactions on Acoustics, Speech, and Signal Processing*, vol. ASSP-34, no. 2, April 1986, pp. 309-316.

[20] Blair Harro. Systems Integration Laboratories, Boeing Defense and Space Group, Helicopters Division. Personal Communication, 1992.

[21] Tim Healey. "Design/Analysis for the Optical Main Rotor RPM Sensor." Boeing Defense and Space Group, Helicopters Division, December 21, 1990.

[22] Kotaro Hirano, Shotard Nishimura, and Sanjit K. Mitra. "Design of Digital Notch Filters." *IEEE Transactions on Circuits and Systems*, vol. CAS-21, no. 4, July 1974, pp. 540-546.

[23] Tilak Lal. "Non-Linear Time Invariant Bandreject Filtering." Boeing Defense and Space Group, Helicopters Division.

[24] I. Laskin, F. K. Orcutt, and E. E. Shipley. "Analysis of Noise Generated by UH-1 Helicopter Transmission." U.S. Army Aviation Material Laboratories, USAAVLABS Technical Report 68-41, Fort Eustis, Virginia, June 1968.

[25] Mitchell S. Mayer. "Acoustic Noise Suppression in Airborne Communications." U.S. Army Electronics Command, Research and Development Technical Report ECOM-4336, Fort Monmouth, New Jersey, July 1975.

[26] Mitchell S. Mayer. "Electronic Voice Communications Improvements for Army Aircraft." U.S. Army Aviation Research and Development Command, Research and Development Technical Report 81-E-1, Fort Monmouth, New Jersey, August 1982.

[27] Ron Mecklin. Pilot, Boeing Defense and Space Group, Helicopters Division. Personal Communication, 1992.

[28] Alan V. Oppenheim and Ronald W. Schafer. *Discrete-Time Signal Processing.* Prentice Hall, Englewood Cliffs, New Jersey, 1989.

[29] Dakshesh D. Parikh, and Nasir Ahmed. "Sequential Regression Considerations of Adaptive Notch Filters." *IEEE Transactions on Acoustics, Speech, and Signal Processing*, vol. ASSP-28, no. 3, June 1980, pp. 313-317.

[30] T. W. Parks and C. S. Burrus. *Digital Filter Design.* John Wiley & Sons, Inc., New York, 1987.

[31] Dennis Carl Pulsipher. "Application of Adaptive Noise Cancellation to Noise Reduction in Audio Signals." University of Utah, Salt Lake City, March 1979.

[32] R. Ramsey. "Linear Noise-Attenuating Earphone." U.S. Army Electronics Command, Research and Development Technical Report ECOM-76-0149-R, Fort Monmouth, New Jersey, November 4, 1977.

[33] D. V. Bhaskar Rao and Sun-Yuan King. "Adaptive Notch Filtering for the Retrieval of Sinusoids in Noise." *IEEE Transactions on Acoustics, Speech, and Signal Processing*, vol. ASSP-32, no. 4, August 1984, pp. 791-802.

[34] Don Reed. Propulsion Technologies, Boeing Defense and Space Group, Helicopters Division. Personal Communication, 1991-92.

[35] Salim Roucos, Vishu Viswanathan, Claudia Henry, and Richard Schwartz. "Word Recognition Using Multisensor Speech Input in High Ambient Noise." Presented at the International Conference on Acoustics, Speech, and Signal Processing, April 8-12, 1986, Tokyo, Japan.

[36] J. Shaw and N. Albion, "Active Control of the Helicopter Rotor for Vibration Reduction." *Journal of the American Helicopter Society*, vol. 26, no. 3, 1981.

[37] J. Shaw, N. Albion, E. Hanker, Jr., and R. Teal, "Higher Harmonic Control: Wind Tunnel Demonstration of Fully Effective Vibratory Hub Force Suppression." *Journal of the American Helicopter Society*, vol. 34, no. 1, 1989.

[38] Lisa A. Sievers and Andreas H. von Flotow. "Comparison and Extensions of Control Methods for Narrowband Disturbance Rejection." Presented at the 1990 ASME Winter Annual Meeting in Dallas Texas, November 1990.

[39] Rajendra Singh and Teik Chin Lim. "A Review of Gear Housing Dynamics and Acoustics Literature." National Aeronautics and Space Administration, NASA-CR-183110, Lewis Research Center, July 1988.

[40] Robert H. Spencer. Noise Technologies, Boeing Defense and Space Group, Helicopters Division. Personal Communication, 1991-92.

[41] R. H. Spencer, M. J. Burke, and G.W. Tye. "Active Control of Helicopter Transmission Noise." Boeing Defense and Space Group, Helicopters Division.

[42] H. J. M. Steeneken and G. Langhout. "Application of Active Noise Reduction for Hearing Protection and Speech Intelligibility Improvement." TNO Institute for Perception Report IZF 1985-7, 1985.

[43] H. J. M. Steeneken and J. G. van Velden. "Application of Active Noise Reduction for Hearing Protection and Speech Intelligibility Improvement." TNO Institute for Perception Report IZF 1988-21, 1988.

[44] Harry Sternfeld, Jr. Noise Technologies, Boeing Defense and Space Group, Helicopters Division. Personal Communication, 1991-92.

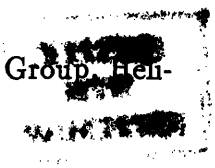

[45] Richard S. Teal. Flight Controls, Boeing Defense and Space Group, Helicopters Division. Personal Communication, 1991-92.

[46] Vishu Viswanathan, Claudia Henry, Richard Schwartz, and Salim Roucos. "Evaluation of Multisensor Speech Input for Speech Recognition in High Ambient Noise." Presented at the International Conference on Acoustics, Speech, and Signal Processing, April 8-12, 1986, Tokyo, Japan.

[47] V. Viswanathan and C. Henry. "Noise-Immune Multisensor Speech Input: Formal Subjective Testing in Operational Conditions." Presented at the International Conference on Acoustics, Speech, and Signal Processing, 1989.

[48] Bernard Widrow, et. al. "Adaptive Noise Cancelling: Principles and Applications." *Proceedings of the IEEE*, vol. 63, no. 12, December 1975, pp. 1692-1716.

6194-10